Comparison of Controlling Techniques for Active and Reactive Power in Wind Energy Conversion System

Beza Abebe Belayneh

A Thesis Submitted to

The Department of Electrical Power and Control Engineering

School of Electrical Engineering and Computing

Presented in Partial Fulfillment of the Requirement for the Degree of Master's in Electrical Power and Control Engineering (Power System Engineering)

Office of Graduate Studies

Adama Science and Technology University

October, 2022

Adama, Ethiopia

Comparison of Controlling Techniques for Active and Reactive Power in Wind Energy Conversion System

Beza Abebe Belayneh

Advisor: Dr. Milkias Berhanu

A Thesis Submitted to

The Department of Electrical Power and Control Engineering

School of Electrical Engineering and Computing

Presented in Partial Fulfillment of the Requirement for the Degree of Master's in Electrical Power and Control Engineering (Power System Engineering)

Office of Graduate Studies

Adama Science and Technology University

October, 2022

Adama, Ethiopia

Declaration

I hereby declare that this Master Thesis entitled "**Comparison of Controlling Techniques for Active and Reactive Power in Wind Energy Conversion System**" is my original work. That is, it has not been submitted for the award of any academic degree, diploma, or certificate in any other university. All sources of materials that are used for this thesis have been duly acknowledged through citation.

Beza Abebe	______________________	__________________
Name of the Student	Signature	Date

Recommendation

I, the advisor of this thesis, hereby certify that I have read the revised version of the thesis entitled "**Comparison of Controlling Techniques for Active and Reactive Power in Wind Energy Conversion System**" prepared under my guidance by **Beza Abebe Belayneh** submitted in partial fulfillment of the requirements for the degree of Masters of Science in Electrical Power and Control Engineering (Power System Engineering). Therefore, I recommend the submission of a revised version of the thesis to the department following the applicable procedures.

Dr. Milkias Berhanu	______________________	_______________
Advisor	Signature	Date

Approval Page

I, the advisor of the thesis entitled "**Comparison of Controlling Techniques for Active and Reactive Power in Wind Energy Conversion System**" and developed by **Beza Abebe Belayneh**, hereby certify that the recommendation and suggestions made by the board of examiners are appropriately incorporated into the final version of the thesis.

Dr. Milkias Berhanu	________________	________________
Advisor	Signature	Date

We, the undersigned, members of the Board of Examiners of the thesis by **Beza Abebe Belayneh** have read and evaluated the thesis entitled "**Comparison of Controlling Techniques for Active and Reactive Power in Wind Energy Conversion System**" and examined the candidate during the open defense. This is, therefore, to certify that the thesis is accepted for partial fulfillment of the requirement of the degree of Master of Science in Electrical Power and Control Engineering (Power System Engineering).

________________	________________	________________
Chairperson	Signature	Date
________________	________________	________________
Internal Examiner	Signature	Date
Dr.Yeshitela Shiferaw	[signature]	28/10/2022
External Examiner	Signature	Date

Finally, approval and acceptance of the thesis is contingent upon submission of its final copy to the Office of Postgraduate Studies (OPGS) through the Department Graduate Council (DGC) and School Graduate Committee (SGC).

________________	________________	________________
Department Head	Signature	Date
________________	________________	________________
School Dean	Signature	Date
________________	________________	________________
Office of Graduate Studies, Dean	Signature	Date

ACKNOWLEDGEMENTS

Foremost, I want to thank our GOD for the wisdom he gives me, the strength, peace of my mind, and good health to finish this research. This thesis becomes a reality with the kind support of many individuals. I would like to extend my sincere thanks to all of them.

I would like to acknowledge and give my thank to my advisor Dr. Milkias Berhanu whose comments and suggestions were valuable throughout my study. His guidance and advice carried me through all stages of writing my project. I would also like to express my gratitude to my family and friends for their moral support and warm encouragement.

Finally, I would like to express my gratitude to Adama Science and Technology University for giving me the opportunity to pursue my master's degree.

CONTENTS

LIST OF TABLES

LIST OF FIGURES

LIST OF ABBREVIATIONS

AC	Alternating Current
DC	Direct Current
DFIG	Doubly-Fed Induction Generator
DFIM	Doubly-Fed Induction Machine
DPC	Direct Power Control
FLC	Fuzzy Logic Controller
FOC	Field Oriented Control
GB	Gearbox
GSC	Grid-Side Converter
IG	Induction Generator
IGBT	Insulated Gate Bipolar Transistor
MPPT	Maximum Power Point Tracking
PI	Proportional-Integral
PWM	Pulse Width Modulation
PMSG	Permanent Magnet Synchronous Generator
RSC	Rotor Side Converter
SCIG	Squirrel Cage Induction Generators
SMC	Sliding Mode Controller
STSMC	Super Twisted Sliding Mode Control
TSR	Tip Speed Ratio
VSC	Voltage Source Converter
WT	Wind Turbine
WECS	Wind Energy Conversion Systems

LIST OF SYMBOLS

β	Blade pitch angle
ρ	Density of the air
λ	Tip speed ratio
Ω_{t-}	Velocity of the turbine on low speed shaft
Ω_m	Velocity of the turbine on high speed shaft
ω_g	Generator rotational speed
ω_t	Rotor angular speed
ω_{ls}	Angular speed of the low speed shaft
ω_s	Frequency of stator voltages and currents
ω_r	Frequency of rotor voltages and currents
ω_m	Electric speed of rotor
ω_{sl}	Angular slip frequency
θ_t	Rotor angular displacement
A_1	Surface Area
Cp	Power coefficient
D	Damping coefficient of turbine
dq	Two phase rotating reference frame
J	Wind turbine inertia
J_g	Generator inertia.
Jr	Rotor moment of inertia
I	Current
K_{ls}	Stiffness of low speed shaft
L_{eq}	Equivalent inductance of the RSC
L_s	Stator inductances
L_m	Magnetizing inductance
$L_{\sigma s}$	Stator leakage inductance
$L_{\sigma r}$	Rotor leakage inductance
L_r	Rotor inductances
N	Gear ratio
P	Number of pole pairs of the generator

P_r	Rotor power
P_s	Stator power
P_g	Power delivered to grid
P_m	Mechanical power
R	Radius of the wind turbine rotor or length of the blades
S	Slip
Ta	Applied torque on the rotor
Tc	Transformation matrix of Clarke transformation
T_{em}	Generator electromagnetic torque
T_{ls}	Low-speed shaft torque
T_{hs}	High-speed shaft torque.
T_t	Torque of the turbine on Low speed shaft
Tm	Torque of the turbine on high speed shaft
V	Voltage
$V_{wa}(t)$	Average value of the wind speed
$V_{wr}(t)$	Ramp wind component
$V_{wg}(t)$	Gust wind component
$V_{wt}(t)$	Turbulence component
V_w	Wind speed
$\vec{V}_{ss}$	Stator voltage space vector
$\vec{\imath}_{ss}$	Stator current space vector
R_s	Stator resistance
$\vec{\Psi}_{ss}$	Stator flux space vector
$\vec{V}_{rr}$	Rotor voltage space vector
$\vec{\imath}_{rr}$	Rotor current space vector
R_r	Rotor resistance
$\vec{\Psi}_{rr}$	Rotor flux space vector
L_f	Inductance of grid side filter
R_f	Resistive part of grid side filter
σ	Leakage coefficient of the generator

ABSTRACT

Wind energy has emerged as one of the sustainable power sources in recent years. One of the major challenges in wind energy is to extract maximum power from the generation of wind farms as wind power generation strongly depends on wind speed variation. The purpose of this thesis is to get the best control mechanism for maximum power extraction in Doubly Fed Induction Generator (DFIG) based wind turbine. The proposed techniques allow the generator to track the optimal operation points under a variable-speed wind energy conversion system. The proposed system contains the model of DFIG, wind turbines, generator side convertor, grid side convertor, and model of the controller. Then establish simulation model for DFIG-based wind turbine with controlling techniques based on MATLAB/Simulink platform with Proportional-Integral Controller (PI), Fuzzy Logic Controller (FLC), and Super Twisted sliding Mode Controller (STSMC). The most extensively used and applicable controller in the wind sector is the conventional PI controller, which requires modification for every change in reference pattern and also has a high overshoot and a prolonged settling time. Hence, to ensure robustness against external disturbances, FLC and SMC are applied to the converters, but the conventional SMC has a chattering problem. To improve this phenomenon, the STSMC technique is implemented on this thesis. The result shows an improved performance in terms of settling time, overshoot and rise time for active power. The response shows that the PI has a settling time of 1.0351 sec and an overshoot of 3.9 %. Whereas FLC has a settling time of 0.8021 sec and an overshoot of 2.8 %. The last STSMC has a settling time of 0.3314 sec and an overshoot of 2.2 %. This leads to the conclusion that the STSMC controller has better-controlling performance.

Keywords: *DFIG, FLC, MATLAB /Simulink, PI, SMC, and STSMC.*

CHAPTER ONE

1.INTRODUCTION

1.1. Background of the Study

To achieve the greenhouse gas reductions needed to sustain a livable climate, we must scale up renewable energy capacity at a rapid pace. In comparison to fossil fuel plants, wind and solar energy facilities produce no air pollution and have little impact on the environment. Since it emits no greenhouse gases or hazardous pollution, generating electricity from the wind is one of the greenest and most sustainable methods available. In addition to being abundant, endless, and inexpensive, the wind can replace fossil fuels on a large scale (Qiao, 2009).

The wind is clean, free, indigenous, and inexhaustible. Wind turbines do not need any type of fuel, so there are no environmental risks or degradation from the exploration, extraction, transport, shipment, processing, or disposal of fuel. Not only is generation produced with zero emissions of carbon dioxide (during the operational phase) but it also does not release toxic pollutants (for example mercury) or conventional air pollutants (for example smog-forming nitrogen dioxide and acid rain-forming Sulphur dioxide). Furthermore, the adverse impacts caused by mountaintop mining and strip mining of coal, including acid mine drainage and land subsidence are avoided, and the negative effects of nuclear power, including radioactive waste disposal, security risks, and nuclear proliferation risks, are not created. Finally, wind power can have a long-term positive impact on biodiversity by reducing the threat of climate change – the greatest threat to biodiversity (European Wind Energy Association, 2012)

Winds are created by differences in atmospheric pressure. The sun warms the water and land at the equator more than it does the rest of the world. Warm air from the equator rises higher in the atmosphere and migrates to the poles. This is a system with low pressure. At the same time, cooler, denser air replaces the warm air as it flows across the earth's surface toward the equator. This is a system with a lot of pressure. High-pressure areas to low-pressure zones are where the winds usually blow. The Earth contains five major wind zones: polar easterlies, westerlies, horse latitudes, trade winds, and doldrums (Ackermann & Söder, 2002).

From the point of view of wind energy, the most striking characteristic of wind resources is their variability. The wind is highly variable, both geographically and temporally. Furthermore, this variability persists over a very wide range of scales, both in space and time (Burton et al., 2011). The primary output of a conversion wind system is wind speed, often known as wind velocity. The metrological circumstances determine it. It is frequently measured in m/s or km/h using an anemometer or a meteorological station. These wind conditions have an impact on the system's mathematical model and necessitate the use of an appropriate model estimating technique (Haile et al., 2021).

Systems that convert wind energy into mechanical power are called wind energy conversion systems (WECS). Wind turbine generators transform this mechanical energy into electricity, which is then employed in windmills to power machines or perform tasks like pumping water or grinding grain. Most likely, the first wind-powered devices were vertical-axis grain-grinding windmills in Persia around 200 BC (Tamaarat, 2019a).

WECS operates at a variable speed and consists of a wind turbine, a generator, a DC bus, a static power converter, and a three-phase current filter. One of the most attractive technologies for wind farms is the DFIG. The advantage of DFIG is that active and reactive power can be controlled separately, and it is more grid compatible than other designs. And also this generator allows the production of electricity has variable speed, this allows them to better exploit the wind resources for different wind velocities (Tapia et al., 2003). In DFIG, the rotor is connected to two bidirectional static converters cascaded through a DC bus, while the stator is connected directly to the grid. The electronic power converter between the rotor circuit of the DFIG and the grid effectively decouples the grid frequency from the rotor frequency (Sellami, n.d.). The control system of DFIG consists of two control subsystems: the control system of the power converter connected to the rotor side (RSC) and the control system of the power converter connected to the electric grid side (GSC) (Tamaarat, 2019a). The three-phase rectifier (RSC) control system controls the rotor current to control the active and reactive power injected into the grid, and three-phase inverter (GSC) control system controls the DC-link voltage(Berhanu et al., 2018). Various types of controllers were used to this control.

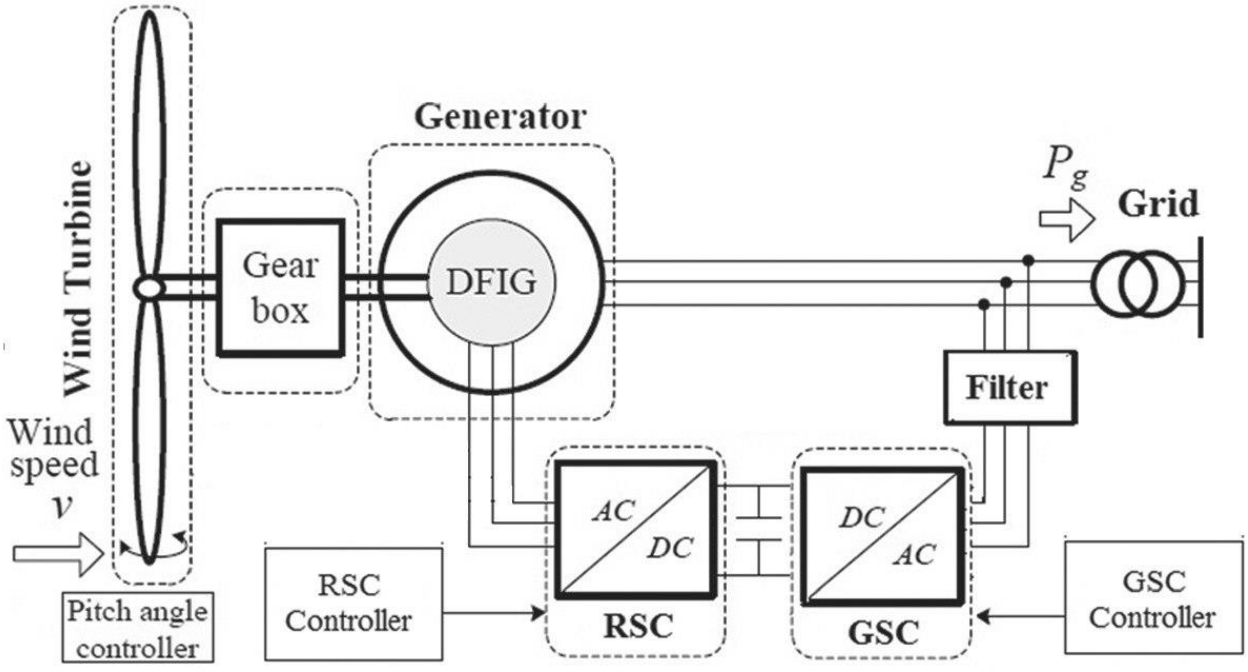

Figure 1.1: DFIG in WECS (Thomas, 2020)

For reasons of simplicity, applicability, moderate cost, and adequacy of linear systems, the classical control techniques using the simplest regulator. One of the classical controllers is the PI, although widely used in many control applications, requires adjustment for every change in reference patterns. This controller's sensitivity to outside disturbances and parameter changes is another major drawback. This type of conventional controller fails to provide quality power generation due to the uncertainty in wind speed variations (Boubzizi et al., 2018).

However, the intelligent control system's FLC is independent of the system's mathematical model. and widely used to solve problems under uncertainty and with high nonlinearities conditions. It provides an algorithm that transforms expert knowledge into an automatic control strategy and can handle approximative data systematically. Therefore, it is appropriate for controlling nonlinear systems and modeling complex systems where an inexact model exists (Tamaarat, 2019a).

The other controller used in this thesis is the sliding mode controller (SMC). It is a nonlinear controller to bring back the state trajectory of a system towards the sliding surface and advance on it with a specific dynamic point balance. This technique has several advantages: high precision, stability, simplicity, a fast response, and especially robustness (Sellami, n.d.). Chattering phenomena is the main drawback caused by high frequency switching near the sliding surface by discontinuous control law in SMC design. This phenomenon has an impact on the system's performance by reducing control accuracy, high wear on moving mechanical parts, and significant high heat losses in the power circuit. So, to reduce the chattering effect, different alternatives are available like composite controllers, different reaching methods, and high order sliding mode controllers (Cherifi & Miloud, 2020).

While studying the performance analysis of DFIG-based wind turbine systems, the main task will be to select the best controller with the best controller technique. By addressing the above concerns, this thesis will conduct a thorough examination of the DFIG-based wind system, particularly in controlling active and reactive powers, by comparing different controllers and recommending the best controller to create a stable system and improve machine performance.

1.2. Statement of the Problem

Wind energy is one of the most important renewable energy sources because it reduces environmental pollution. The main problem in wind energy systems is the fluctuating nature of wind speed can cause instability in voltage and frequency of the system in the grid-connected generator. When the voltage at the grid system is higher than the rated value, the grid provides reactive power to the generator, or when the voltage is lower than the rated value, reactive power is delivered to the grid. This reactive power flow cause instability in the power system. When a wind turbine is designed with an effective control system, the power extracted from wind energy is increased and improved. The control system proposed in this thesis is the vector control scheme used to control the active and reactive power using different controllers. The most extensively used and applicable controller in the wind sector is the conventional PI controller, which requires modification for every change in reference pattern and also has a high overshoot and a long settling time.

Hence, to ensure the robustness against external disturbances, FLC and SMC are applied to the converters, but the conventional SMC has a chattering problem. There are a various techniques available to deal with this problem. To improve this phenomenon, the Super Twisted Sliding Mode Controller (STSMC) technique is implemented.

1.3. Objective of the Study

1.3.1. General Objective

The main objective of the study is to compare controlling techniques for active and reactive power in wind energy conversion systems.

1.3.2. Specific Objective

- To model a DFIG-based wind turbine using MATLAB/Simulink software.
- To model and control the rotor and grid side bidirectional converters using PI, FLC, and STSMC for active and reactive power control.
- To conduct a comparative study between the controllers.

1.4. Scope of the Study

The thesis focused on the model, analysis, and control of DFIG used in the WECS using MATLAB/Simulink 2019a, comparing and contrasting different controller results and selecting the best controller for active and reactive power.

1.5. Motivation of the Study

Wind energy has been a rapidly developing energy supply in recent years, and most WECS now uses a DFIG-based wind energy system. DFIG plays a major role in operating in grid system. It has attracted more attention to its variable speed, reduced converter cost, less switching losses, higher energy efficiency, and improved power quality. However, this generator is subjected to several limitations, including the nonlinear features of the wind and the effect of other parametric variables. This causes the system to differ from its normal operating point. Controlling active power and reducing reactive power transmitted to the grid are two ways to achieve maximum output power generation while maintaining a unity power factor. To keep the system stable, we must control both active and reactive power, which necessitates the development of appropriate wind energy models and control mechanisms.

1.6. Significance of the Study

The main advantages of this proposed work are:

- ▶ It introduces how to improve output power from WECS by using STSMC.
- ▶ It contributes to a better understanding of the variable speed wind turbine operation, generator, and converters and their modeling as well as control concepts

- It helps in reducing a large percentage of power loss in wind energy.
- It helps to reduce the lack of sustainable energy supply and demand.

Therefore, controlling the rotor and grid side converter in WECS using STSMC is significant for supplying optimized power because there is a continuous growth of electricity demand.

1.7. Thesis Organization

This thesis work is organized into five chapters.

Chapter One: Includes introduction, statement of problem, objectives, scope, limitation, motivation, and significance of the research.

Chapter Two: Includes the literature review on the system components and different control mechanisms briefly and some related works with the title.

Chapter Three: Discussed the general methods used to accomplish the objectives of the study and the modeling of the whole WECS is aerodynamic, DFIG, and power converter modeling with a selection of appropriate control techniques and suitable controllers.

Chapter Four: The results of the controllers are discussed, and a comparison between controllers depending on the results.

Chapter Five: Presents conclusions of the whole work and recommendations for future work.

CHAPTER TWO

2.LITERATURE REVIEW

2.1. Theoretical Background

2.1.1. Wind Energy Conversion Systems (WECS) and its Components

The basic configuration of a DFIG in WECS is shown in the Figure 2.1. A mechanical shaft system consisting of a low-speed shaft, a high-speed shaft, and a gearbox in the middle connects the wind turbine to the DFIG. The stator of the DFIG is directly linked to the grid, while the rotor is connected through a back-to-back converter, which only has to handle a small portion of the total power (25–30%) to obtain full control of the generator. The power flow between the rotor circuit and the utility grid must be controlled in magnitude and direction to generate electrical power at constant voltage and frequency to the utility grid over the large operating range from sub-synchronous to super-synchronous speeds. Therefore, the back-to-back converter consists of two four-quadrant IGBT PWM converters, namely RSC and GSC, connected by a dc-link capacitor. The crow-bar circuit is used to prevent the RSC from over-current in the rotor circuit during transient disturbances (Faculty et al., 2008).

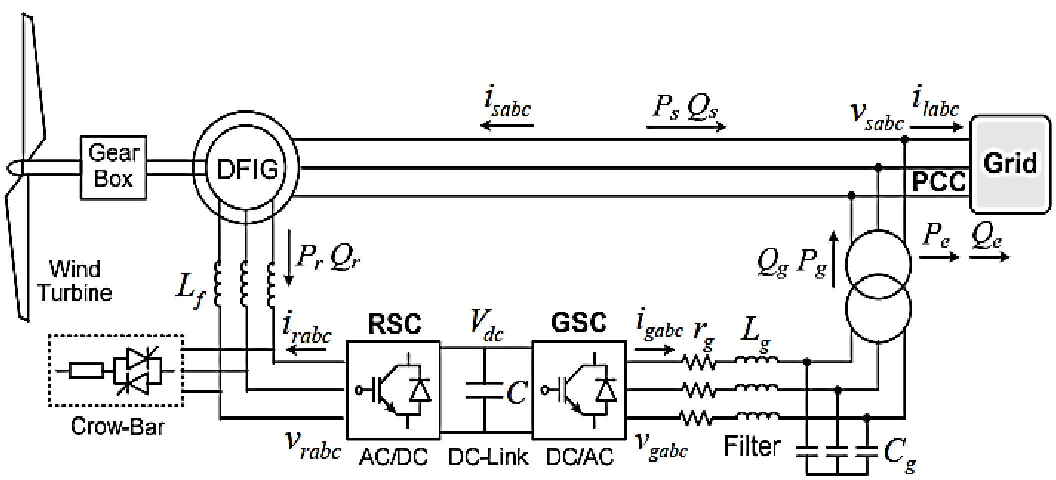

Figure 2.1: Configuration of WECS with a DFIG (Faculty et al., 2008)

2.1.1.1. Wind Turbine

The translation of air kinetic energy into spinning mechanical power of the turbine rotor blades is the principle of wind turbines in power generation. The most prevalent wind turbine now is the horizontal-axis propeller with two or three blades positioned on a tower's top. The number of blades on a wind turbine is a difficult design decision. Three-blade systems are more expensive than two-blade systems yet two-blade wind generators have to operate at higher rotational speeds than three-blade ones.

Betz's law says that only 59% of the kinetic energy is converted to mechanical energy using a wind turbine. German physicist Albert Betz first proposed Betz's law in 1919 (Sumathi et al., 2015).

Wind turbine classification

Wind turbines can be classified according to the turbine generator configuration, airflow path relatively to the turbine rotor, turbine capacity, the generator-driving pattern, and, the power supply mode.

1. **Horizontal-axis and vertical-axis wind turbines**

The rotors in the earliest wind turbine design have a vertical axis of rotation. But initially, only pure drag-type vertical-axis rotors could be constructed. Well-known examples of rotors having a vertical axis of rotation are the "Savonius rotor," which is used as a ventilator on railroad carriages or delivery vans, and the cup anemometer used to measure wind velocity (Hau, 2005).

It was only recently that engineers succeeded in developing vertical-axis designs which could also efficiently use aerodynamic lift. The design proposed in 1925 by the French engineer Darrieus, in particular, has been considered a promising concept for modern wind turbines. In the “Darrieus rotor”, the blades are shaped and rotate in the pattern of a surface line on a geometric solid of revolution, a troposkien (i. e. “turning rope” in Greek), with a vertical axis of rotation. This makes the geometric shape of the rotor blades complicated and thus difficult to manufacture. Darrieus rotors are often constructed with two or three rotor blades, as is the case with horizontal-axis rotors. A variation of the Darrieus rotor is the so-called H-rotor. Straight blades attached to the rotor shaft by struts are utilized in place of curved rotor blades (Hau, 2005).

The specific advantages of vertical axis turbine concepts are that their simple design includes the possibility of housing mechanical and electrical components, gearbox, and generator at ground level and that there is no yaw system. This is offset by drawbacks like its poor tip-speed ratio, inability to self-start, and inability to adjust speed or power output by pitching the rotor blades (Rekioua, 2014).

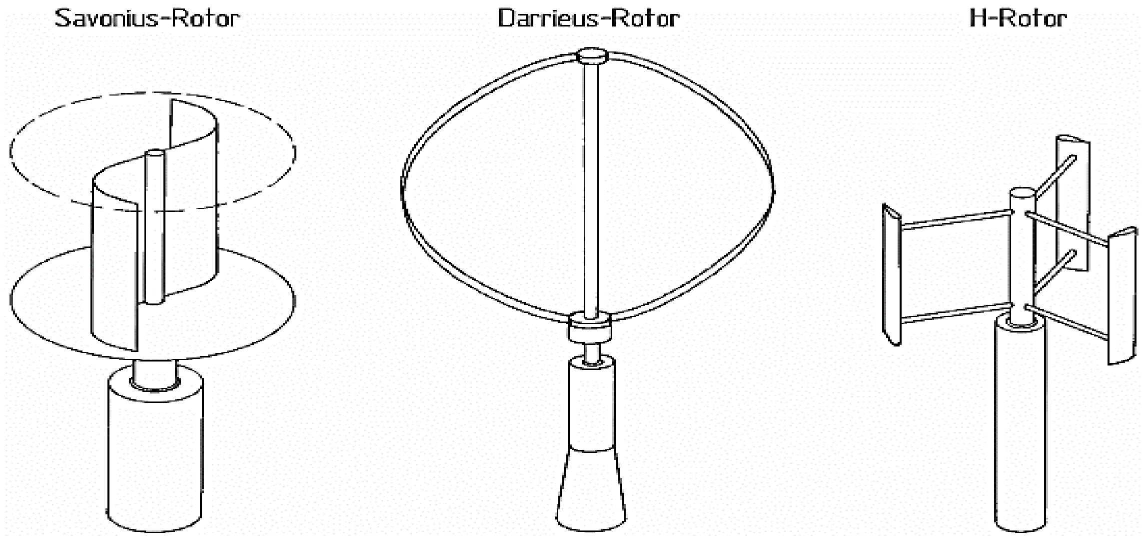

Figure 2.2: Rotor turbine Concepts with a Vertical Axis (Hau, 2005)

Wind energy converters that have their axis of rotation in a horizontal position are realized almost exclusively based on "propeller-like" concepts in Figure 2.3. This design, which includes European windmills as much as the American wind turbine or modern wind turbines, is the dominant design principle in wind energy technology today. The undisputed superiority of this design to date is largely based on the following characteristics (Hau, 2005):

- Pitching the rotor blades along their longitudinal axis allows for control of rotor speed and power production in propeller designs (blade pitch control). The best defense against Overspeed and extremely high wind speeds, particularly in large wind turbines, is rotor blade pitching.
- The rotor blade form can be aerodynamically tuned, and it has been demonstrated that it will operate most effectively when the aerodynamic lift is utilized to the fullest extent possible.
- Not least, the technological lead in the development of propeller design is a decisive factor

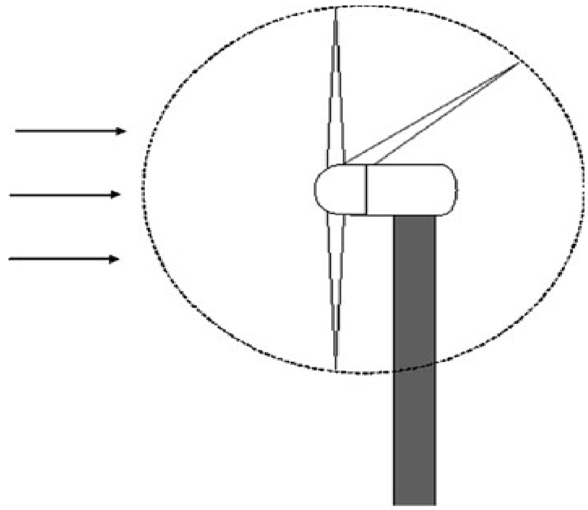

Figure 2.3: Horizontal-Axis Wind Turbine (Rekioua, 2014)

2. Wind Turbine Capacity

Based on their rated capabilities, wind turbines can be grouped into the following basic categories: micro, small, medium, large, and ultra-large wind turbines. Even though there isn't a precise definition of what constitutes a micro wind turbine, it is generally agreed that any turbine with a rated power of under a few kilowatts falls into this category. Micro wind turbines are particularly useful in areas without access to the electricity grid. The most common wind turbines have medium sizes with power ratings from 100 kW to 1 MW. Large wind turbines are those that produce up to10 MW of power. Wind turbines having a capacity of more than 10 MW are referred to as ultra-large wind turbines. The study and development of this kind of wind turbine are still in their infancy (Christensen, 2009).

3. Direct Drive and Geared Drive Wind Turbines

According to the drivetrain condition in a wind generator system, wind turbines can be classified as either direct drive or geared drive groups. A conventional geared drive wind turbine employs a multi-stage gearbox to convert the low-speed shaft of the blade rotor's rotational speed into a fast rotation on the high-speed shaft of the generator rotor to raise the generator rotor's rotating speed and increase power output. The advantages of geared generator systems include lower cost and smaller size and weight. However, the use of a gearbox can dramatically reduce the reliability of wind turbines and raise mechanical losses and noise levels. The generator shaft is directly connected to the blade rotor in a generator system by removing the multi-stage gearbox. The direct-drive system is therefore preferable in terms of the energy economy, dependability, and ease of design (Christensen, 2009).

4. On-Grid and off-Grid Wind Turbines

Wind turbines can be used for either on-grid or off-grid applications. Most medium-sized and almost all large-size wind turbines are used in grid-tied applications. One of the obvious advantages of on-grid wind turbine systems is that there is no energy storage problem. In the contrast, most small wind turbines are off-grid for residential homes, farms, telecommunications, and other applications. Wind power generated by off-grid wind turbines, on the other hand, can shift substantially over a short time with little notice because it is an intermittent source of energy. To increase the reliability of the wind power supply, off-grid wind turbines are typically utilized in conjunction with batteries, diesel engines, and photovoltaic systems (Christensen, 2009).

5. Fixed- and Variable-Speed Turbines

wind turbine systems rotate at almost a constant speed, which is determined by the gear ratio, the grid frequency, and the number of poles of the generator. The maximum conversion efficiency can be achieved only at a given wind speed, and the system efficiency degrades at other wind speeds. The turbine is shielded from potential harm brought on by strong wind gusts by aerodynamic control of the blades. The fixed-speed turbine disrupts the power system by producing output power that is excessively unpredictable for the grid. To withstand severe mechanical loads, this sort of turbine also needs a strong mechanical design (Luis & Moncayo, n.d.).

Variable-speed wind turbines, on the other hand, can maximize energy conversion efficiency over a broad range of wind speeds. The utility grid is not immediately connected to it. Instead, a power electronic interface is placed between the generator and the grid to provide decoupling and control of the system (J.~Marques et al., 2003)(Becheri et al., 2018). According to the wind speed, the turbine's rotational speed can be continually adjusted. By doing this, the tip speed ratio, which measures the relationship between the speed of the blade tip and the wind speed, may be maintained at an ideal level to maximize power conversion efficiency at various wind speeds (Luis & Moncayo, n.d.).

Type 1

It is a fixed-speed wind turbine that operates with less than 1% variation in rotor speed with a squirrel cage induction generator. The aerodynamic active power can be controlled using passive or active stall control, and the reactive power can be controlled by using capacitor banks or additional active power electronics (Singh & Santoso, 2012).

Type 2

Such type of wind turbine is the fixed speed with a wound rotor induction generator. It has a limited operating range the aerodynamic power is controlled using pitch control, and the reactive power can be controlled using capacitor backs or additional active power electronics (Singh & Santoso, 2012).

Type 3

It is a variable speed type wind turbine with a wound rotor induction generator, and power converters rated 30% of nominal rated power. It has a wide speed operating range and can control active and reactive power independently. Pitch control is used for controlling the aerodynamic power (Singh & Santoso, 2012).

Type 4

It is a variable speed type wind turbine with fully rated power converters that are directly coupled generator's stator. The generators can be permanent magnet synchronous generators, wound rotor synchronous generators, or squirrel cage induction generators (Singh & Santoso, 2012).

2.1.1.2. Gearbox

A big three-bladed wind turbine's rotor typically spins between 6 and 20 revolutions per minute (rpm). Compared to a typical 4- or 6-pole wind generator, which has a rated speed of 1500 or 1000 rpm for a 50 Hz stator frequency and 1800 or 1200 rpm for a 60 Hz stator frequency, this is substantially slower. As a result, a gearbox is required to convert the turbine rotor's low speed to the generator's high speed (Luis & Moncayo, n.d.).

2.1.1.3. Wind Turbine Generators

Over four decades, the advancement of wind generation conversion engineering has generated the development of several different adjustments to wind generators, which employ a wide selection of electric turbines. The group of most popular electric source types utilized in megawatt variety WECS is presented in the Figure below (Sumathi et al., 2015).

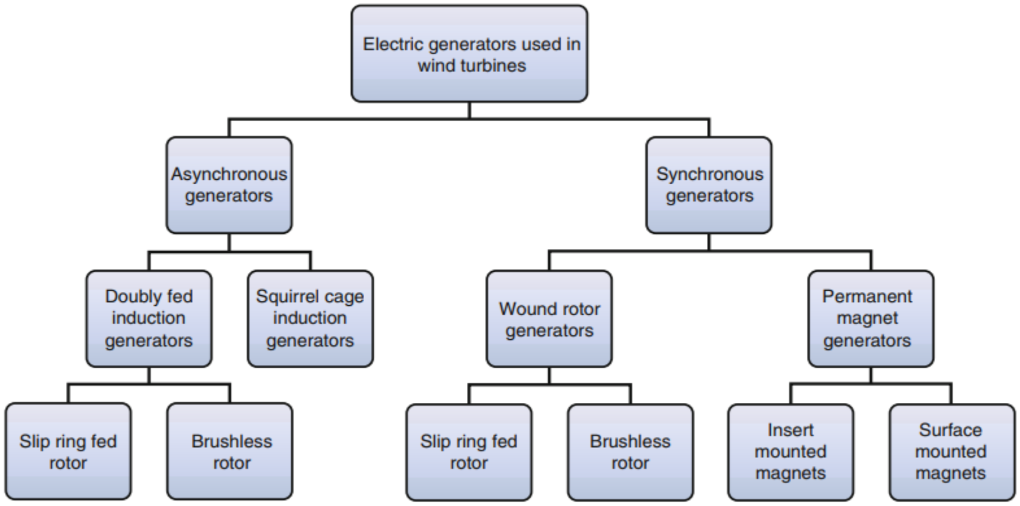

Figure 2.4: Types of Generators in WECS (Sumathi et al., 2015)

Doubly Fed Induction Generator (DFIG)

The DFIG is currently the system of choice for multi-MW wind turbines. To obtain the best aerodynamic efficiency, the aerodynamic system needs to be able to track the ideal tip-speed ratio while working at a variable rotating speed. As a result, the DFIG system can operate in both sub-synchronous and super-synchronous modes at rotor speeds that are close to synchronous. While the rotor winding is connected to a three-phase converter via slip rings, the stator circuit is directly connected to the grid. The DFIG delivers adequate performance and is sufficient for the speed range needed to harness typical wind resources for variable-speed systems where the speed range needs are small, for example, ±30% of synchronous speed (Fletcher & Yang, n.d.).

The capacity to produce output greater than their rated power without overheating could be the benefit of using doubly-fed induction generators (DFIG). Other advantages of the generator are the power converter rating is 33% of the total power so that the cost of the converter is reduced and Reduced losses in the converter (Hussein et al., 2004).

2.1.1.4. Back-to-Back PWM Converters

Converter can typically output zero volts or Vdc, where Vdc is the voltage of the dc link. Figure 2.5 depicts two of these converters coupled in a back-to-back configuration with a DC link. IGBTs are probably used as the switching components in higher power converters. With the restriction that the peak line voltage is smaller than the DC link voltage, the six-switch converter can provide a three-phase output voltage of any magnitude, frequency, and phase.

The converter can change the output voltage almost instantly, the limit is related to the switching frequency of the pulse-width modulated switching devices, and delays introduced by any filtering on the output (typical on the grid-side converter). The converter switches are switched ON and OFF with a fixed frequency but with a pulse width that is varied to control the output voltage (Fletcher & Yang, n.d.).

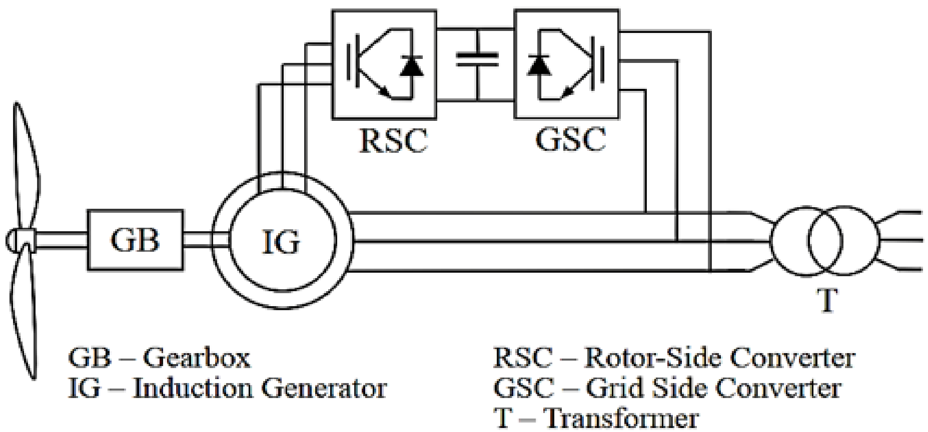

Figure 2.5: Typical Back-to-Back Arrangement of Inverter and Converter Circuits (Fletcher & Yang, n.d.)

A more highly advanced method of applying back-to-back converters has also been developed. One option is to employ vector control on the supply-side ripper tools, with a frame of reference orientated with the actual d-axis along the stator voltage vector. The grid-side converter is controlled to maintain the DC-link electric potential constant through regulation of the d-axis current. It can be responsible for reactive power control using the alteration of the actual q-axis stream. For the rotor side, choosing decoupled control in the electrical torque in addition to the rotor excitation current is displayed. Conversely, inwards the rotor coil current was decomposed into d–q components in which the d-axis current is used to manage the electromagnetic torque, and the q-axis current controls the power factor (Sumathi et al., 2015).

The Rotor-Side Converter (RSC)

The RSC applies the voltage to the rotor windings of the doubly-fed induction generator. The RSC's function is to regulate the rotor currents in such a way that the rotor flux position is ideally orientated with the stator flux, resulting in the development of the desired torque at the machine's shaft. The reactive power (voltage) measured at the machine stator terminals is regulated by the RSC using a torque controller. To track the maximum PowerPoint, the power is adjusted to adhere to a previously established turbine power-speed characteristic. The reference power derived from the wind turbine characteristic is compared with the actual electrical output power from the generator terminals, added to the overall power losses (mechanical and electrical) (Fletcher & Yang, n.d.).

The Grid-Side Converter (GSC)

The GSC's goal is to maintain a constant voltage for the dc bus capacitor. Moreover, it is allowed to generate or absorb reactive power for voltage support requirements. The function is realized with two control loops as well: an outer regulation loop consisting of a dc voltage regulator (Luis & Moncayo, n.d.).

2.1.2. Control Strategies for a Wind Turbine Generator System (WTGS)

Some of the control techniques for a wind turbine generator system are Pitch angle control, MPPT control, and DFIG control.

I. Pitch Angle Control

Mechanical output power regulation is accomplished through pitch angle control. The wind turbine's output torque is utilized to regulate the angular speed, which regulates the mechanical output power. Pitch angles are incorporated into the high-rated generator turbines to shield the wind generator from a sudden wind gust. Lower wind speeds require adjusting the blade pitch so that the rotor rotates at a faster rate, hence boosting the machine's power. The pitch angle controller limits the rotor speed when the wind speed is higher, protecting the generator. If the controller is unable to limit the rotor speed below the ideal speed, the generator is protected. It serves as a braking mechanism. By changing the wind turbine's pitch angle, the aerodynamic power it generates can be managed (Tiwari & Babu, 2016).

II. Maximum Power Point Tracking (MPPT) Control

Some regulator schemes have been offered to achieve MPPT control. The control of MPPT can be classified into two categories. There are two types of control schemes: conventional and intelligent. The conventional control schemes can also be divided into current mode control and speed mode control, which depend on the setting of reference values. For current-mode control, the reference values are the active power and electromagnetic torque, and for speed mode control, the rotating speed. The FLC and the hill-climbing control are typically applied to the MPPT control by intelligent control techniques. However, this control method is usually slow because the step disturbance is fixed. Therefore, a perturbation was proposed to mitigate the drawback (Senapati, 2014).

III. DFIG Control

Many other DFIG control systems exist, including Field-Oriented Control (FOC) or vector control, direct torque or power control, predictive control, sensor-less control, and nonlinear control.

- Field Oriented Control (FOC) or vector control

  It is the most widely used control approach in wind power systems with DFIG. Among its many advantages, it primarily provides independent control of active and reactive power and the ability to control motor speed more efficiently with a low-cost system to construct (Senapati, 2014).

- Direct torque/power control

  Direct torque mechanisms do not require current controllers, coordinate conversions, specific variations, and current control loops. Thus, direct torque control can directly control the rotor flux linkage magnitude and generator torque by carefully selecting the inverter switching states (Senapati, 2014).

2.1.3. Controllers

2.1.3.1. Proportional Integral (PI) Controller

A PI controller is a type of controller that combines proportional and integral control actions. It is a feedback control loop that figures out the error signal by using the difference between the system output and the set point.

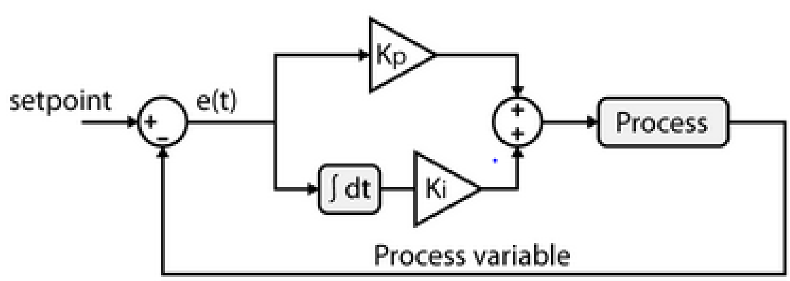

Figure 2.6: Block Diagram of PI Controller (O'Dwyer, 2006)

The controller can play a greater role in attenuating the signal to the required level while reducing error and optimizing the process output.

2.1.3.2. Fuzzy Logic Controller (FLC)

Fuzzy control is an intelligent control system that combines fuzzy sets, fuzzy language variables, and knowledge of fuzzy logical inference to control complex systems based on analogous human fuzzy thinking. The benefits of fuzzy control include high performance and robustness. This control approach is used to control uncertain systems without computing a mathematical model. Fuzzy logic is conceptually easy to understand, flexible, tolerant of imprecise data, and based on natural language. Can also model nonlinear functions of any complexity, combining standard control methods with the insight of experts (Sumathi et al., 2015).

The structure of FLC consists of four blocks (Sumathi et al., 2015):

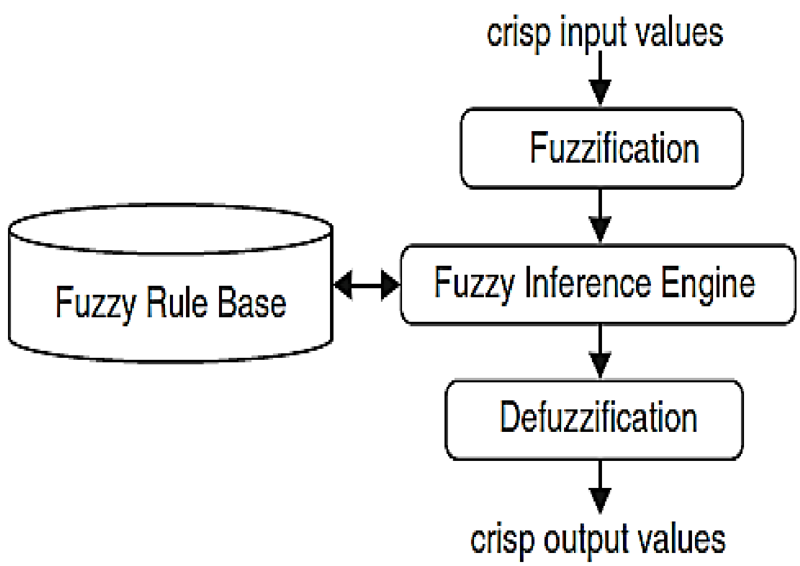

Figure 2.7: Structure of FLC (Sumathi et al., 2015)

- Fuzzification is a process of converting inputs, such as crisp numbers, into fuzzy sets that the inference mechanism can easily understand and use to activate rules.
- A fuzzy inference engine refers to the fuzzy rule base containing fuzzy IF-THEN rules to derive the linguistic values for the intermediate and output linguistic variables.
- Defuzzification is a process of converting the fuzzy sets obtained by the inference engine into a crisp value.

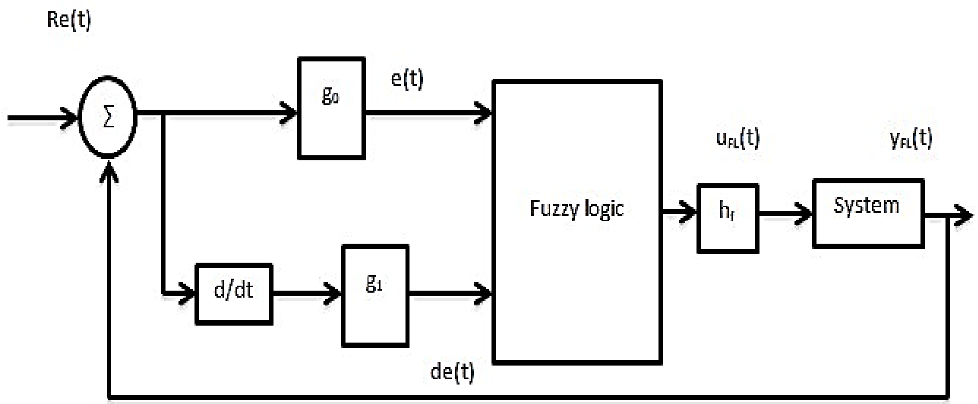

Figure 2.8: Block Diagram of FLC (Alta, n.d.)

2.1.3.3. Sliding Mode Controller (SMC)

A Sliding Mode Controller (SMC) is a particular type of variable structure control system designed as a robust control to drive and constrain the system to lie within the switching function. It is a non-linear type of controller which is unaffected by internal parameter variations and external disturbances compared to other linear and non-linear controllers. By introducing a discontinuous control signal across the sliding surface that meets the sliding requirement, it achieves robust control. Also, it could achieve active and reactive power tracking and improve the dynamic. Therefore it is highly appreciated in the control of the wind system (Khalfallah et al., 2015).

Although it has its drawback, namely the chattering phenomena caused by high frequency switching near the system's sliding surface caused by the discontinuous control rule used in SMC design. There are several ways to remove this problem, including sliding surface design modification, composite controllers, different reaching methods, and high order sliding mode controllers (Zouggar et al., 2019).

The design of the control can be obtained in three important steps, and each step is dependent on another one (Rekioua, 2014):

- The choice of sliding surface
- Setting of the convergence conditions
- Determination of the control law

2.2. Review of Related Works

DFIG-based wind turbine control systems have drawn a lot of attention recently. Various researchers have been engaged in DFIG modeling, designing, and controlling activities. The following are literature reviews related to DFIG-based wind turbine control systems.

The authors in (Hamane & Member, n.d.), have proposed a power control study of a WECS based on a DFIG connected to the electric power grid by a direct power control system. . Direct torque control of a DFIG control system led to the development of the direct power control principle. This control approach was created as a result of the torque and flux relationship. The main advantages of the Direct power control (DPC) approach are high performance, robustness, and low sensitivity to the system parameter variations. But, this approach has a high ripple in produced torque or power and a non-constant switching frequency. It is demonstrated that the power slope that depends on shaft speed has a significant impact on the switching frequency of the rotor side converter. The variable switching frequency decreases the stator side AC filter's efficiency due to an increase in size and power loss.

The authors in (Senani & Rah, n.d.) study the control of active and reactive power of DFIG typically used in electrical energy production, particularly in wind turbines. The modeling and simulation were done using MATLAB-Simulink software using direct power control with a PI controller. According to the simulation results, the controllers provide good responses for the active or reactive power dynamic tracking. However, compared to recent controllers, the PI controller has a lower level of stability and a higher initial overshoot.

A wind turbine that worked in variable wind speed situations with DFIG was described in (Tamaarat, 2019b) as part of a system that also comprised a stator that was directly connected to the grid and a power converter that supplied the electricity on the rotor side. In this research, the active and reactive power flow between the stator of the DFIG and the grid is individually managed to utilize control techniques using standard PI, fuzzy logic, and fuzzy self-tuning PI controllers. To obtain active and reactive power at the specified reference levels, the postulated controllers produce the reference rotor voltages needed. Simulated data under random wind fluctuations were used to compare these three controllers. The result suggests that when compared to the PI controller, the proposed fuzzy logic-based intelligent controllers exhibit greater robustness and have high control precision. However, these results demonstrate that it is not possible to precisely track the stator active and reactive power references with a traditional PI controller with fixed values of proportional and integral gains. With a fuzzy logic controller, the system has better performance, but this controller needs high expert knowledge to design it.

The authors in (Mazouz et al., 2018) analyzed Vector Control with SMC for DFIG of 5 KW. The simulation result was used to evaluate the efficiency and robustness of the suggested control strategy. The SMC approach is the best because it minimizes steady-state error, reduces high power ripple, and ensures that the performance is unaffected by changes in machine parameters. The problem with this controller is the existence of chattering, even though the authors didn't discuss it.

In (Djeriri & Massoum, n.d.), was presented a modeling and SMC of a DFIM integrated with a wind energy system for independent control of active and reactive power. In this paper comparative study was done between two controllers. The first controller is a proportional-integral (PI) controller, and the second is a sliding mode (SM) controller based on a field-oriented control (FOC) strategy using MATLAB / SIMULINK software. The optimized performances of the FOC method based on a sliding mode controller are shown by the simulation results. It has excellent response times and references tracking without overshoots through the response characteristics. The chattering effect, however, continues to be a significant issue with this method.

Related work listed above is summarized as follow:

Table 2.1: Summary of Related Works

Author	Control techniques / Controller	Findings	Gap
(Hamane & Member, n.d.)	Direct power control (DPC)	This approach has high performance, robustness, and low sensitivity to the system parameter variations.	It has a high ripple in produced torque or power and a non-constant switching frequency.
(Senani & Rah, n.d.)	PI controller	good responses for the active or reactive power dynamic tracking.	PI controller has a lower level of stability and a higher initial overshoot.

(Tamaarat, 2019b)	PI, fuzzy logic, and fuzzy self-tuning PI controllers	Fuzzy logic-based intelligent controllers exhibit greater robustness and have high control precision.	This controller needs high expert knowledge to design it.
(Mazouz et al., 2018)	Sliding Mode Control (SMC)	It minimizes steady-state error, reduces high power ripple, and ensures that the performance is unaffected by changes in machine parameters.	The problem with this controller is the existence of chattering, even though the authors didn't discuss it.
(Djeriri & Massoum, n.d.)	PI and SMC	SMC has excellent response times and references tracking without overshoots through the response characteristics.	The chattering effect.

CHAPTER THREE

3. METHODOLOGY

3.1. Introduction

This chapter mainly focuses on the methodology used to complete this thesis and a detailed analysis of the DFIG-based wind turbine system's modeling and control system, including the wind turbine's mathematical model, DFIG with both RSC and GSC, and vector control method. Finally, the Simulink model with an appropriate control system will be explained using MATLAB software.

3.2. Methodology of the System

To attain the above general and specific objectives of the study, the following methods and techniques are followed.

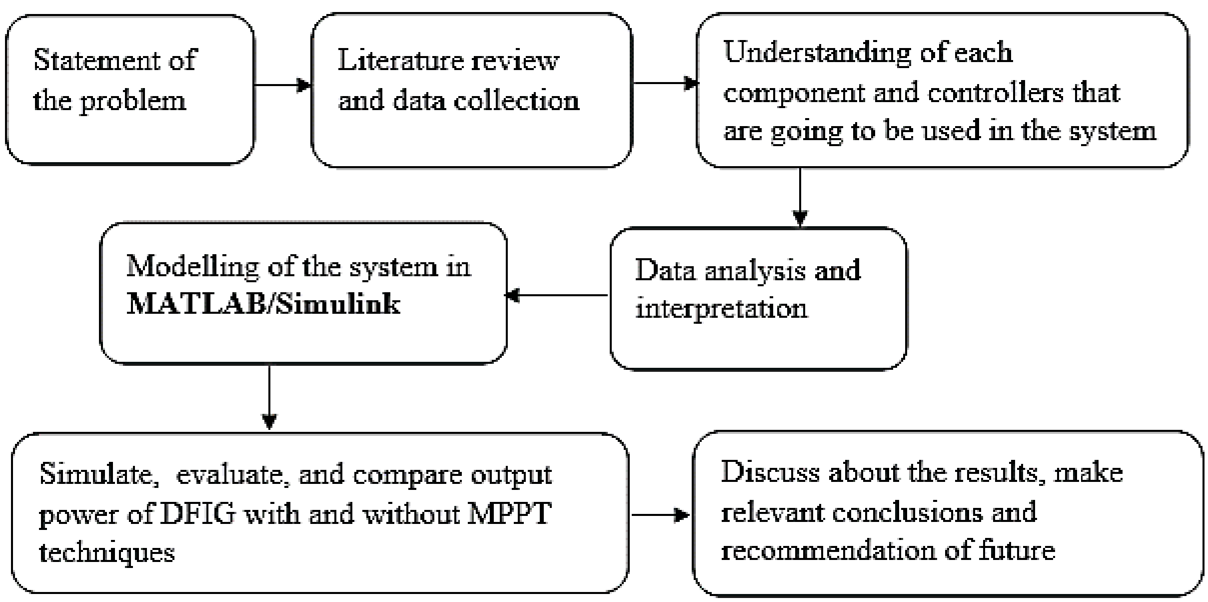

Figure 3.1: Block schematic of Proposed System Methodology

3.3. Wind Energy Conversion System Modeling

The aerogenerator, the power electronics, and the load make up the overall structure of a wind energy conversion system. The system's components are each individually modeled.

3.3.1. Wind Turbine Aerodynamic Modeling

Aerodynamic model, evaluates the turbine torque Tt as a function of wind speed Vv and the turbine angular speed Ωt. It represents the power extraction of the rotor, calculating the mechanical torque as a function of the air flow on the blades. The wind speed can be regarded as the instantaneous wind speed averaged over the area swept by the blades in order to assess the average torque in the low speed axles (Abad et al., 2011).

The power contained in the form of kinetic energy in the wind crossing at a speed V_w, surface A_1, is expressed by (Mabrouk & Boumediene, 2018):

$$P_w = \frac{1}{2}\rho A_1 V_w^3 \tag{3.1}$$

Turbine power is expressed by the maximum power coefficient, which is given by (Rajendran & Jena, 2014):

$$P_t = P_w C_p = \frac{1}{2}\rho\pi R^2 V_w^3 C_p \tag{3.2}$$

Where: ρ is density of the air, R is wind turbine's rotor radius or length of the blades, C_p is the power coefficient. The power coefficient, which is a dimensionless parameter, measures how well a wind turbine converts wind kinetic energy into mechanical energy (Abad et al., 2011)

C_p is the function of blade pitch angle (β) and tip speed ratio (λ). The tip speed ratio is defined as ratio between linear tip speed and wind speed (Rajendran & Jena, 2014):

$$\lambda = \frac{\mathrm{R\,\Omega t}}{\mathrm{Vw}} \tag{3.3}$$

Where: Ωt is the angular speed of the rotor.

The turbine's torque is defined in terms of angular speed of the rotor and the power received of the turbine by the following relation (Mabrouk & Boumediene, 2018):

$$T_t = \frac{P_t}{\Omega_t} = \frac{\frac{1}{2}\rho\pi R^2 V_w^3 C_p}{\Omega_t} = \frac{\rho\pi R^2 V_w^3}{2\Omega_t} C_p = \frac{\rho\pi R^3 V_w^2}{2\lambda} C_p = \frac{\rho\pi R^3 V_w^2}{\lambda} C_t \tag{3.4}$$

Where: Ct is the coefficient of torque. The coefficients of power and torque are related by the equation (Abad et al., 2011):

$$C_p(\lambda) = \lambda\, C_t(\lambda) \tag{3.5}$$

The expression of the Cp is a nonlinear equation of the tip speed λ,is given by (Mabrouk & Boumediene, 2018):

$$\begin{cases} \frac{1}{\lambda i} = \frac{1}{\lambda + 0.02\beta} - \frac{0.003}{\beta 3 + 1} \\ Cp = Cp(\lambda + \beta) = 0.46(\frac{151}{\lambda i} - 0.58\beta - 0.02\beta 2.14 - 13.2)(e^{\frac{-18.4}{\lambda i}}) \end{cases} \quad (3.6)$$

3.3.2. Dynamic Turbine Model

A. Turbine Gearbox

The mechanical connection between an electrical generator and the turbine rotor may be direct or through a gearbox. In essence, the gearbox converts the blades' turning speed into a rotational speed of an electrical generator. The turbine gearbox aims at the adaptation between the shaft velocity of the turbine (Low speed shaft) and that of the generator (High speed shaft). In the case of an ideal gearbox, the gear ratio can be modeled mathematically by (Mabrouk & Boumediene, 2018):

$$N = \frac{\Omega_m}{\Omega_t} = \frac{T_t}{T_m} \quad (3.7)$$

where N is the gear ratio, T_t and T_m are torque of the turbine on Low and high speed shaft respectively, Ω_t and Ω_m are velocity of the turbine on Low and high speed shaft respectively.

Most of the simple wind turbine gear box consists of two main shafts, the low speed shaft, which is essentially attached to the wind turbine blades, and the second shaft, known as the high speed shaft, which is directly connected to the generator, make up the majority of simple wind turbine gear boxes. The shaft system of the wind turbine generator can be represented either by a two-mass system or by a single lumped-mass system. Two mass shaft models are wanted to study in this thesis (Ahmed, 2013).

Two-mass model

In this model, The low-speed turbine and high-speed generator are modeled as separate masses, and the connecting robust shaft is modeled as a spring and a damper and it can show flexible modes in the gear train model that cannot be done using the one mass model (Ahmed, 2013)(Qiao, 2009).

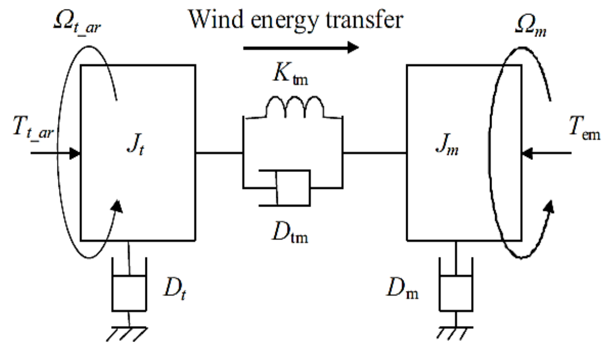

Figure 3.2: Two Mass System [28]

By applying Newton's second law for rotation system or using energy principles on the rotor, the mathematical model will be (Ahmed, 2013):

$$J_r\dot{\omega}_t + B_r\omega_t = T_a - T_{ls} \tag{3.8}$$

Where, J_r is rotor moment of inertia, ω_t is rotor angular speed, B_r is rotor damping effect, Ta is applied torque on the rotor, and T_{ls} is low-speed shaft torque.

Whereas the same mechanism is used for the driving gear, which practically cancels out its moment of inertia, producing:

$$T_{ls} = B_{ls}(\omega_t - \omega_{ls}) + K_{ls}(\theta_t - \theta_{ls}) \tag{3.9}$$

Where, B_{ls} is low speed damping effect and K_{ls} is stiffness of low speed shaft, ω_{ls} is angular speed of the low speed shaft, θ_t is rotor angular displacement, and θ_t is low speed shaft angular displacement.

Using the gearbox G, torque and speed of low shaft are provided to generate a torque on high shaft (Rekioua, 2014):

$$T_{hs} = \frac{T_{ls}}{G} \tag{3.10}$$

$$\theta_g = G\theta_{ls} \tag{3.11}$$

$$\omega_g = G\omega_{ls} \tag{3.12}$$

Through the gearbox, the low-shaft speed is enhanced by the gearbox ratio to obtain the generator speed, while the low-speed shaft torque is decreased. Assuming an ideal gearbox with a ratio of G, we can write the following (Rekioua, 2014):

$$G = \frac{T_{ls}}{T_{hs}} = \frac{\omega_g}{\omega_{ls}} = \frac{\theta_g}{\theta_{ls}} \quad (3.13)$$

The generator is driven by the high-speed shaft Torque (T_{hs}) and braked by the generator electromagnetic torque (T_{em}). Its dynamic equation is given as:

$$J_g \dot{\omega}_g = T_{hs} - T_{em} - B_g \omega_g \quad (3.14)$$

Where J_g is generator inertia, ω_g is generator rotational speed, and B_g is high speed shaft.

B. Equation Dynamic of Wind Turbine

The fundamental equation of the dynamics which makes it possible to determine the evolution mechanical speed from the torque exerted on the shaft of the rotor of the wind turbine T_t and the electromagnetic torque T_{em} (Mabrouk & Boumediene, 2018)(J.~Marques et al., 2003):

$$J \frac{d\Omega_m}{dt} = T_m - T_{em} - D\Omega_m \quad (3.15)$$

where D is the damping coefficient of turbine, J is the wind turbine inertia.

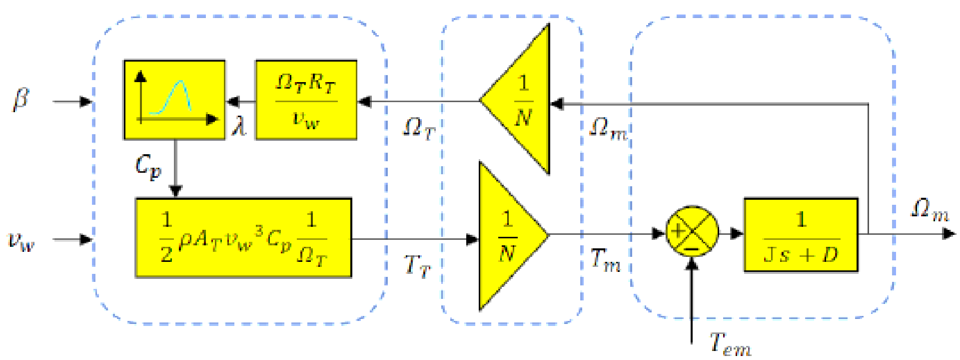

Figure 3.3: Dynamic Model of the Wind Turbine (Mabrouk & Boumediene, 2018)

3.3.3. Wind Speed Model

The primary output of a conversion wind system is wind speed, often known as wind velocity. The metrological circumstances determine it. It is frequently measured in (m/s) or (km/h) using an anemometer or a weather station (Rekioua, 2014).

The short-term wind speed fluctuations with specific features, such as speed range or turbulence intensity, that a WT will encounter are generated using this model. The wind speed V_w is modeled as the sum of the four components and this wind speed expression has the form (Ibrahim & Watson, n.d.)(Ganthia & Barik, 2020):

$$V_w(t) = V_{wa}(t) + V_{wr}(t) + V_{wg}(t) + V_{wt}(t) \qquad (3.16)$$

Where, V_{wa}(t)is the average value of the wind speed, V_{wr}(t) is the ramp wind component, V_{wg}(t) is the gust wind component and V_{wt}(t) is the turbulence component, all of them in m/s.

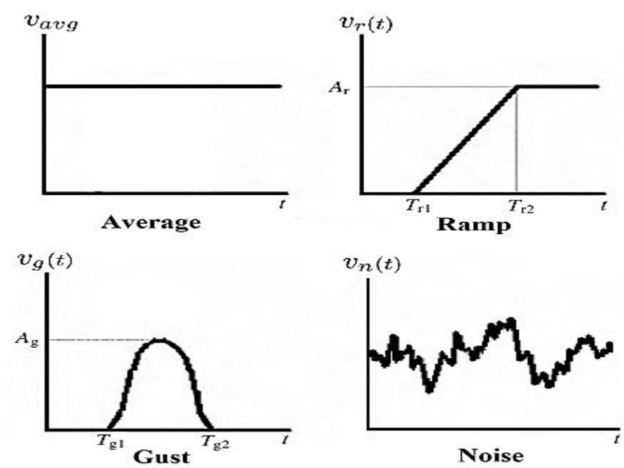

Figure 3.4: Wind Speed Components (Ibrahim & Watson, n.d.)

The gust component may be useful to simulate an abnormal temporary increase of the speed of the wind and Its expression is (Junyent-ferré et al., 2010):

$$V_{wg}(t) \ = \begin{cases} 0, t < T_{g1} \\ A_g(1 - cos[\,2\pi(\frac{t-T_{g1}}{T_{g2}-T_{g1}})]) \,, T_{g1} \leq t \leq T_{g2} \\ 0, t > T_{g2} \end{cases} \qquad (3.17)$$

Where, Ag is gust's amplitude and T_{g1} and T_{g2} are the times representing the starts and ends of the ramp respectively.

Turbulence component is a signal which has a power spectral density of the following form (Junyent-ferré et al., 2010):

$$P_{Dt}(t) = \frac{lV_w[\ln(\frac{k}{z_o})]^{-2}}{[1+1.5\frac{fl}{V_w}]^{5/3}} \qquad (3.18)$$

Where, l is a turbulence scale which is 20 times the high and its maximum value is 300m, Vw is average wind speed, h is the height of interest (wind wheel height) and Zo is roughness length parameter which depends on the type of landscape.

The following equation can be used to compute the wind velocity ramp component (Junyent-ferré et al., 2010):

$$V_{wr}(t) = \begin{cases} 0, t < T_{r1} \\ A_r(1 - cos[\,2\pi(\frac{t-T_{r1}}{T_{r2}-T_{r1}})]) \,, T_{r1} \leq t \leq T_{r2} \\ 0, t > T_{r2} \end{cases} \quad (3.19)$$

Where, A_r is the amplitude of the ramp and T_{r1} and T_{r2} are the times representing the starts and ends of the ramp respectively.

3.3.4. DFIG Modeling

3.3.4.1. Steady State Model of DFIG

The induction generator steady-state model is extremely useful for evaluating the performance of steady-state generators. The machine's dynamic behavior will then be created using this information. In a steady-state, the stator is powered by three-phase ac signals from the grid that are balanced and constant in frequency and voltage amplitude. In addition to the stator, the rotor is supplied with balanced and constant three-phase ac signals via back-to-back power converters (Wu & Xie, 2018).

The frequency of stator voltages and currents (ω_s), frequency of rotor voltages and currents (ω_r), and the electric speed of rotor (ω_m) are given by (Senapati, 2014):

$$\omega_s = \omega_r + \omega_m \quad (3.20)$$

The relation between the mechanical rotational speed at the rotor in rad/s Ω_m and the electrical speed depends on the pole pairs of the machine:

$$\omega_m = P\Omega_m \quad (3.21)$$

The slip *s* of the machine is defined as follows:

$$S = \frac{\omega_s - \omega_m}{\omega_s} = \frac{\omega_r}{\omega_s} \quad (3.22)$$

There are three distinct operating modes for the machine, depending on the sign of the slip:

- $\omega_m < \omega_s \Rightarrow \omega_r > 0 \Rightarrow S > 0 \Rightarrow$ Sub-synchronous operation
- $\omega_m > \omega_s \Rightarrow \omega_r < 0 \Rightarrow S < 0 \Rightarrow$ Super-synchronous operation
- $\omega_m = \omega_s \Rightarrow \omega_r = 0 \Rightarrow S = 0 \Rightarrow$ Synchronous operation

a) Sub-synchronous operation

In this mode, the generator operates below the synchronous speed and the slip is positive. The rotor circuit can take power from or send it to the grid depending on whether the slip is positive or negative.. For this operation, The grid provides power to the rotor for this operation. Through the stator, the grid receives both mechanical power (Pm) and rotor power (Pr).Since the mechanical power Pm from the generator shaft is lower in the sub-synchronous mode than it is in the super-synchronous mode, even if the stator power (PS) is the sum of Pm and Pr, it won't go over its power rating. Neglecting the losses in the generator and convertor, the total amount of power provided to the grid (Pg) is the input mechanical power (Pm) (Luis & Moncayo, n.d.)(Rao, 2012).

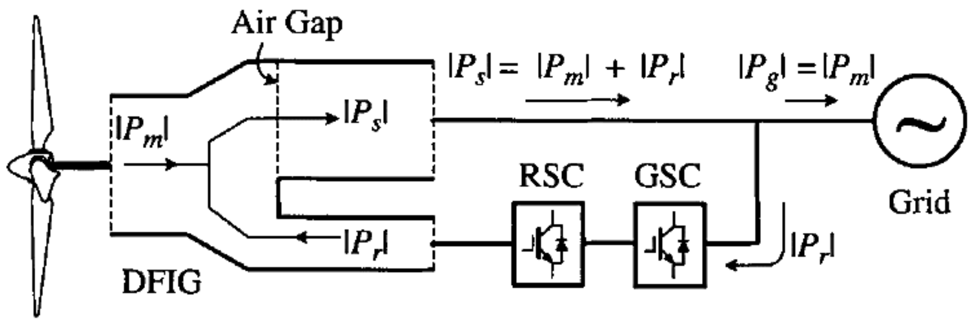

Figure 3.5: Power Flow in DFIG at Sub-Synchronous Model (Luis & Moncayo, n.d.)

b) Super-synchronous operation

In super-synchronous mode, the generator operates above the synchronous speed and slip is negative. In this mode of operation, the stator and rotor circuits each deliver mechanical power (Pm) from the shaft to the grid. Stator power (PS) is sent directly to the grid, whereas rotor power (Pr) is transferred to the grid by power converters in the rotor circuit. The power delivered to the grid (Pg) is equal to the mechanical power (Pm) of the generator after neglecting losses in the generator and converters(Luis & Moncayo, n.d.)(Rao, 2012).

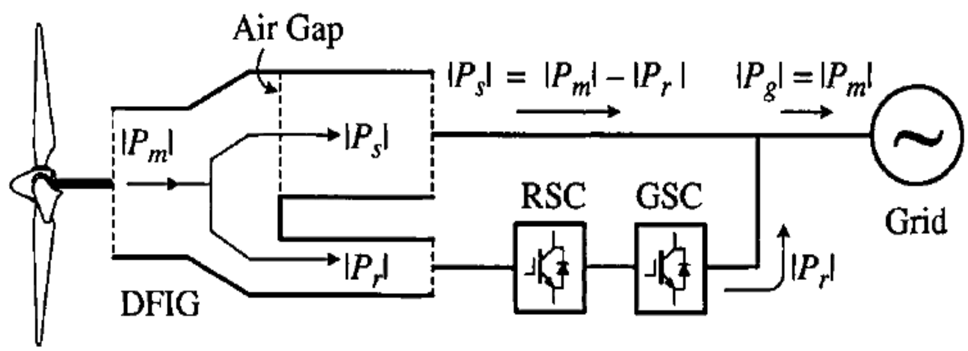

Figure 3.6: Power Flow in DFIG at Super-Synchronous Model (Luis & Moncayo, n.d.)

c) Synchronous operation

In this operation mode, the RSC shall provide DC excitation for the rotor so that the generator operates as a synchronous machine. Since the rotor winding does not provide any current or power, the rotor power is zero, but the stator winding delivers a large amount of reactive power to the network. The generated nominal speed is similar to generator's operating speed, and the slip is zero (Chandrasekaran, 2014).

Steady-state equivalent circuit of DFIG with rotor-side convertor

In order to examine the steady-state performance of the DFIG wind energy system, it is possible to model the RSC by an equivalent impedance. Figure 3.9 shows a steady-state equivalent circuit of DFIG WECS. This equivalent circuit is developed by adding the converter equivalent impedance to the SCIG steady-state model (Luis & Moncayo, n.d.).

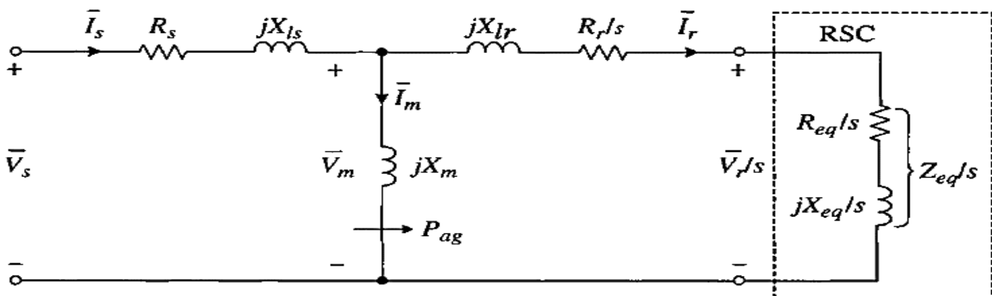

Figure 3.7: Steady- State Equivalent Circuit of DFIG with the Rotor-Side Converter (Luis & Moncayo, n.d.)

The equivalent impedance of the converter is defined by (Luis & Moncayo, n.d.):

$$\bar{Z}_{eq} = R_{eq} + jX_{eq} = R_{eq} + j\omega_{sl}L_{eq} \qquad (3.23)$$

where ω_{sl} is the angular slip frequency and L_{eq} is the equivalent inductance of the RSC. Note that the frequency of the rotor current in the actual rotor winding flowing into the converter is ω_{sl}, not the stator frequency ω_s. For the converter to be integrated equivalent impedance into the steady-state model with the stator frequency ω_s, the impedance Z_{eq} should be divided by slip s. The equivalent impedance referred to the stator side is then given by (Luis & Moncayo, n.d.):

$$\frac{\bar{Z}_{eq}}{s} = \frac{R_{eq}}{s} + \frac{j\omega_{sl}L_{eq}}{s} = \frac{R_{eq}}{s} + j\omega_s L_{eq} \qquad (3.24)$$

Assuming that the stator operates at a unity power factor, the air-gap power of the generator can be calculated by:

$$P_{ag} = 3(V_S - I_s R_s) I_s \tag{3.25}$$

The air-gap power from the induction machine theory can alternatively be calculated using by:

$$P_{ag} = \frac{\omega_s T_m}{P} \tag{3.26}$$

where T_m is the mechanical torque and P is the number of pole pairs of the generator.

Substituting (3.26) into (3.25) yields

$$\frac{\omega_s T_m}{P} = P_{ag} = 3(V_S - I_s R_s) I_s \tag{3.27}$$

From which

$$R_s I_s^2 - V_s I_s + \frac{\omega_s T_m}{3P} = 0 \tag{3.28}$$

Solving (17), we have

$$I_s = \frac{V_s \pm \sqrt{V_s^2 - \frac{4 R_s \omega_s T_m}{3P}}}{2 R_s} \tag{3.29}$$

With the magnitude of the stator current calculated, we can use the equivalent circuit of Figure 5 to find the rotor voltage $\bar{V}_r$ and rotor current $\bar{I}_r$. The voltage across the magnetizing branch is (Luis & Moncayo, n.d.):

$$\bar{V}_m = \bar{V}_s - \bar{I}_s (R_s + j\omega_s L_{ls}) \tag{3.30}$$

where the stator voltage and current are given by

$$\bar{V}_s = V_s < 0^{\circ} and\ \bar{I}_s = I_s < 180^{\circ} \tag{3.31}$$

The stator voltage and current are 180° out of phase, indicating that the DFIG is in the generating mode and the stator power factor (PF_s) is unity (Luis & Moncayo, n.d.).

The magnetizing current can be determined by

$$\bar{I}_m = \frac{\bar{V}_m}{j\omega_s L_m} \tag{3.32}$$

The rotor current is

$$\bar{I}_r = \bar{I}_s - \bar{I}_m \tag{3.33}$$

The rotor voltage can be determined by (Luis & Moncayo, n.d.):

$$\frac{\bar{V}_r}{S} = \bar{V}_m - \bar{I}_r \left(\frac{R_r}{S} + j\omega_s L_{lr}\right) \tag{3.34}$$

From which

$$\bar{V}_r = S\bar{V}_m - \bar{I}_r(R_r + jS\omega_s L_{lr}) \quad (3.35)$$

The rotor voltage and current relate to the equivalent resistance R_{eq} and reactance X_{eq} by (Luis & Moncayo, n.d.):

$$R_{eq} + jX_{eq} = \frac{\bar{V}_r}{\bar{I}_r} \quad (3.36)$$

3.3.4.2. Dynamic DFIG model

To investigate the actual behavior of DFIG, it is necessary to consider dynamic equations to achieve a more reasonable perspective. It is critical to use Clarke and Park to turn the machine model into a space vector before controlling and analyzing its performance. This will make simulation and implementation of the control scheme much easier. The voltage equations, flux linkage equations, and motion equations are the three sets of equations that make up the Induction Generator space-vector model (Abad et al., 2011).

There are three different rotating reference frames typically utilized to develop space vector-based models of the DFIM. The stator reference frame (α–β) is a stationary reference frame, the rotor reference frame (DQ) rotates at ωm and the synchronous reference frame (dq) rotates at ωs. Subscripts "s" and "r" are used to denote that one space vector is reference to the stator, and rotor respectively. By using direct and inverse rotational transformation, a space vector can be represented in any of these frames (Rajendran & Jena, 2014).

.

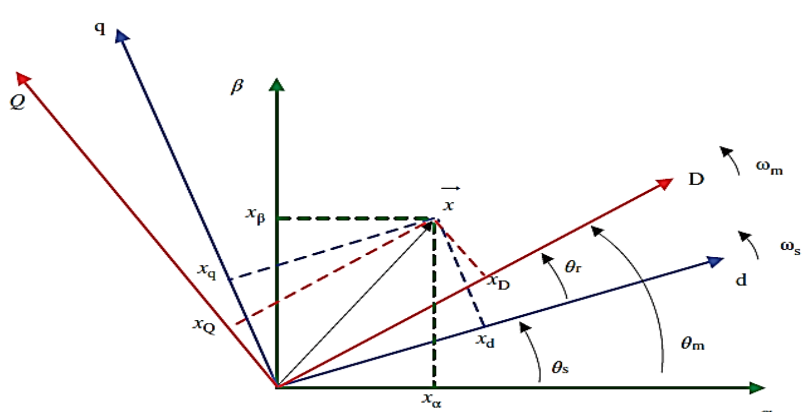

Figure 3.8: Different Reference Frames to Represent Space Vectors of the DFIM (Rajendran & Jena, 2014).

A. αβ model

The transformation of three-phase variables in the stationary reference frame into the two-phase variables also in the stationary frame is often referred to as abc/αβ (Clarke) transformation and can be represented in the matrix as (Luis & Moncayo, n.d.):

$$X_{\alpha\beta} = T_c X_{abc} \tag{3.37}$$

Where Tc is the transformation matrix of Clarke transformation.

$$T_c = \frac{2}{3}\begin{bmatrix} 1 & -1/2 & -1/2 \\ 0 & \sqrt{3}/2 & -\sqrt{3}/2 \end{bmatrix} \tag{3.38}$$

$$\begin{bmatrix} X_\alpha \\ X_\beta \end{bmatrix} = \frac{2}{3}\begin{bmatrix} 1 & -1/2 & -1/2 \\ 0 & \sqrt{3}/2 & -\sqrt{3}/2 \end{bmatrix}\begin{bmatrix} X_a \\ X_b \\ X_c \end{bmatrix} \tag{3.39}$$

Similarly, the two-phase to three-phase transformation in the stationary reference frame, known as αβ/abc (inverse clarke) transformation, can be performed by (Luis & Moncayo, n.d.):

$$\begin{bmatrix} X_a \\ X_b \\ X_c \end{bmatrix} = \begin{bmatrix} 1 & 0 \\ -1/2 & \sqrt{3}/2 \\ -1/2 & -\sqrt{3}/2 \end{bmatrix}\begin{bmatrix} X_\alpha \\ X_\beta \end{bmatrix} \tag{3.40}$$

The three coils of the stator and rotor separately, by using space vector theory, can be represented by two stationary αβ coils for the stator and two rotating coils DQ for the rotor, providing the following voltage equation (Rajendran & Jena, 2014).

:

$$\vec{V}_s^s = R_s \vec{i}_s^s + \frac{d\vec{\Psi}s}{dt} \tag{3.41}$$

$$\vec{V}_r^r = R_r \vec{i}_r^r + \frac{d\vec{\Psi}r}{dt} \tag{3.42}$$

Where $\vec{V}_s^s$ is the stator voltage space vector, $\vec{i}_s^s$ is the stator current space vector, R_s is the stator resistance and $\vec{\Psi}_s^s$ is the stator flux space vector. Equation (3.41) is represented in stator coordinates (αβ reference frame). $\vec{V}_r^r$ is the rotor voltage space vector, $\vec{i}_r^r$ is the rotor current space vector, R_r is rotor resistance and $\vec{\Psi}_r^r$ is the rotor flux space vector. Equation (3.42) is represented in rotor coordinates (DQ reference frame) (Abad et al., 2011).

If both voltage equations are represented in stationary reference frame αβ, then the rotor equation must be multiplied by $e^{j\theta m}$, which yields the following set of equations (Senapati, 2014):

$$\vec{V}_s^{\,s} = R_s \vec{i}_s^{\,s} + \frac{d\vec{\Psi}s}{dt} \Rightarrow \begin{cases} V_{\alpha s} = R_s i_{\alpha s} + \frac{d\Psi\alpha s}{dt} \\ V_{\beta s} = R_s i_{\beta s} + \frac{d\Psi\beta s}{dt} \end{cases} \tag{3.43}$$

While on the other hand, the correlation between the fluxes and the currents, in space vector notation, is given by (Abad et al., 2011):

$$\vec{\Psi}_s^{\,s} = L_s \vec{i}_s^{\,s} + L_m \vec{i}_r^{\,s} = L_s \vec{i}_s^{\,s} + L_m e^{j\theta m} \vec{i}_r^{\,r} \tag{3.44}$$

$$\vec{\Psi}_r^{\,r} = L_m \vec{i}_s^{\,r} + L_r \vec{i}_r^{\,r} = L_m e^{-j\theta m} \vec{i}_s^{\,s} + L_r \vec{i}_r^{\,r} \tag{3.45}$$

$$\begin{cases} Ls = L\sigma s + Lm \\ Lr = L\sigma r + Lm \end{cases} \tag{3.46}$$

Where L_s and L_r are the stator and rotor inductances, L_m is the magnetizing inductance, they are related to the stator leakage inductance $L_{\sigma s}$ and the rotor leakage inductance $L_{\sigma r}$ and equation (3.44) is represented in the stator reference frame, while equation (3.45) is in the rotor reference frame.

The following equations can be used to determine the active and reactive powers of the stator and rotor sides:

$$P_s = \frac{3}{2}\left(V_{\alpha s} i_{\alpha s} + V_{\beta s} i_{\beta s}\right) \quad P_r = \frac{3}{2}\left(V_{\alpha r} i_{\alpha r} + V_{\beta r} i_{\beta r}\right) \tag{3.47}$$

$$Q_s = \frac{3}{2}\left(V_{\beta s} i_{\alpha s} - V_{\alpha s} i_{\beta s}\right) \quad Q_r = \frac{3}{2}\left(V_{\beta r} i_{\alpha r} + V_{\alpha r} i_{\beta r}\right) \tag{3.48}$$

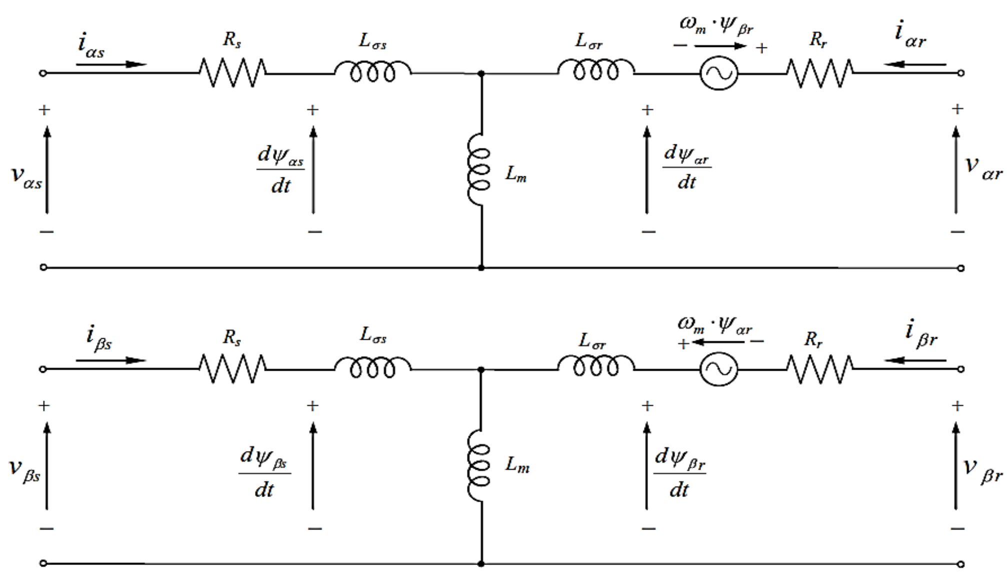

Figure 3.9: αβ model of the DFIM in Stator Coordinates (Abad et al., 2011)

B. dq model

The transformation of two-phase variables in the stationary reference frame (αβ) into the a two-phase rotating reference frame (dq) through the rotation transformation matrix Tp(θ) is park transformation (Mitra & Sengupta, 2006).

$$\begin{bmatrix} \mathrm{d} \\ \mathrm{q} \end{bmatrix} = T_p(\theta) \begin{bmatrix} \alpha \\ \beta \end{bmatrix} \tag{3.49}$$

Where $T_p(\theta)$ is the transformation matrix of park transformation.

$$T_p(\theta) = \begin{bmatrix} cos\theta & sin\theta \\ -sin\theta & cos\theta \end{bmatrix} \tag{3.50}$$

The transformation from (abc) to (dq) (Luis & Moncayo, n.d.):

$$\begin{bmatrix} X_d \\ X_q \end{bmatrix} = \frac{2}{3} \begin{bmatrix} cos\theta & \cos(\theta - 2\pi/3) & cos(\theta - 4\pi/3) \\ sin\theta & -\sin(\theta - 2\pi/3) & -\sin(\theta - 4\pi/3) \end{bmatrix} \begin{bmatrix} X_a \\ X_b \\ X_c \end{bmatrix} \tag{3.51}$$

The transformation from (dq) to (αβ) or inverse park transformation is done by (Senapati, 2014):

$$\begin{bmatrix} \alpha \\ \beta \end{bmatrix} = \begin{bmatrix} cos\theta & -sin\theta \\ sin\theta & cos\theta \end{bmatrix} \begin{bmatrix} d \\ q \end{bmatrix} \tag{3.52}$$

The transformation from (dq) to (abc) (Luis & Moncayo, n.d.):

$$\begin{bmatrix} X_a \\ X_b \\ X_c \end{bmatrix} = \begin{bmatrix} cos\theta & sin\theta \\ \cos(\theta - 2\pi/3) & -\sin(\theta - 2\pi/3) \\ cos(\theta - 4\pi/3) & -\sin(\theta - 4\pi/3) \end{bmatrix} \begin{bmatrix} X_d \\ X_q \end{bmatrix} \tag{3.53}$$

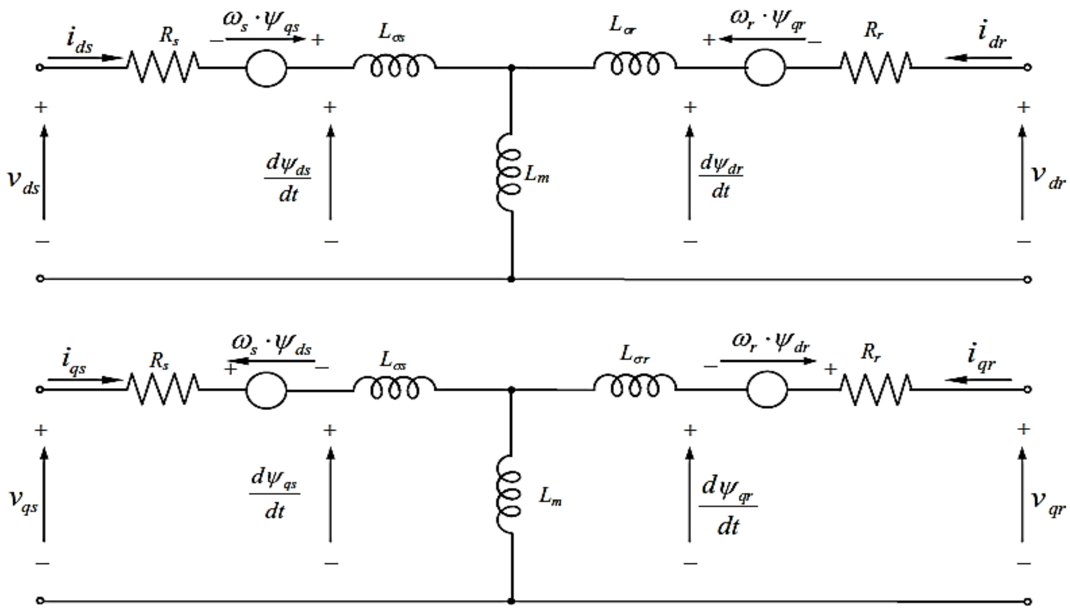

Figure 3.10: dq Model of the DFIM in Synchronous Coordinates (Abad et al., 2011)

The most widely used model for doubly fed induction generator is the Park model, which allows writing a dynamic model in a d−q reference frame as follows (Jaballaafou et al., 2020):

The stator and rotor voltage equations are:

$$\begin{cases} V_{ds} = R_s i_{ds} + \frac{d\Psi_{ds}}{dt} - \omega_s \Psi_{qs} \\ V_{qs} = R_s i_{qs} + \frac{d\Psi_{qs}}{dt} - \omega_s \Psi_{ds} \\ V_{dr} = R_r i_{dr} + \frac{d\Psi_{dr}}{dt} - \omega_r \Psi_{qr} \\ V_{qr} = R_r i_{qr} + \frac{d\Psi_{qr}}{dt} - \omega_r \Psi_{dr} \end{cases} \tag{3.54}$$

The stator and rotor flux:

$$\begin{cases} \Psi_{ds} = L_s i_{ds} + L_m i_{dr} \\ \Psi_{qs} = L_s i_{qs} + L_m i_{qr} \\ \Psi_{dr} = L_m i_{ds} + L_r i_{dr} \\ \Psi_{qr} = L_m i_{qs} + L_r i_{qr} \end{cases} \tag{3.55}$$

The electromagnetic torque T_{em} is written as:

$$T_{em} = \frac{3}{2} P \frac{L_m}{L_s} (\Psi_{qs} i_{dr} - \Psi_{ds} i_{qr}) \tag{3.56}$$

The active and reactive stator and rotor powers are given in dq reference frame by:

$$\begin{cases} P_s = \frac{3}{2}\left(V_{ds}i_{ds} + V_{qs}i_{qs}\right) \\ Q_s = \frac{3}{2}\left(V_{qs}i_{ds} - V_{ds}i_{qs}\right) \\ P_r = \frac{3}{2}\left(V_{dr}i_{dr} + V_{qr}i_{qr}\right) \\ Q_r = \frac{3}{2}\left(V_{qr}i_{dr} - V_{dr}i_{qr}\right) \end{cases} \tag{3.57}$$

3.3.5. Back-to-Back Converter Model

In WECS, back-to-back converter are commonly utilized. The DFIG is commonly uses two back-to-back PMW converters. While the other converter operates in the inverting mode, one of the converters functions in the rectifying mode. Through a DC-link composed of a capacitor, these two converters are linked together. The GSC (the invertor) is utilized to maintain the dc-link voltage constant and to make the grid-side work at unit power factor, so no reactive power flows between rotor and grid. The rotor side converter (the rectifier) allowed stator voltage and reactive power to be regulated by the stator or controls the rotor current for the purpose of controling the active and reactive power injected in to the grid (Luis & Moncayo, n.d.)(Rekioua, 2014)(Ganthia & Barik, 2020). Generally, this convertor is important to convert variable frequency and voltage from variable speed to fixed frequency and voltage that is suitable for the grid.

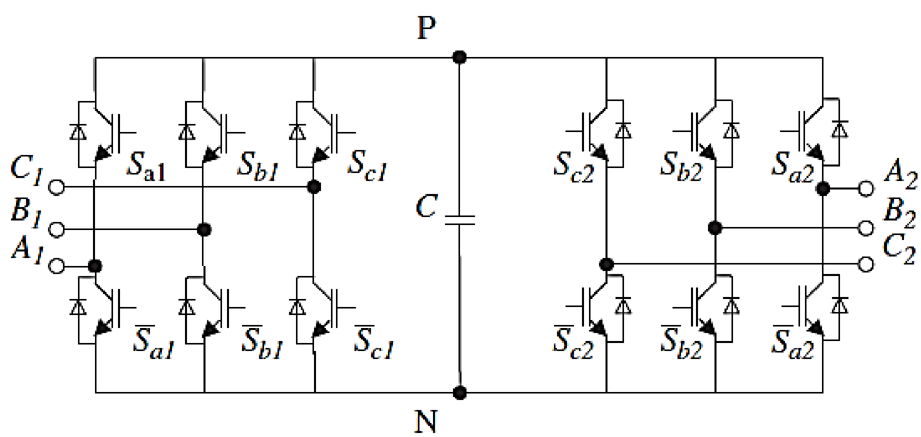

Figure 3.11: Back-to-Back Converter (Luis & Moncayo, n.d.)

3.3.5.1. Two-Level Grid Side Voltage Source Converter (VSC)

The most widely used power converter for three-phase drive applications is the two-level VSC, which generates the output waveform using PWM with two voltage levels. The grid side system is composed by the grid side converter, the grid side filter, and the grid voltage. This converter is modeled with ideal bidirectional switches. It converts DC currents and voltages into AC, while Power transfer is possible in both the AC to DC (rectifier mode) and the DC to AC directions (inverter mode). The ideal switch normally is created by a controlled semiconductor with a diode in antiparallel to allow the flow of current in both directions. In this exposition, the controlled semiconductor used is an insulated gate bipolar transistor (IGBT) (Abad et al., 2011).

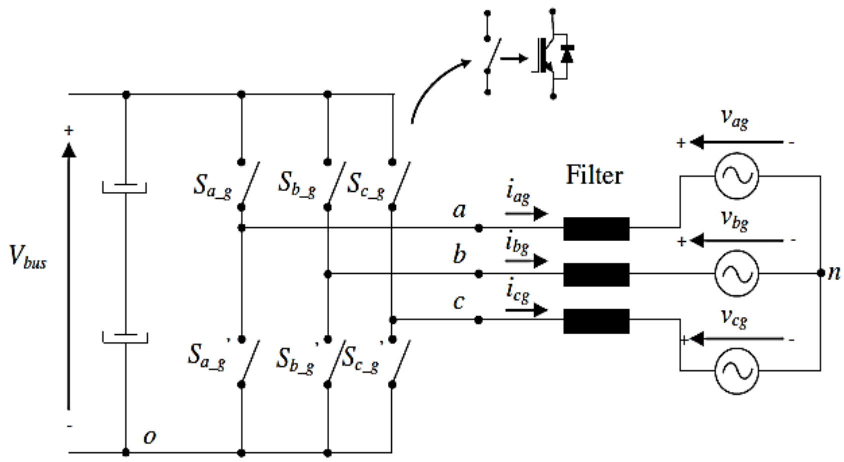

Figure 3.12: Simplified Model of the Grid Side System (Abad et al., 2011)

The two-level converter is modeled with ideal switches that allow the flow of current in both directions. The output voltages of the converter are synthesized by commanding the appropriate switching orders of the IGBTs: S_{a_g}, S_{b_g}, and S_{c_g} .The output voltages referred to the zero point of the DC bus can be calculated according to the following general expression (Abad et al., 2011)(Abad, 2016):

$$V_{jo} = V_{bus} S_{j\_g} \tag{3.58}$$

With $S_{j\_g} \in \{0,1\}$ $and\ j = a, b, c$

Thus, by different combinations of S_{a_g}, S_{b_g}, and S_{c_g} it is feasible to create AC output voltages with a fundamental component of different amplitude and frequency. The converter provides two possible voltage levels at each phase and the voltage levels are 0 and V_{bus}.

On the other hand, for modeling purposes, it is very useful to know the converter output voltages referred to the neutral point of the grid three-phase system (n). As Figure 3.15 illustrates, the following voltage relationships are true (Abad et al., 2011):

$$V_{jn} = V_{jo} - V_{no}\ with\ j = a, b, c \tag{3.59}$$

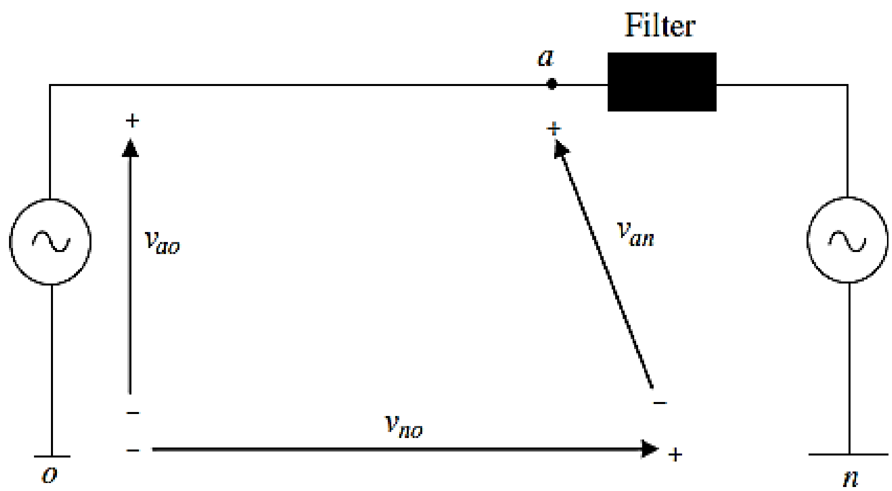

Figure 3.13: Simplified Equivalent Single-Phase Grid Circuit (a phase) (Abad et al., 2011)

The voltage between the neutral point (n) and the negative point of the DC bus (o) is needed, so assuming a three-phase grid system that holds, we have (Abad et al., 2011).

$$V_{an} + V_{bn} + V_{cn} = 0 \tag{3.60}$$

Substituting expression (3.59) into the last expression yields

$$V_{no} = \frac{1}{3}\,(V_{ao} + V_{bo} + V_{co}) \tag{3.61}$$

Substituting again into Equation (3.59) this last expression, we finally obtain

$$\begin{cases} V_{an} = \frac{2}{3}\,V_{ao} - \frac{1}{3}(V_{bo} + V_{co}) \\ V_{bn} = \frac{2}{3}\,V_{bo} - \frac{1}{3}(V_{ao} + V_{co}) \\ V_{cn} = \frac{2}{3}\,V_{co} - \frac{1}{3}(V_{bo} + V_{ao}) \end{cases} \tag{3.62}$$

Or more simply, directly from the order commands,

$$\begin{cases} V_{an} = \frac{V_{bus}}{3}(2S_{a\_g} - S_{b\_g} - S_{c\_g}) \\ V_{bn} = \frac{V_{bus}}{3}(2S_{b\_g} - S_{a\_g} - S_{c\_g}) \\ V_{cn} = \frac{V_{bus}}{3}(2S_{c\_g} - S_{a\_g} - S_{b\_g}) \end{cases} \tag{3.63}$$

According to the eight permitted switching states of S_{a_g}, S_{b_g}, and S_{c_g}, there are eight different combinations of output voltages. As previously stated, the output voltages V_{ao}, V_{bo}, and V_{co} only accept two voltage levels: V_{bus} and 0; that is why this converter is identified as a “two-level converter". On the other hand, output voltages V_{an}, V_{bn}, and V_{cn} take five different voltage levels: $-2V_{bus}/3, -V_{bus}/3, 0, V_{bus}/3, and\ 2V_{bus}/3$.

Steady State Model of the Grid Side System

The steady state model of the grid side system is developed by using phasor theory, that allowing to understand the basic relationships between active and reactive powers, voltage, and currents at different operating modes. The grid voltage $(V_{ag}, V_{bg}, and\ V_{cg})$ is sinusoidal with constant amplitude and frequency. The voltage imposed by the grid side converter $(V_{af}, V_{bf}, and\ V_{cf})$ can be modified in amplitude and phase [43]. The filter considered in this thesis is a pure inductive filter (L_f) and resistance (R_f) is also considered within the model of the filter.

It is easier to create subsequent analyses by considering one of the phases. Only one phase (for example, a phase) needs to be examined in order to extrapolate the other two phases from the system's behavior.

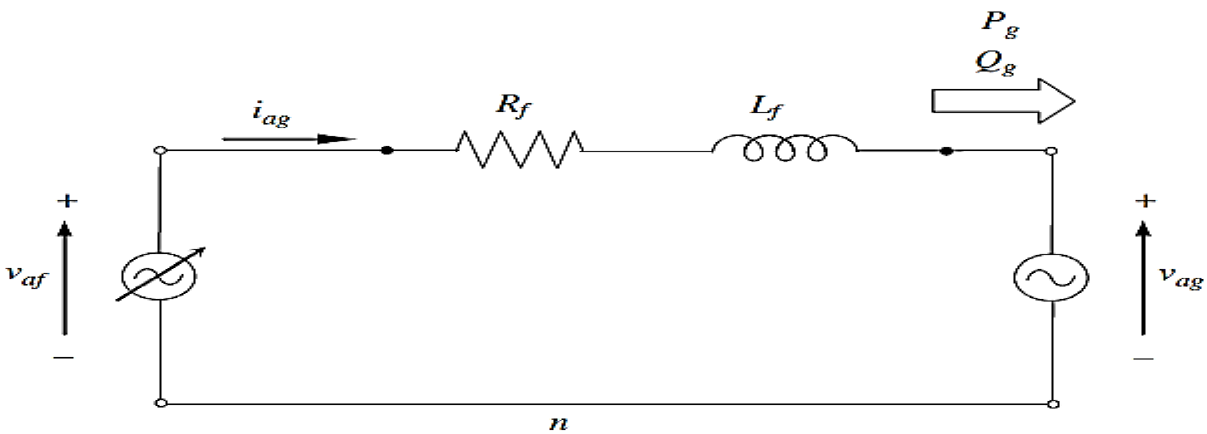

Figure 3.14: Simplified Model of Single-Phase Grid Side System (Abad et al., 2011)

Therefore, the voltage imposed by the converter can be modified depending on the requirements of the application (Abad, 2016). So, at steady-state operation, the electric equation of the system represented in the above figure is:

$$V_{af} = V_{ag} + (R_f + jL_f\omega_s)I_{ag} \quad (3.64)$$

Dynamic Modeling of the Grid Side System

By applying the space vector notation to the abc modeling equations, it is possible to represent the electric equations in αβ components (Abad, 2016).

The αβ expression become:

$$\begin{cases} V_{\alpha f} = R_f i_{\alpha g} + L_f \frac{di_{\alpha g}}{dt} + V_{\alpha g} \\ V_{\beta f} = R_f i_{\beta g} + L_f \frac{di_{\beta g}}{dt} + V_{\beta g} \end{cases} \tag{3.65}$$

Also by multiplying the above Equation by $e^{-j\theta}$, from the αβ expressions the dq expressions are also derived (rotating frame) (Abad et al., 2011).

The basic equations for vector orientation are obtained:

$$\begin{cases} V_{df} = R_f i_{dg} + L_f \frac{di_{dg}}{dt} + V_{dg} - \omega_a L_f i_{qg} \\ V_{qf} = R_f i_{qg} + L_f \frac{di_{qg}}{dt} + V_{qg} + \omega_a L_f i_{dg} \end{cases} \tag{3.66}$$

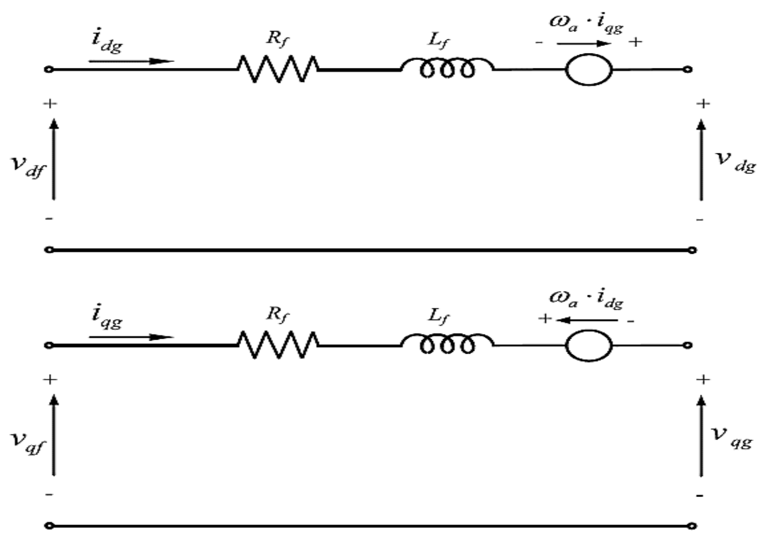

Figure 3.15: dq Model of the Grid Side System in Stationary Coordinates (Abad et al., 2011)

3.3.5.2. Rotor Side Converter and dv/dt Filter

The rotor side converter that supplies the rotor of the DFIG, in general terms, is equal to the grid side converter. In this case also, a two-level VSC feeds the rotor. Between the rotor and the converter, in general, a dv/dt filter is located mainly with the objective to protect the machine from the harmful effects of the voltage source converter, such as capacitive leakage currents, bearing currents, and increased stress on the motor insulation (Abad et al., 2011).

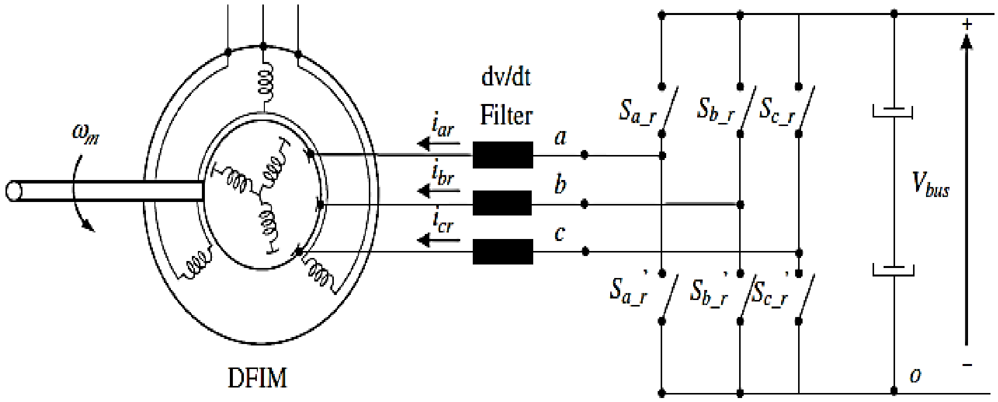

Figure 3.16: RSC and dv/dt Filter Supplying the Rotor at the Machine (Abad et al., 2011)

3.3.6. DC-Link Model

The DC part of the back-to-back converter is typically called the DC link. It stores a certain amount of energy in the capacitor (or combination of several capacitors), it tries to maintain a constant voltage in its terminals. Figure 3.16 shows a possible model for the DC-link. A resistor in parallel with the capacitors bank has been introduced. This R_{bus} is typically of very high resistive value (Abad et al., 2011)(Abad, 2016).

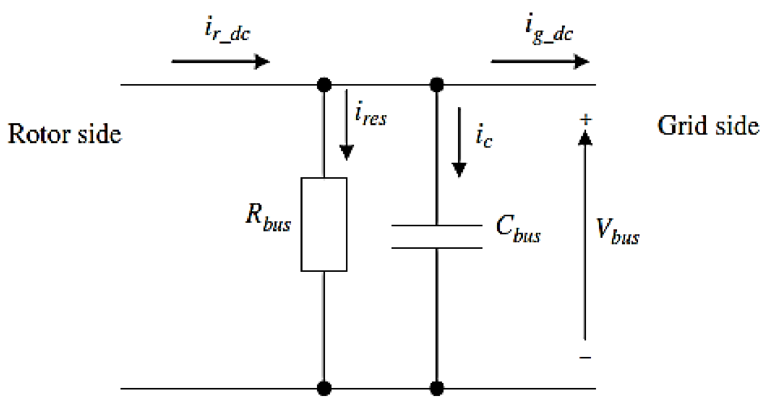

Figure 3.17: DC- Link System (Abad et al., 2011)

It is necessary to determine the DC bus voltage in order to derive the model of the DC-link. This voltage is dependent on the current through the capacitor (Abad, 2016):

$$V_{bus} = \frac{1}{C_{bus}} \int i_c \; dt \tag{3.67}$$

The capacitor's current can be calculated as:

$$i_c = i_{r\_dc} - i_{g\_dc} - i_{res} \tag{3.68}$$

Where, i_{res} is the current through the resistance (A), i_{g_dc} is the DC current flowing from the DC-link to the grid (A), and i_{r_dc} is the DC current flowing from the left part to the DC-link (A).

Additionally, the converters' output AC currents can be used to calculate the DC currents in the manner shown below:

$$i_{g\_dc} = S_{a\_g}i_{ag} + S_{b\_g}i_{bg} + S_{c\_g}i_{cg} \tag{3.69}$$

$$i_{r\_dc} = -S_{a\_r}i_{ar} - S_{b_r}i_{br} - S_{c\_r}i_{cr} \tag{3.70}$$

The current through the resistance is

$$i_{res} = \frac{V_{bus}}{R_{bus}} \tag{3.71}$$

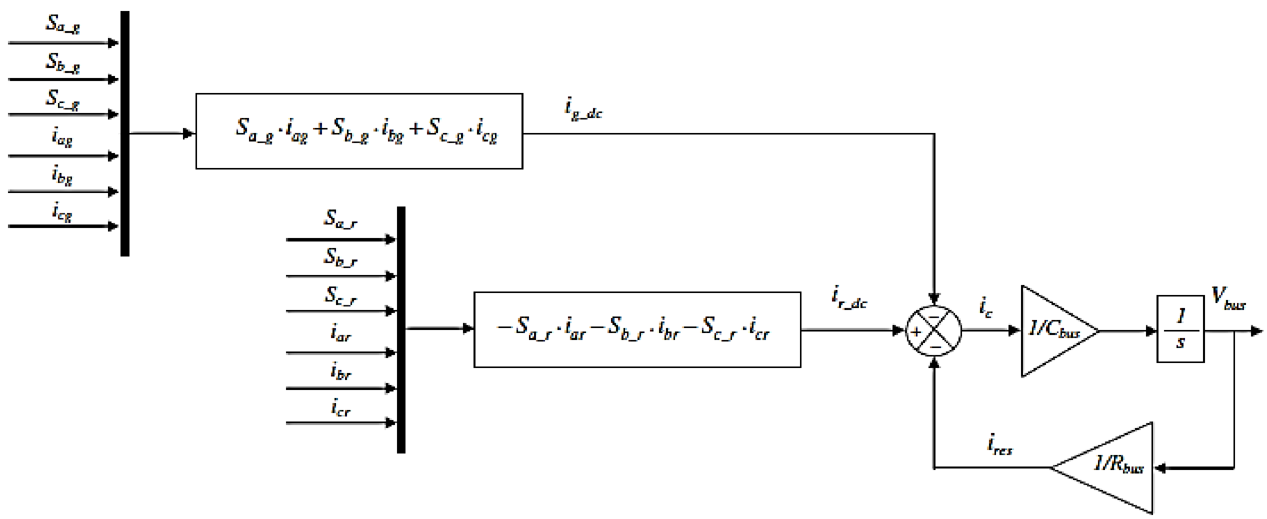

Figure 3.18: DC-Link Model (Abad et al., 2011)

3.3.7. Filter Model

The grid side filter, which is located between the grid and the converter is important to minimize the current and voltage harmonics generated by the switching of the converter. A simple and reliable solution adopts an inductive filter, locating an inductance in each phase. The grid voltage is modeled as an ideal three-phase balanced voltage. The three-phase system can be modeled as three independents, but equivalent, single-phase systems as depicted in Figure 3.18. Note that the output AC voltages of the converter, referred to the neutral point are named with the sub-index 'f' (Abad et al., 2011)(Abad, 2016).

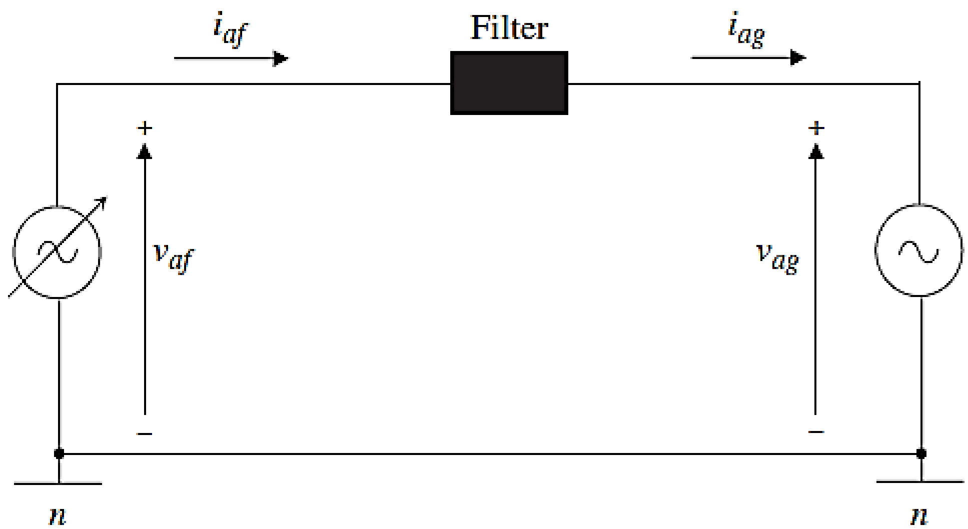

Figure 3.19: Equivalent Single-Phase Grid Circuit (a phase) (Abad, 2016)

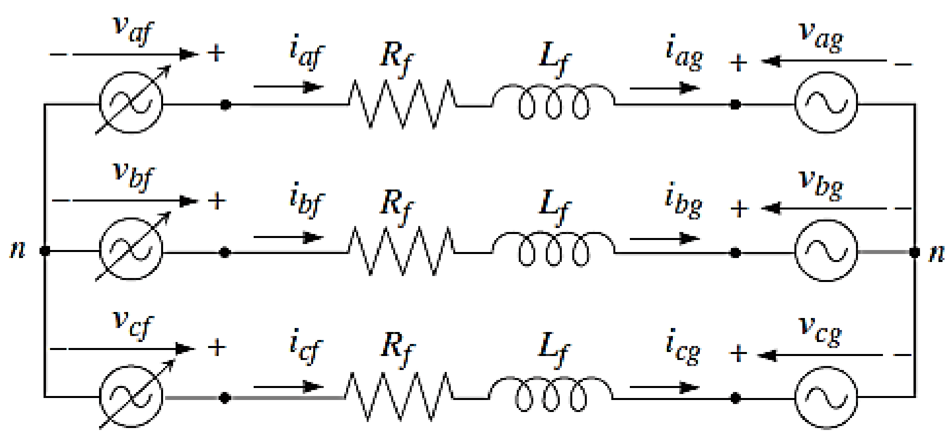

Figure 3.20: Simplified Representation of the Three-Phase Grid System with an L Filter (Abad, 2016)

Thus, the electric equation of the system can easily be derived as (Abad et al., 2011)

$$\begin{cases} V_{af} = R_f i_{ag} + L_f \frac{di_{ag}}{dt} + V_{ag} \\ V_{bf} = R_f i_{bg} + L_f \frac{di_{bg}}{dt} + V_{bg} \\ V_{cf} = R_f i_{cg} + L_f \frac{di_{cg}}{dt} + V_{cg} \end{cases} \quad (3.72)$$

Where, L_f is inductance of the grid side filter (H), R_f is resistive part of the grid side filter (O), $V_{ag}, V_{bg}, and\ V_{cg}$ are grid voltages (V), with ω_s electric angular speed in (rad/s), $i_{ag}, i_{bg}, and i_{cg}$

are currents flowing thorough the grid side converter's output (A), and $V_{af}, V_{bf}, and\ V_{cf}$ are output voltages of the converter referred to the neutral point of the load n (V).

Consequently, for modeling purposes, it is necessary to isolate the first derivative of the currents and the currents exchanged with the grid are calculated, taking into consideration the filter, according to expressions:

$$\begin{cases} \frac{di_{ag}}{dt} = \frac{1}{L_f}(V_{af} - R_f i_{ag} - V_{ag}) \\ \frac{di_{bg}}{dt} = \frac{1}{L_f}(V_{bf} - R_f i_{bg} - V_{bg}) \\ \frac{di_{cg}}{dt} = \frac{1}{L_f}(V_{cf} - R_f i_{cg} - V_{cg}) \end{cases} \tag{3.73}$$

3.3.8. Control System

When generating electricity in a wind turbine, the DFIG must and must be controlled. For proper and effective energy generation, control keeps generator magnitudes like torque and active and reactive power, as well as magnitudes related to the grid side converter like reactive power and DC bus voltage, close to their optimum values. DFIG control strategies come in a variety of forms, including Field Oriented Control (FOC) or vector control, direct torque/power control, predictive control, sensor-less control, and nonlinear control (Abad et al., 2011).

The ability to individually manage the generator's active and reactive power as well as low construction cost are the reasons that FOC or vector control was chosen for this thesis. Vector control of a grid-connected DFIG is controlled in a synchronously rotating dq reference frame, to govern the active and reactive power, the rotor current's d and q axis components are regulated.

3.3.8.1. Vector Control Strategy for RSC

Vector Control Strategy for RSC Stator voltage-oriented control and stator flux-oriented control are the two different types of vector control. For RSC if a reference frame orientated with the stator flux is used, the active and reactive power flows of the stator can be controlled independently by using the quadrature and the direct current, respectively.

The working principle is by neglecting the voltage drop in the stator resistance and assuming the stator flux is proportional to the grid voltage that is when the stator flux is oriented with the direct axis, and the voltage aligns with the quadrature axis (Abad et al., 2011)(Benbouhenni et al., 2018). The stator voltages in d-q axis become:

$$\begin{cases} V_{ds} = 0, \Psi_{ds} = \Psi_s \\ V_{qs} = V_g \approx \omega_s \Psi_s \end{cases} \tag{3.74}$$

The stator active and reactive power can be written as:

$$\begin{cases} P_s = \frac{3}{2}\left(V_{ds} i_{ds} + V_{qs} i_{qs}\right) = \frac{3}{2} V_{qs} i_{qs} \\ Q_s = \frac{3}{2}\left(V_{qs} i_{ds} - V_{ds} i_{qs}\right) = \frac{3}{2} V_{qs} i_{ds} \end{cases} \tag{3.75}$$

Under stator flux orientation, the equation for determining the relation between the current and flux is:

$$\begin{cases} i_{ds} L_s + i_{dr} L_m = \Psi_s \\ i_{qs} L_s + i_{qr} L_m = 0 \end{cases} \tag{3.76}$$

The relationship between the rotor and the stator current is determined by applying the above equation is:

$$\begin{cases} i_{ds} = \frac{\Psi_s}{L_s} - \frac{L_m}{L_s} i_{dr} \\ i_{qs} = -\frac{L_m}{L_s} i_{qr} \end{cases} \tag{3.77}$$

Substituting equation (3.74) into (3.72) and solving for the rotor currents which has the main role in controlling the stator active and reactive powers:

$$\begin{cases} i_{qr} = \frac{-2}{3} \frac{L_s}{L_m} \frac{P_s}{V_g} \\ i_{dr} = \frac{V_g}{\omega_s L_m} \frac{-2}{3} \frac{L_s}{L_m} \frac{Q_s}{V_g} = \frac{-L_s}{L_m} \left(\frac{-V_g}{\omega_s L_s} + \frac{2}{3} \frac{Q_s}{V_g}\right) \end{cases} \tag{3.78}$$

By using the last equation, the SIMULINK model of PQ control for RSC becomes:

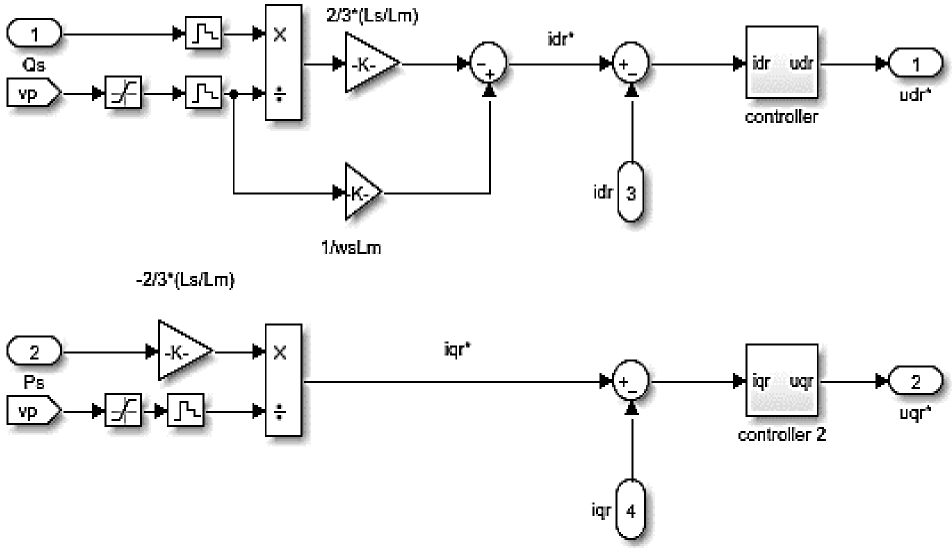

Figure 3.21: SIMULNK Model of PQ Control for RSC with PI Controller

To calculate the controller parameters, the relationship between the rotor voltage and the rotor currents must be known (Abad et al., 2011).

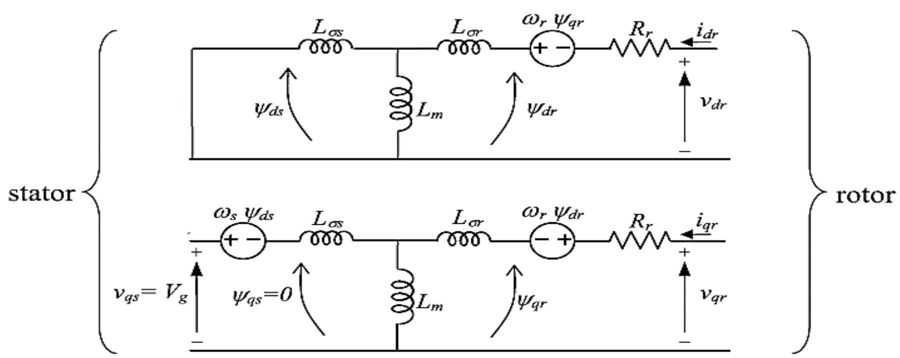

Figure 3.22: Equivalent Circuit of the DFIG (Abad et al., 2011)

The voltage at rotor terminals corresponds to the sum of the voltage drop in the resistance Rr and the voltage induced by the flux (Abad et al., 2011).

This can be written mathematically as:

$$\begin{cases} V_{dr} = R_r i_{dr} - \omega_r \Psi_{qr} + \frac{d\Psi_{dr}}{dt} \\ V_{qr} = R_r i_{qr} + \omega_r \Psi_{dr} + \frac{d\Psi_{qr}}{dt} \end{cases} \tag{3.79}$$

The relationship between this flux and the rotor current is:

$$\begin{cases} \Psi_{dr} = \left(L_r - \frac{{L_m}^2}{L_s}\right) i_{dr} + \frac{L_m}{L_s} \Psi_{ds} \\ \Psi_{qr} = \left(L_r - \frac{{L_m}^2}{L_s}\right) i_{qr} \end{cases} \tag{3.80}$$

The proportionality ratio between the fluxes and the currents is referred to as the transitory inductance of the rotor, σLr, and is the result of adding in series the rotor leakage inductance with the parallel magnetizing and the stator leakage inductance:

$$\left(L_r - \frac{{L_m}^2}{L_s}\right) = L_{\sigma r} + L_m // L_{\sigma s} = \sigma L_r \tag{3.81}$$

Where σ is leakage coefficient of the generator.

$$\sigma = 1 - \frac{L_m^2}{L_s L_r} \tag{3.82}$$

Substituting equation (3.77) into (3.76),then the voltage equation become:

$$\begin{cases} V_{dr} = R_r i_{dr} - \omega_r \sigma L_r i_{qr} + \sigma L_r \frac{di_{dr}}{dt} + \frac{L_m}{L_s} \frac{d\Psi_{ds}}{dt} \\ V_{qr} = R_r i_{qr} + \omega_r \sigma L_r i_{dr} + \sigma L_r \frac{di_{qr}}{dt} + \omega_r \frac{L_m}{L_s} \Psi_{ds} \end{cases} \tag{3.83}$$

During regular operation, when the grid voltage is constant in amplitude, the derivative of the flux Ψ_{ds} is zero.

So, V_{dr} become:

$$V_{dr} = R_r i_{dr} - \omega_r \sigma L_r i_{qr} + \sigma L_r \frac{di_{dr}}{dt} \tag{3.84}$$

From a control perspective, the term $\omega_r \frac{L_m}{L_s} \Psi_{ds}$ is a perturbation since it depends on the stator flux or the grid voltage, an external variable independent of the loop. As it is constant, it will easily be compensated for by the controller.

In the Figure 3.25, the resulting equations are graphically represented as:

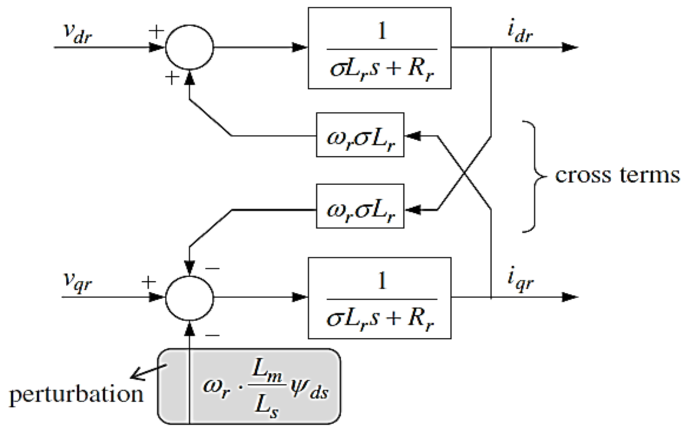

Figure 3.23: Current Control Loop for Rotor Side Control (Abad et al., 2011)

The cross-terms are the terms represented in the middle of the figure. When the reference frame rotates at a different rate than the rotor terminals, then these terms appear. Although, these components are constant throughout a permanent regime and do not impact how the control loops function.

3.3.8.2. Vector Control Strategy for GSC

Controlling the GSC is mostly done to regulate the DC bus voltage and the transmission of power through the converter, with regulated reactive power exchange. The active power that is generated for the wind turbine flow through the rotor must cross the DC-link and then it must be transmitted to the grid. Therefore, by controlling the bus voltage to a constant value, it is possible to ensure the flow of active power through the converters.

The vector control strategy of the grid-connected converter is typically developed from the system modeled in *dq* components. Thus, in order to further simplify the model equations (3.66), typically, the space vector of the grid voltage V_g is aligned with the *d* axis of the *dq* rotating reference frame (Abad, 2016). Therefore, the resulting *dq* components of the grid voltage yield:

$$\begin{cases} V_{dg} = V_g \\ V_{qg} = 0 \end{cases} \tag{3.85}$$

The active and reactive power in the grid side can be simplified as:

$$\begin{cases} P_g = \frac{3}{2}\left(V_{dg} i_{dg} + V_{qg} i_{qg}\right) = \frac{3}{2} V_{dg} i_{dg} \\ Q_g = \frac{3}{2}\left(V_{qg} i_{dg} - V_{dg} i_{qg}\right) = -\frac{3}{2} V_{dg} i_{qg} \end{cases} \tag{3.86}$$

On other hand, the active and reactive power calculated in the terminals of the converter is not the same as the power in the grid terminals.

The power at the converter output is calculated as follows:

$$\begin{cases} P_f = \frac{3}{2}\left(V_{df} i_{dg} + V_{qf} i_{qg}\right) \\ Q_f = \frac{3}{2}\left(V_{qf} i_{dg} - V_{df} i_{qg}\right) \end{cases} \tag{3.87}$$

This grid voltage alignment not only slightly simplifies the active and reactive power equations of the system, but also reduces the voltage equation.

Therefore, expressions (3.66) is simplified to

$$\begin{cases} V_{df} = R_f i_{dg} + L_f \frac{di_{dg}}{dt} + V_{dg} - \omega_s L_f i_{qg} \\ V_{qf} = R_f i_{qg} + L_f \frac{di_{qg}}{dt} + \omega_s L_f i_{dg} \end{cases} \tag{3.88}$$

Then, substituting the voltage expression in to equation (3.87) and the power at the converter output is:

$$\begin{cases} P_f = \frac{3}{2}\left(R_f i_g^2 + V_{dg} i_{dg}\right) \\ Q_f = \frac{3}{2}\left(L_f \omega_s i_g^2 - V_{dg} i_{qg}\right) \end{cases} \tag{3.89}$$

Finally, the SIMULINK model of PQ control for GSC becomes:

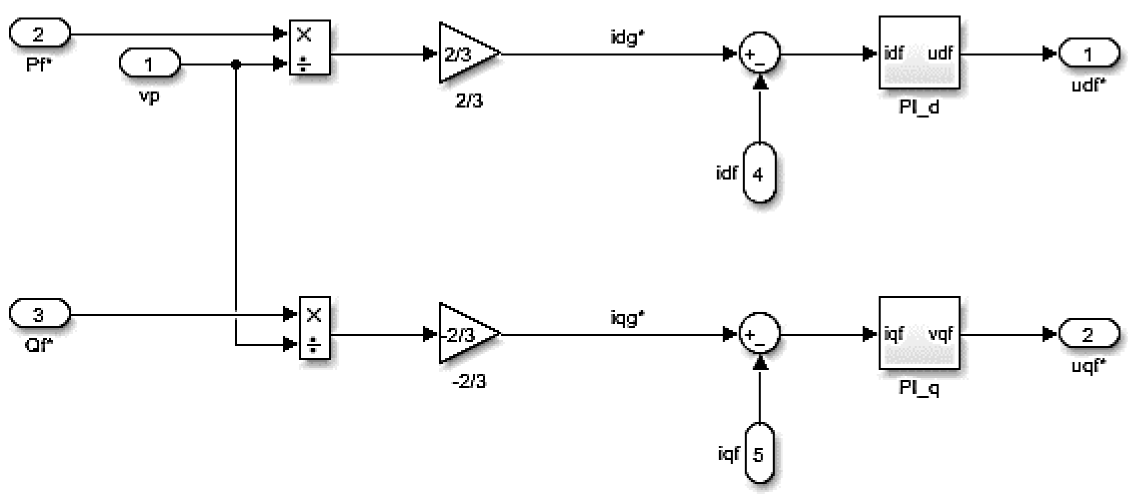

Figure 3.24: SIMULNK Model of PQ Control for GSC with PI Controller

3.4. Controller Design

In any control system, controllers are critical for minimizing the error between actual and measured values. In this system the controllers ensure that the actual currents follow the references current to control active and reactive power. Different controllers are available to control the power. In this thesis work PI controller, fuzzy logic controller, and super twisted sliding mode controller are used.

3.4.1. PI Controller

This controller is the simplest control method but it is highly affected by internal and external parameter variations and the gains are calculated according to the DFIG parameters.

3.4.1.1. PI Controller for RSC Control

To calculate the controller parameters, It is necessary to understand how the rotor voltage and currents relate to one another. The relationship between the rotor voltage and current is stated in equation (3.83).

The simplified transfer function is:

$$\frac{i_{dr}(s)}{i_{dr}^{*}(s)} = \frac{sk_p + k_i}{s^2\sigma L_r + s(k_p + R_r) + k_i} \tag{3.90}$$

$$\frac{i_{qr}(s)}{i_{qr}^{*}(s)} = \frac{sk_p + k_i}{s^2\sigma L_r + s(k_p + R_r) + k_i} \tag{3.91}$$

There are various methods provided by classical control theories that tune the PI regulators of closed current control loops. But, the simple method is the second order of the general control transfer function (Abad et al., 2011). Then denominator of this transfer function is compared to the above transfer function:

$$s^2\sigma L_r + s(k_p + R_r) + k_i = s^2 + 2\xi\omega_n + \omega_n^2 \tag{3.92}$$

Where, ω_n is the natural frequency and ξ is the damping ratio.

$$s^2 + s\left(\frac{k_p + R_r}{\sigma L_r}\right) + \frac{k_i}{\sigma L_r} = s^2 + 2\xi\omega_n + \omega_n^2 \tag{3.93}$$

From the above equation k_p and k_i became:

$$\begin{cases} k_p = 2\xi\sigma L_r\omega_n - R_r \\ k_i = \sigma L_r\omega_n^2 \end{cases} \tag{3.94}$$

The poles of the closed-loop system ω_n can be *x* times faster than the open-loop poles $\frac{\sigma L_r}{R_r}$.

Then, ω_n become:

$$\omega_n = \frac{x}{\frac{\sigma L_r}{R_r}} \tag{3.95}$$

The system is with double poles, then the damping ratio ξ= 1, and let taking x =100, then k_p and k_i become: $K_p = 2.204\ and\ K_i = \frac{2.204}{0.0003}$

$K_t = \frac{1}{0.0003}$, the main goal of K_i is to avoid the over value in the Integrator, therefore the Integration output will be kept with in a limited range.

3.4.1.2. PI Controller for GSC Control

Once the dq current reference components are obtained. Then, they are passed by their corresponding PI regulators. Note that the cancelation of the coupling terms is also carried out at the output of the current PI regulators. The current versus voltage equations of the electric model equations for the L filter yield (Senapati, 2014):

$$\begin{cases} V_{df} = R_f i_{dg} + L_f \frac{di_{dg}}{dt} \\ V_{qf} = R_f i_{qg} + L_f \frac{di_{qg}}{dt} \end{cases} \tag{3.96}$$

When applying the Laplace transformation to the above equation, the following transfer functions are derived:

$$\begin{cases} \frac{i_{dg}(s)}{V_{df}(s)} = \frac{1}{L_f s + R_f} \\ \frac{i_{qg}(s)}{V_{qf}(s)} = \frac{1}{L_f s + R_f} \end{cases} \tag{3.97}$$

The simplified transfer function is:

$$\frac{i_{dg}(s)}{i^*_{dg}(s)} = \frac{s k_p + k_i}{s^2 L_f + s(k_p + R_f) + k_i} \tag{3.98}$$

$$\frac{i_{qg}(s)}{i^*_{qg}(s)} = \frac{s k_p + k_i}{s^2 L_f + s(k_p + R_f) + k_i} \tag{3.99}$$

There are various methods provided by classical control theories that tune the PI regulators of closed current control loops. But, the simple method is the second order of the general control transfer function (Abad et al., 2011). Then denominator of this transfer function is compared to the above transfer function:

$$s^2 L_f + s(k_p + R_f) + k_i = s^2 + 2\xi\omega_n + \omega_n^2 \tag{3.100}$$

From the above equation k_p and k_i become: $\begin{cases} k_p = 2\xi L_f \omega_n - R_f \\ k_i = L_f \omega_n^2 \end{cases}$ (3.101)

And ω_n and ξ values can be chosen by any of the pole placement methods of classic control theories. For this system ξ and $\omega_n = 2\pi 200$ rad/sec has been chosen, which means we obtain two equal real poles, then k_p and k_i become: $K_p = 1.25,\ K_i = \frac{1.25}{0.0016}\, and\ K_t = \frac{1}{0.0016}$

3.4.1.3. PI Controller for DC-Link Voltage Control

The dc link voltage has to get controlled to deliver optimized power through the converter to the grid. Due to variations in the power the generator produces, the DC voltage may experience transient circumstances. Voltage overshoot and voltage undershoot are both caused by changes in the amount of power produced.

To control this voltage variation using PI the k_p and k_i be

$$\begin{cases} k_p = 2\xi C_{dc} - \omega_n \\ k_i = C_{dc}\omega_n^2 \end{cases} \tag{3.102}$$

Where C_{dc} =15μF and k_p and k_i become: $K_p = 0.19,\ K_i = \frac{0.19}{0.00031}\ and\ K_t = \frac{1}{0.00031}$

The PI controller design on MATLAB Simulink is:

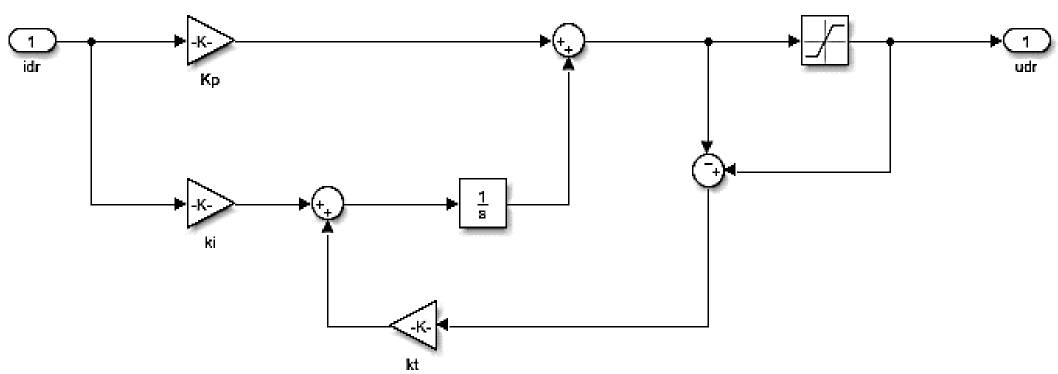

Figure 3.25: PI Controller in MATLAB Simulink

3.4.2. Fuzzy Logic Controller (FLC)

For modeling FLC in MATLAB, the first is identifying the number and defining input-output parameters. After that, the next step is creating the membership function and rule base. In this thesis, the FLC has two inputs, namely current error and change in current error, and has one output, namely voltage.

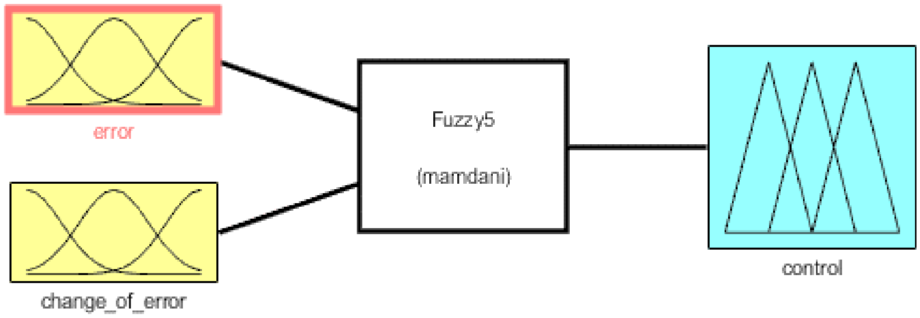

Figure 3.26: Fuzzy Logic Design

The design consists of seven triangular membership functions for Mamdani-type inputs and output. The membership function is expressed as NB: negative big, NM: negative medium, NS: negative small, Z: zero, PS: positive small, PM: positive medium, and PB: positive big. The ranges of MFs are determined simply by trial and error method.

The range of error is chosen as [-290 1600].

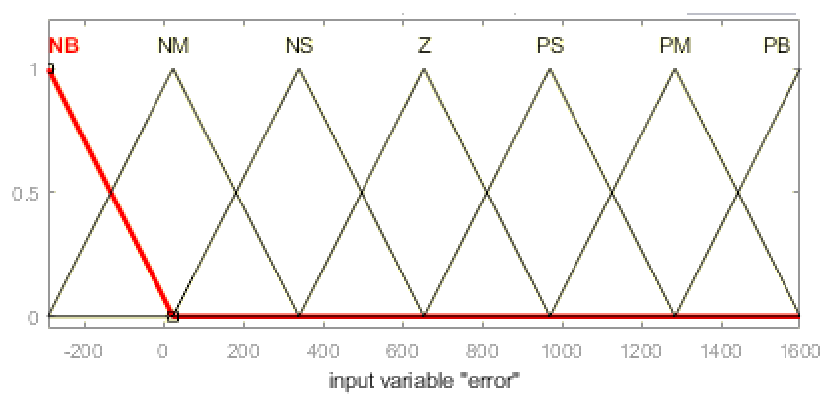

Figure 3.27: Current Error Membership Function

The range of change in error is chosen as $[-1.2 \times 10^7 \quad 3 \times 10^7]$.

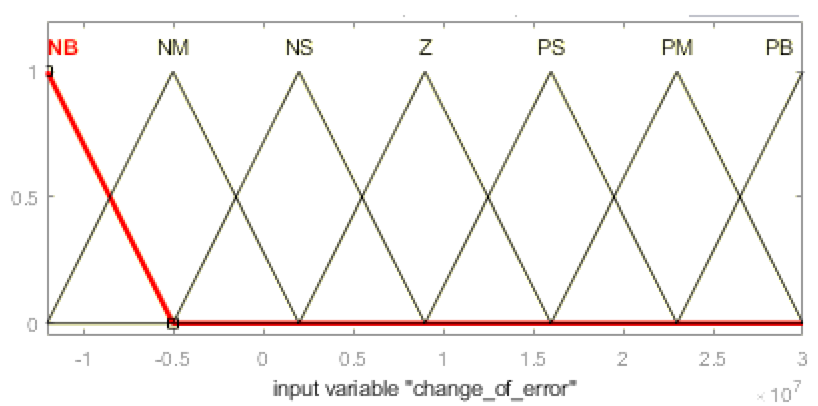

Figure 3.28: Change in Current error Membership Function

The range of output is chosen as [-290 1600].

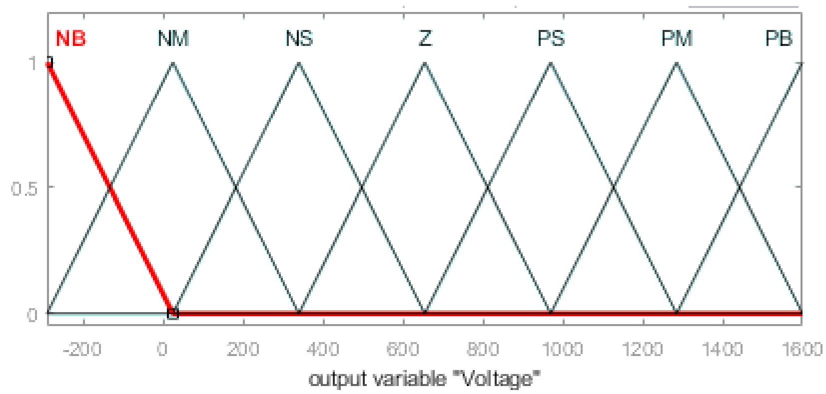

Figure 3.29: Voltage Membership Function

In this thesis, the rule base taken is a common control rule base (CRB) and is designed with 49 'If-Then' rules as shown in table 3.1.

Table 3.1: Fuzzy Rule Base with Seven MFs

Δe \ e	NB	NM	NS	Z	PS	PM	PB
NB	NB	NB	NB	NB	NM	NS	Z
NM	NB	NB	NB	NM	NS	Z	PS
NS	NB	NB	NM	NS	Z	PS	PM
Z	NB	NM	NS	Z	PS	PM	PB
PS	NM	NS	Z	PS	PM	PB	PB
PM	NS	Z	PS	PM	PB	PB	PB
PB	Z	PS	PM	PB	PB	PB	PB

The FLC design on MATLAB Simulink is:

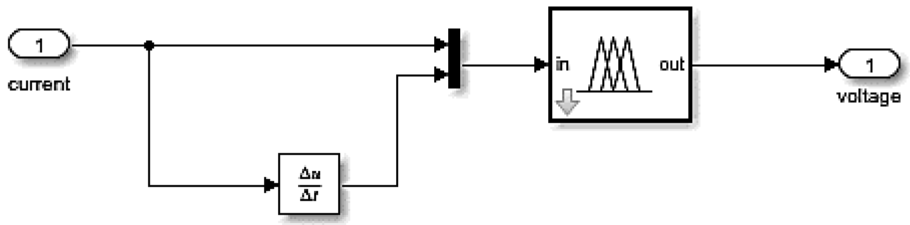

Figure 3.30: FLC in MATLAB Simulink

3.4.3. Super Twisted Sliding Mode Controller (STSMC)

The controller structure is divided into two sections, one of which represents dynamics in the sliding mode and the other of which represents the discontinuous dynamics system in the convergence mode. Three crucial phases can be taken to create the control's design, and each of these processes depends on the previous one (Senapati, 2014):

1. The choice of surface

There are various types of sliding surfaces, and each one performs better in a particular application. In general, the surface must a nonlinear surface. The nonlinear form is a function of the error on the controlled variable (x), and it is given by (Senapati, 2014):

$$S(x) = \left(\frac{\partial}{\partial t} + \lambda\right)^{r-1} * e(x) \quad (3.103)$$

where, r is the relative degree of the system, it means the number of times to derive the surface to obtain the control, λ is a positive constant and $e(x)$ is the error between the variable and its reference.

When r = 1, then $S(x) = e(x)$

2. Setting of the convergence conditions

The conditions different dynamics of the convergence criteria enable the system to converge to the sliding surface and maintain it regardless of the disturbance. There are two considerations to ensure the convergence mode (Senapati, 2014).

- The discrete function switching

This is the first convergence condition. We have to give to the surface a dynamic converging to zero. It is given by:

$$\begin{cases} \dot{S}(X) > 0 \; if \; S(X) < 0 \\ \dot{S}(X) < 0 \; if \; S(X) > 0 \end{cases} \tag{3.104}$$

It can be written as:

$$\dot{S}(X).S(X) < 0 \tag{3.105}$$

- Lyapunov function

The Lyapunov function is a positive scalar function $V(x) > 0$ for the state variables of the system. The idea is to choose a scalar function to ensure the attraction of the variable to be controlled to its reference value or to guarantee the stability of the nonlinear systems (Senapati, 2014).
The Lyapunov function as follows:

$$V(X) = \frac{1}{2} S^2(X) \tag{3.106}$$

To ensure the convergence of the Lyapunov function, it is sufficient to guarantee that:

$$\dot{S}(X).S(X) < 0 \tag{3.107}$$

3. Determination of the control law

The structure of a sliding mode controller consists of two parts. The first one concerns the exact linearization (U_{eq}), and the second one concerns the stabilization (U_n).

$$U = U_{eq} + U_n \tag{3.108}$$

where U_{eq}corresponds to the control. It serves to maintain the variable control on the sliding surface and U_n is the discrete control determined to check the convergence condition.

$$U_n = -K_s \; sgn(S) \tag{3.109}$$

Where K_s is a positive number and $sgn(S)$ is defined as follows (Senapati, 2014):

$$sgn(S) = \begin{cases} 1 & for \; S > 0 \\ 0 & for \; S = 0 \\ -1 & for \; S < 1 \end{cases} \tag{3.110}$$

In this control law, when selecting the gain K_s, there has be a compromise between chattering and reaching time. If K_s is too small the reaching time for the system would be too long and if K_s is too high there will be too much chattering in the system. So, when selecting this gain there has to be a compromise between the two.

- **Mathematical Model of Conventional SMC for RSC using the above steps**

To control Q_s

Sliding surface become:

$$S(Q_s) = e(Q_s) = i_{dr}^* - i_{dr} \tag{3.111}$$

In order to force the chosen variables to converge to their reference values it needs that surface of sliding are driven to zero.

$$\dot{S}(Q_s) = \dot{e}(Q_s) = \frac{d}{dt}(i_{dr}{}^* - i_{dr}) = 0 \tag{3.112}$$

From equation (3.84) find $\frac{di_{dr}}{dt}$ and substitute to $\dot{S}(Q_s)$

$$\frac{di_{dr}}{dt} = \frac{V_{dr} - R_r i_{dr} + \omega_r \sigma L_r i_{qr}}{\sigma L_r} \tag{3.113}$$

$$\frac{d}{dt}(i_{dr}{}^* - i_{dr}) = \dot{i}_{dr}{}^* - \left(\frac{V_{dr} - R_r i_{dr} + \omega_r \sigma L_r i_{qr}}{\sigma L_r}\right) = 0 \tag{3.114}$$

$$\sigma L_r \dot{i}_{dr}{}^* - V_{dr} + R_r i_{dr} - \omega_r \sigma L_r i_{qr} = 0 \tag{3.115}$$

Finally, find V_{dr}

$$V_{dr} = \sigma L_r \dot{i}_{dr}{}^* + R_r i_{dr} - \omega_r \sigma L_r i_{qr} \tag{3.116}$$

This V_{dr} is V_{dr_eq}. So, the total V_{dr} become:

$$V_{dr} = \sigma L_r \dot{i}_{dr}{}^* + R_r i_{dr} - \omega_r \sigma L_r i_{qr} - K_s\, sgn(S) \tag{3.117}$$

To control P_s

Sliding surface become:

$$S(P_s) = e(P_s) = i_{qr}^* - i_{qr} \tag{3.118}$$

In order to force the chosen variables to converge to their reference values it needs that surface of sliding are driven to zero.

$$\dot{S}(P_s) = \dot{e}(P_s) = \frac{d}{dt}\left(i_{qr}{}^* - i_{qr}\right) = 0 \tag{3.119}$$

From equation (3.83) find $\frac{di_{qr}}{dt}$ and substitute to $\dot{S}(P_s)$

$$\frac{di_{qr}}{dt} = \frac{V_{qr} - R_r i_{qr} - \omega_r \sigma L_r i_{dr} - \omega_r \frac{Lm}{L_s} \Psi_{ds}}{\sigma L_r} \tag{3.120}$$

$$\frac{d}{dt}({i_{qr}}^{*} - i_{qr}) = \dot{\iota_{qr}}^{*} - (\frac{V_{qr} - R_r i_{qr} - \omega_r \sigma L_r i_{dr} - \omega_r \frac{L_m}{L_s}\Psi_{ds}}{\sigma L_r}) = 0 \quad (3.121)$$

$$\sigma L_r \dot{\iota_{qr}}^{*} - V_{qr} + R_r i_{qr} - \omega_r \sigma L_r i_{dr} + \omega_r \frac{L_m}{L_s}\Psi_{ds} = 0 \quad (3.122)$$

Finally, find V_{qr}

This V_{qr} is V_{qr_eq}. So, the total V_{qr} become:

$$V_{qr} = \sigma L_r \dot{\iota_{qr}}^{*} + R_r i_{qr} + \omega_r \sigma L_r i_{dr} + \omega_r \frac{L_m}{L_s}\Psi_{ds} - K_s\, sgn(S) \quad (3.123)$$

- **Mathematical Model of Conventional SMC for GSC using the above steps**

To control P_f

Sliding surface become:

$$S(P_f) = e(P_f) = i_{dg}^{*} - i_{dg} \quad (3.124)$$

In order to force the chosen variables to converge to their reference values it needs that surface of sliding are driven to zero.

$$\dot{S}(P_f) = \dot{e}(P_f) = \frac{d}{dt}({i_{dg}}^{*} - i_{dg}) = 0 \quad (3.125)$$

From equation (3.88) find $\frac{di_{dg}}{dt}$ and substitute to $\dot{S}(P_f)$

$$\frac{di_{dg}}{dt} = \frac{V_{df} - R_f i_{dg} - V_{dg} + \omega_s L_f i_{qg}}{L_f} \quad (3.126)$$

$$\frac{d}{dt}({i_{dg}}^{*} - i_{dg}) = \dot{\iota_{dg}}^{*} - (\frac{V_{df} - R_f i_{dg} - V_{dg} + \omega_s L_f i_{qg}}{L_f}) = 0 \quad (3.127)$$

$$L_f \dot{\iota_{dg}}^{*} - V_{df} + R_f i_{dg} + V_{dg} - \omega_s L_f i_{qg} = 0 \quad (3.128)$$

Finally, find V_{df}

$$V_{df} = L_f \dot{\iota_{dg}}^{*} + R_f i_{dg} + V_{dg} - \omega_s L_f i_{qg} \quad (3.129)$$

This V_{df} is V_{df_eq}. So, the total V_{df} become:

$$V_{df} = L_f \dot{\iota_{dg}}^{*} + R_f i_{dg} + V_{dg} - \omega_s L_f i_{qg} - K_s\, sgn(S) \quad (3.130)$$

To control Q_f

Sliding surface become:

$$S(Q_f) = e(Q_f) = i_{qg}^{*} - i_{qg} \tag{3.131}$$

In order to force the chosen variables to converge to their reference values it needs that surface of sliding are driven to zero.

$$\dot{S}(Q_f) = \dot{e}(Q_f) = \frac{d}{dt}\left(i_{qg}{}^{*} - i_{qg}\right) = 0 \tag{3.132}$$

From equation (3.88) find $\frac{di_{qg}}{dt}$ and substitute to $\dot{S}(Q_f)$

$$\frac{di_{qg}}{dt} = \frac{V_{qf} - R_f i_{qg} - \omega_s L_f i_{dg}}{L_f} \tag{3.133}$$

$$\frac{d}{dt}(i_{qg}{}^{*} - i_{qg}) = \dot{i}_{qg}{}^{*} - \left(\frac{V_{qf} - R_f i_{qg} - \omega_s L_f i_{dg}}{L_f}\right) = 0 \tag{3.134}$$

$$L_f \dot{i}_{qg}{}^{*} - V_{qf} + R_f i_{qg} + \omega_s L_f i_{dg} = 0 \tag{3.135}$$

Finally, find V_{qf}

$$V_{qf} = L_f \dot{i}_{qg}{}^{*} + R_f i_{qg} + \omega_s L_f i_{dg} \tag{3.136}$$

This V_{qf} is V_{qf_eq}. So, the total V_{qf} become:

$$V_{qf} = L_f \dot{i}_{qg}{}^{*} + R_f i_{qg} + \omega_s L_f i_{dg} - K_s\, sgn(S) \tag{3.137}$$

Super Twisted Sliding Mode Controller (STSMC)

A higher-order sliding mode control called STSMC prevents chattering while maintaining other sliding mode properties. A discontinuous sliding variable function and a continuous derivative function are part of it and expressed as

$$\begin{cases} U_n = -K_1\sqrt{|s|}\; sgn(S) + v \\ \dot{v} = -K_2\; sgn(S) \end{cases} \tag{3.138}$$

The gains are tuned by changing them until getting the best result using the trial and error method. $K_s = 4.5,\ K_1 = 6.2\ and\ K_2 = 9.3$ is selected.

The STSMC design for RSC on MATLAB Simulink is:

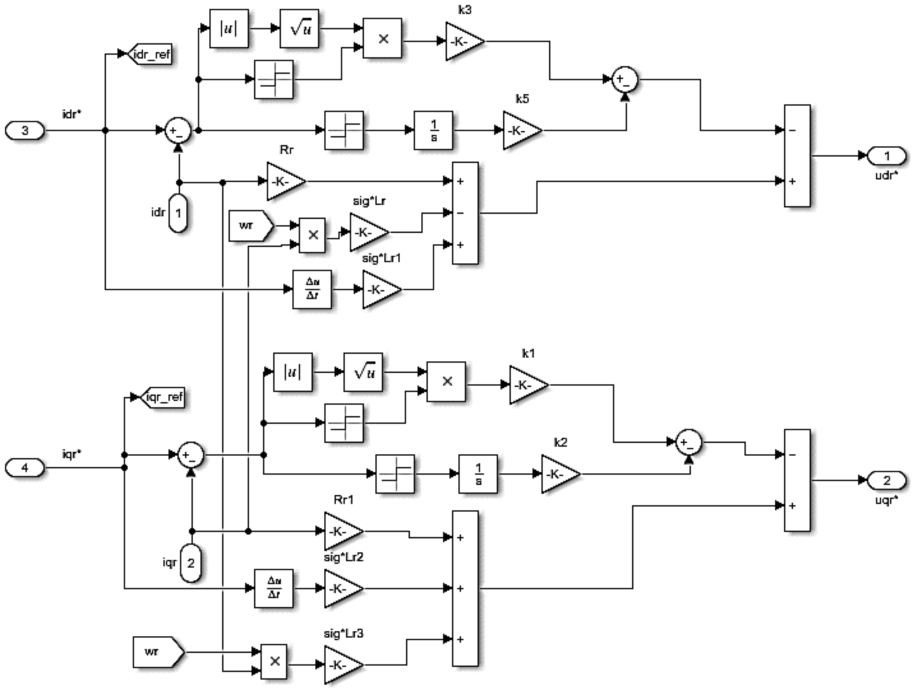

Figure 3.31: STSMC for RSC MATLAB Simulink

The STSMC design for GSC on MATLAB Simulink is:

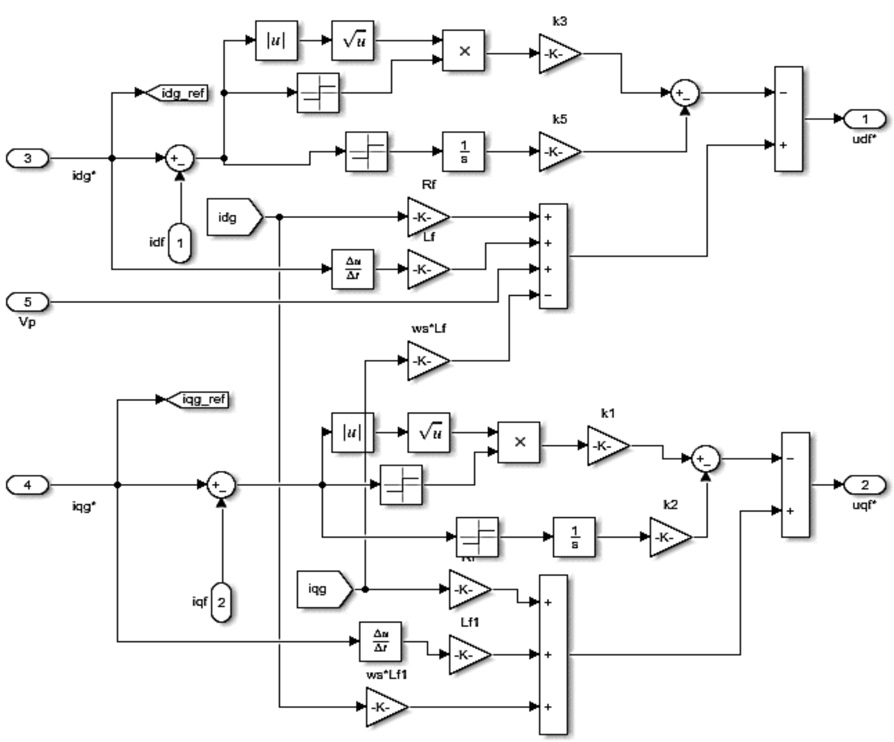

Figure 3.32: STSMC for GSC MATLAB Simulink

CHAPTER FOUR

4. RESULTS AND DISCUSSIONS

This section discusses the results of the MATLAB/SIMULINK simulation and displays the simulation results for the designed controller system. The objective of this work was to control active and reactive power flow for wind speed variation and comparative analysis of controllers.

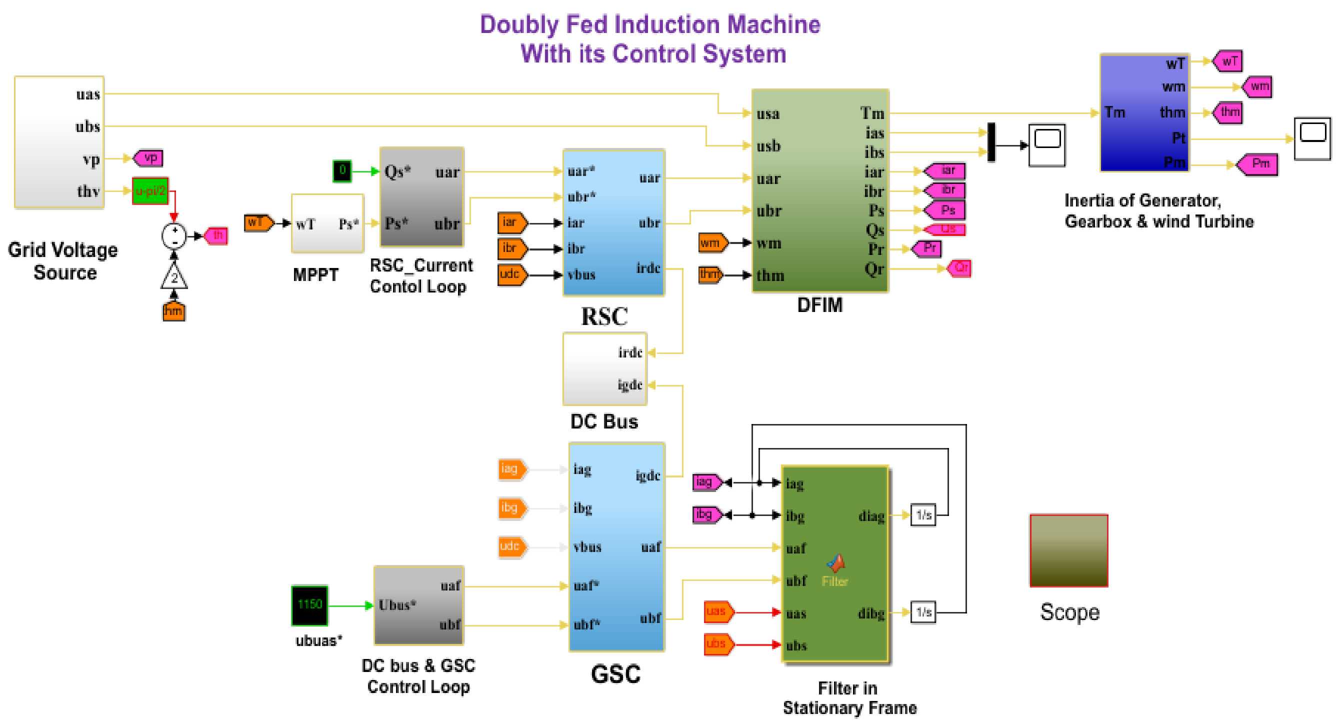

Figure 4.1: Overall Model of the WECS with Control System

4.1. Results

This section will analyze the different results of the simulation. The simulated system comprises a DFIG connected to the 690V, 50Hz grid. The time for the simulation is 10 sec. Variable wind speed from lower to higher [6 6 9 9 12 12 9 9 6 6] taken. The active and reactive powers are controlled using PI, Fuzzy, and STSMC controllers separately with the vector control techniques. All controllers' references and actual power are plotted side by side on the same scale and according to the time domain specification for comparison.

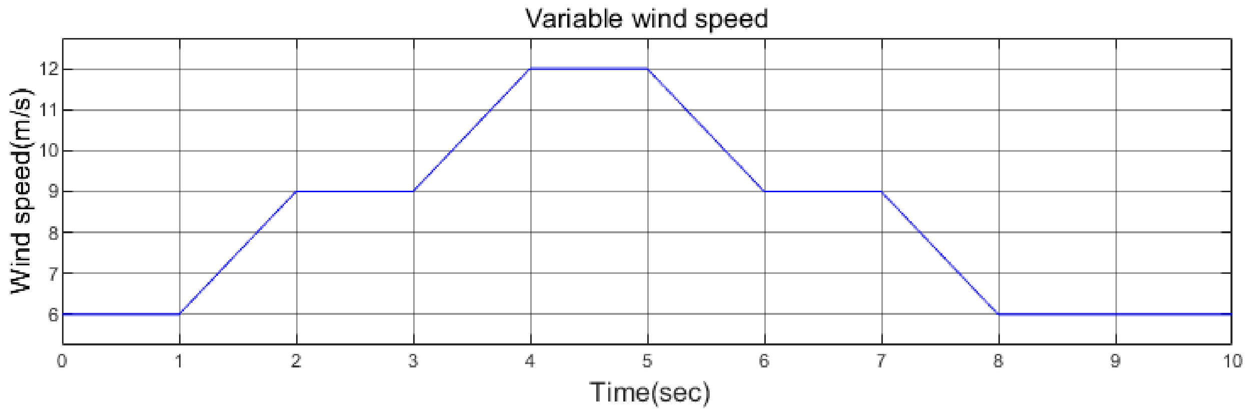

Figure 4.2: Variable Wind Speed

4.1.1. Active and reactive power result using PI controller

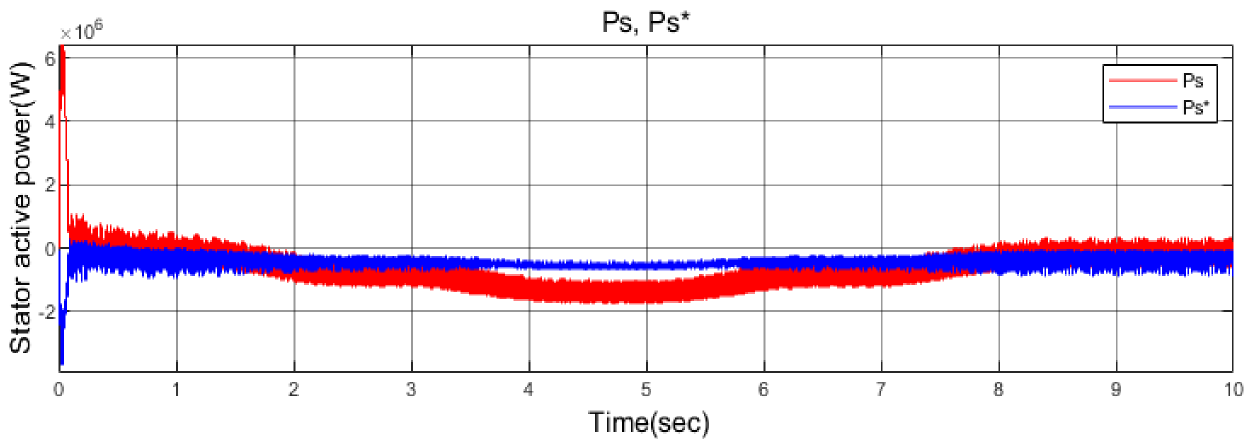

(a)

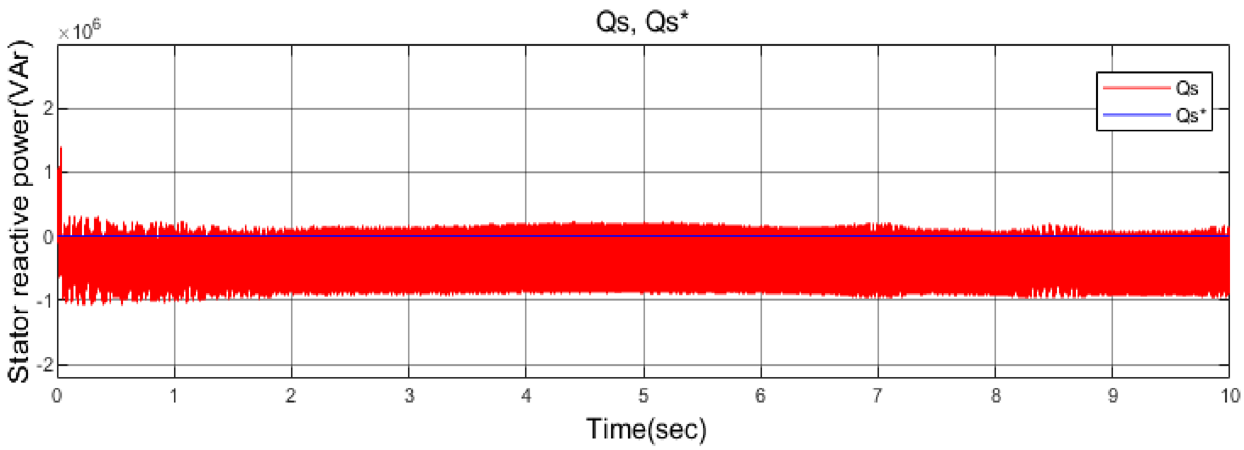

(b)

Figure 4.3: Stator Active and Reactive Power

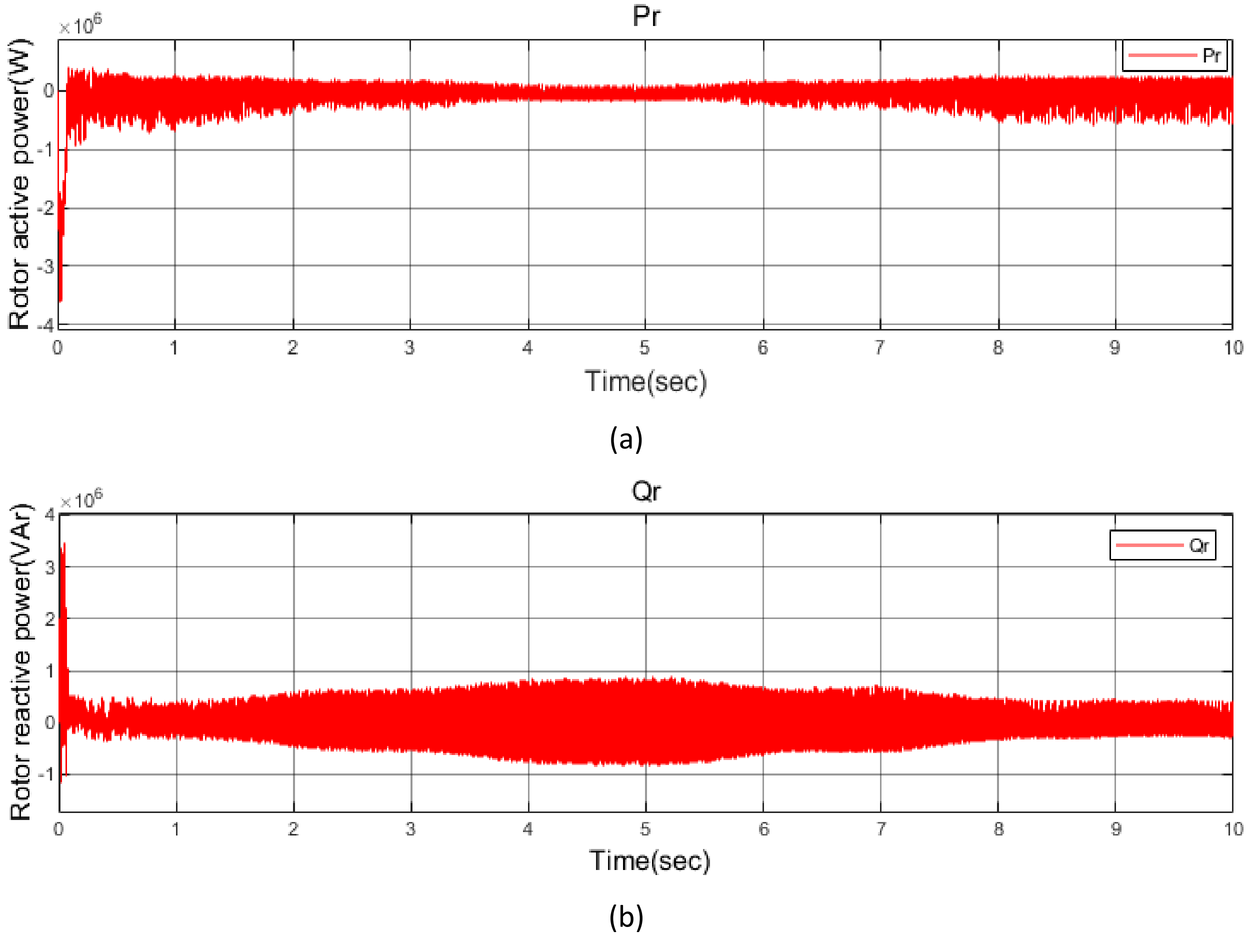

Figure 4.4: Rotor Active and Reactive Power

The active and reactive powers supplied by the stator and rotor utilizing the PI controller are shown in Figures 5.3 and 5.4, respectively. Due to the machine's super synchronous speed and operation as a generator, the active powers of the stator and rotor are negative. The stator and rotor supply active power to the grid by directly connecting to the grid and using power converters, respectively. The stator generates almost all of the power, but the rotor at maximum speed generates close to zero. Depending on the wind speed, varying amount of power are generated as the wind speed increases, and so does the power. Both stator and rotor reactive power are near zero. However, there is a high deviation at high wind speeds as the machine tries to support the grid with reactive power. As a result, the power factor is not kept at unity, and results have chattering. Therefore, the system's stability cannot be maintained.

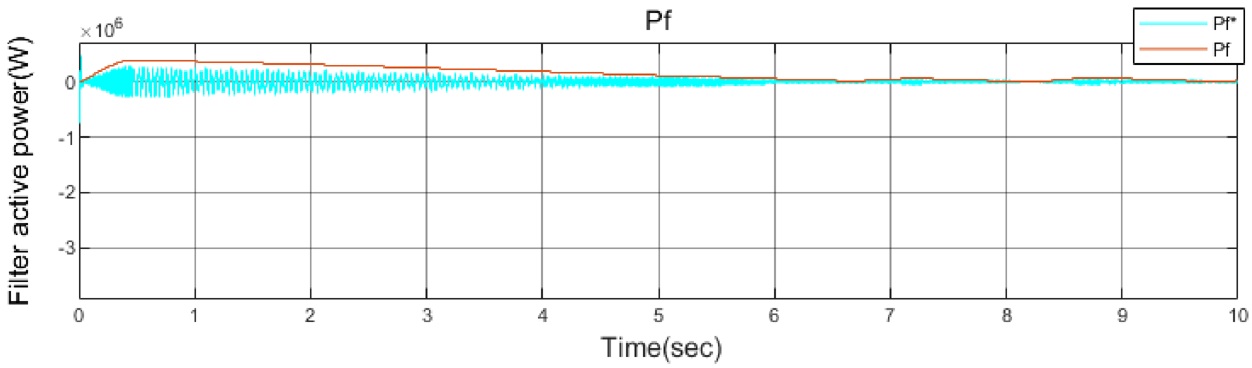

(a)

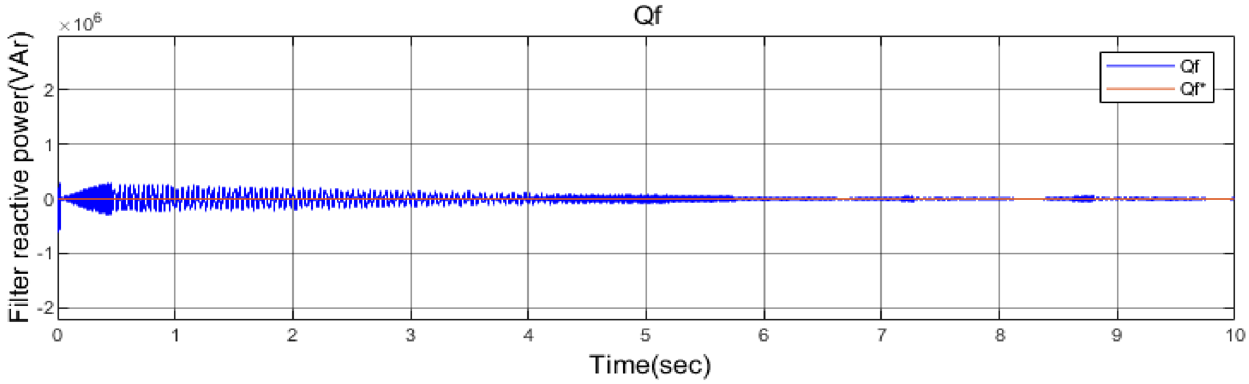

(b)

Figure 4.5: Grid Active and Reactive Power

The grid's active power is near 0.3 MW, and its reactive power is approaching zero. Due to the machines operating at super synchronous speed, the power flows from the generator to the grid through the stator and rotor, so the active and reactive power approach to zero. Also, have chattering.

4.1.2. Active and reactive power result using FLC

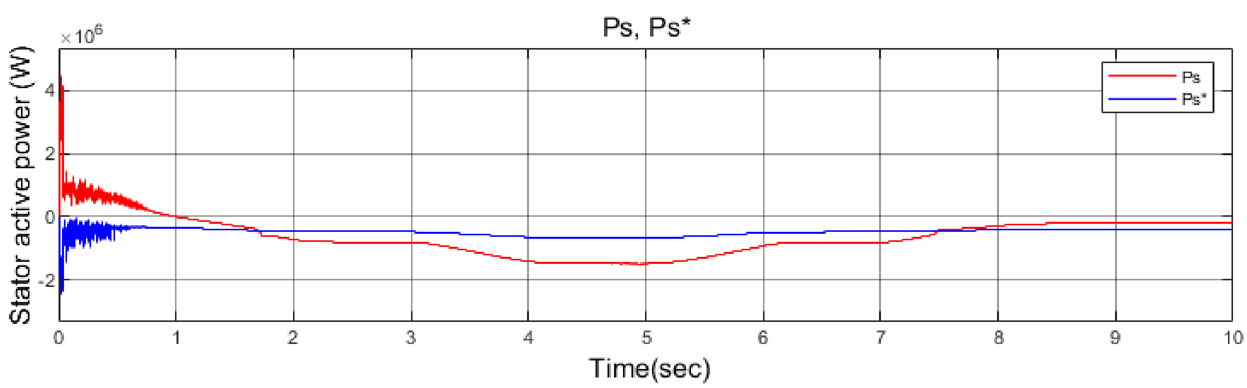

(a)

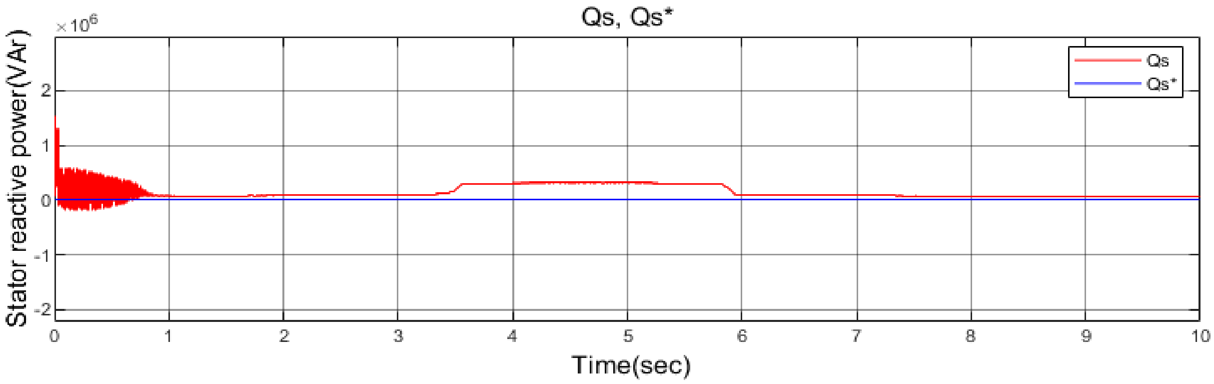

(b)

Figure 4.6: Stator Active and Reactive Power

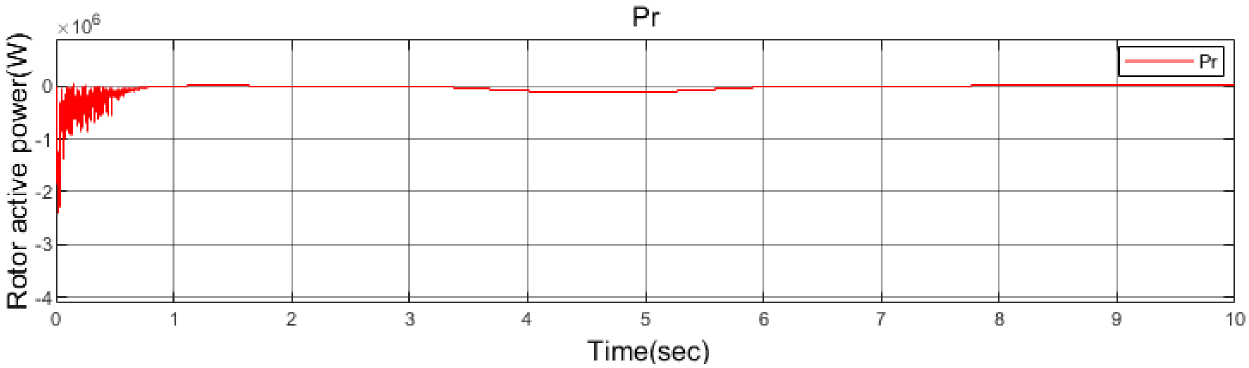

(a)

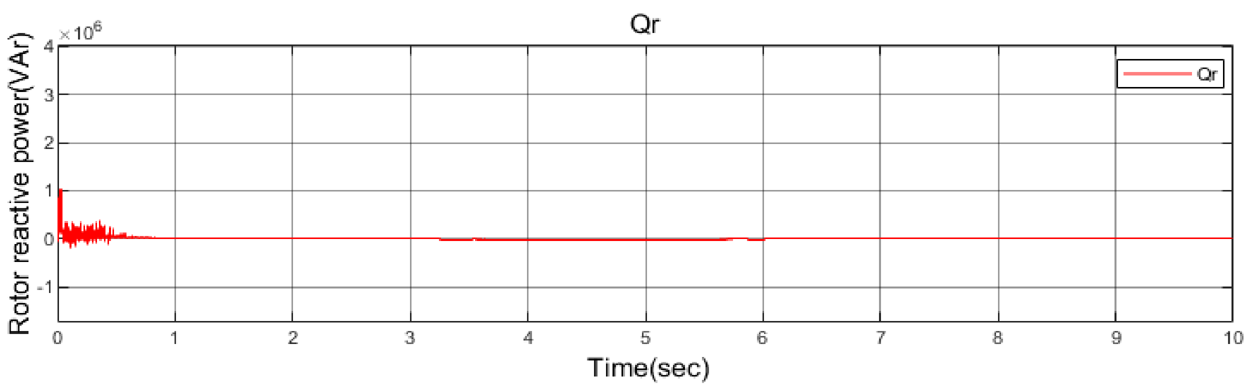

(b)

Figure 4.7: Rotor Active and Reactive Power

The stator and rotor active power is similar to the results in PI, but it is free for chattering, and the deviation is a starting point only. And both have low overshoot and settle less than 1 sec than the PI. The stator and rotor reactive power is more approach to zero, but at maximum speed, stator reactive power is slightly generated. However, this controller is better than PI in maintaining stability.

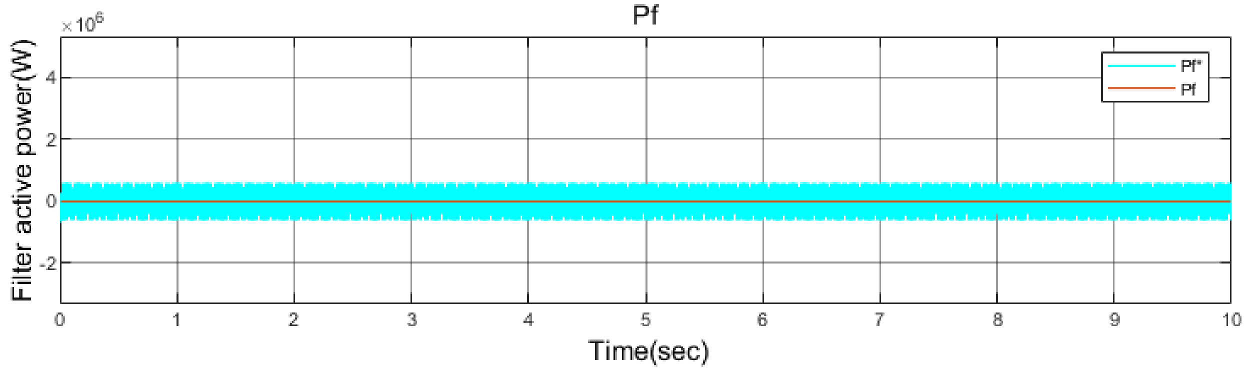

(a)

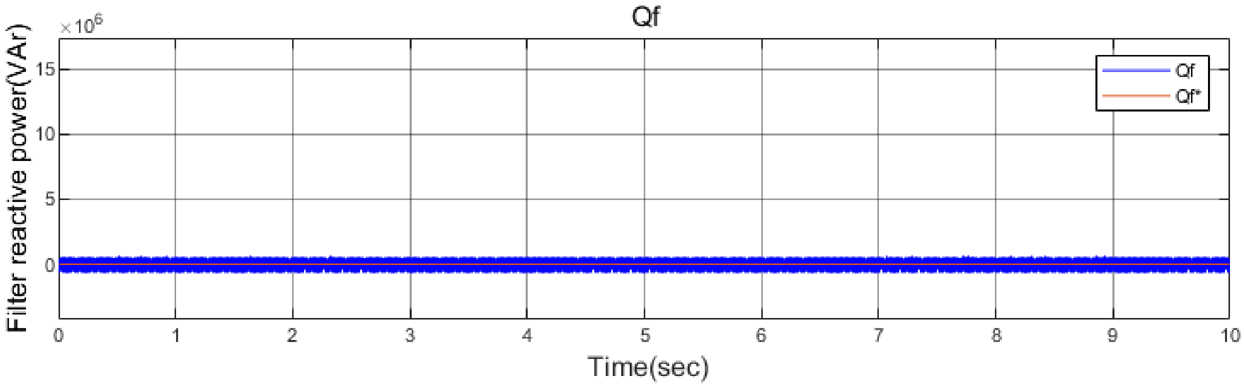

(b)

Figure 4.8: Grid Active and Reactive Power

Both the grid's active and reactive power approach to zero is because the generator is supplying the power to the grid, and it is a better faster to settle than PI.

4.1.3. Active and reactive power result using STSMC

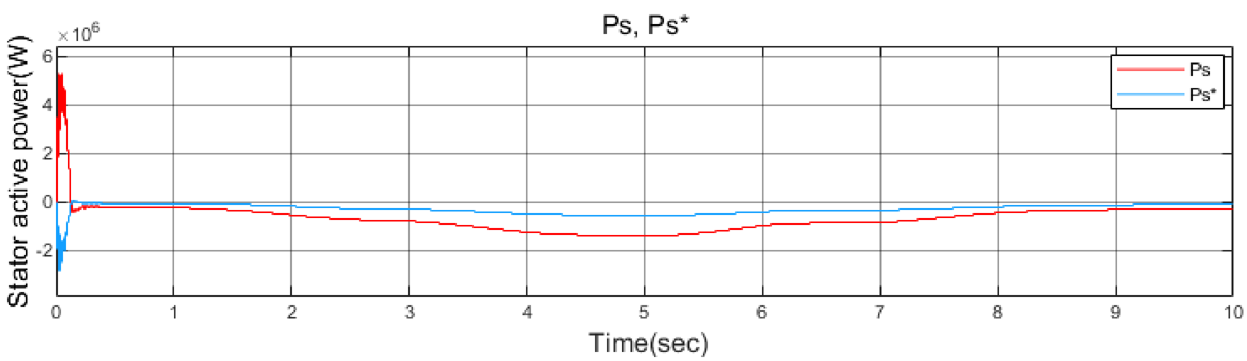

(a)

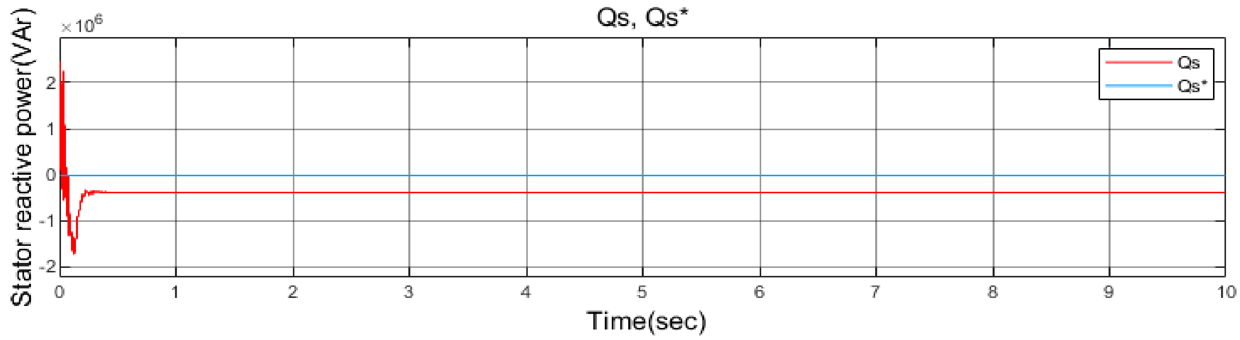

(b)

Figure 4.9: Stator Active and Reactive Power

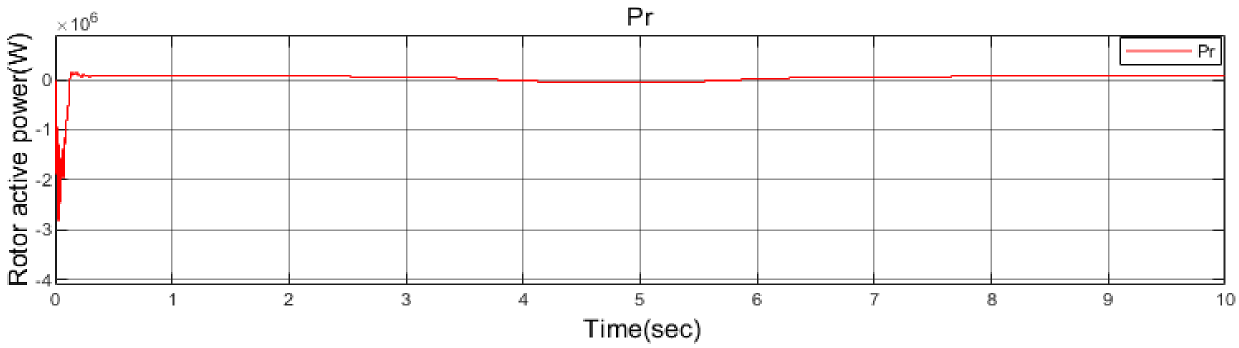

(a)

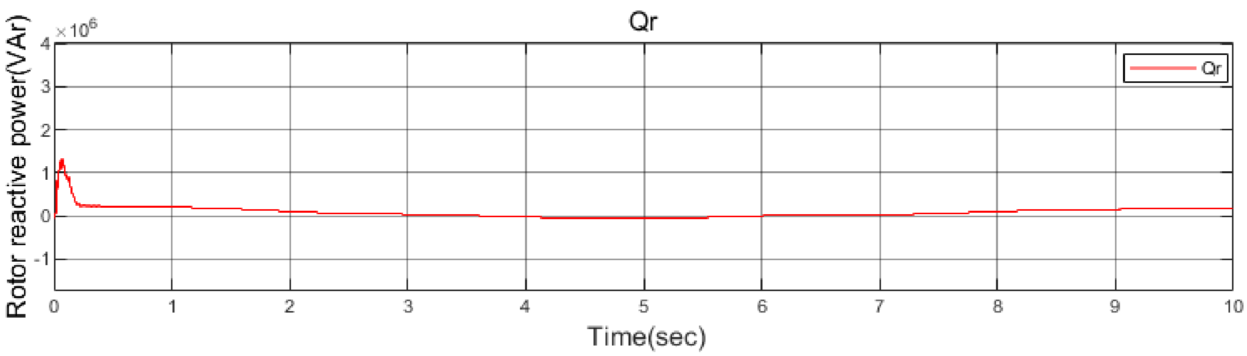

(b)

Figure 4.10: Rotor Active and Reactive Power

Performance-wise, this controller outperforms FLC and PI. As can be observed from the Figure 5.9 a and 5.10 a, the variation at the beginning has been significantly decreased to 0.1 seconds and is chatter-free. The stator and rotor reactive power is close to zero and constant. Consequently, it is possible to improve the system's stability.

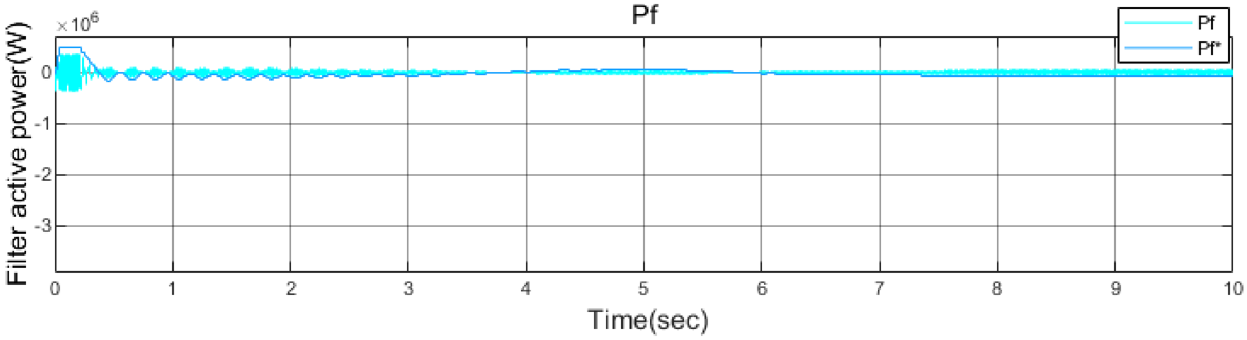

(a)

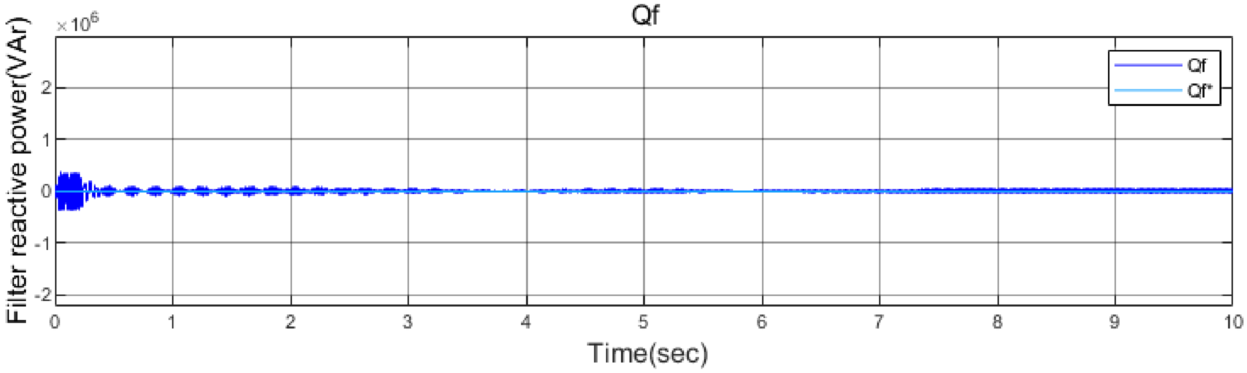

(b)

Figure 4.11: Grid Active and Reactive Power

The simulation is at Super-synchronous speed, so the active and reactive power of the grid approach to zero because the power flow is from the generator to the grid.

4.2. Discussions

Comparison of controllers performance based on rise time, settling time, and overshoot for stater active power.

Table 4.1: Controllers Dynamic Performance Comparison

Controllers	Controller performance		
	Rise time(sec)	Settling time(sec)	Overshoot (%)
PI	0.2134	1.0351	3.9
FLC	0.1082	0.8021	2.8
STSMC	0.0017	0.3314	2.2

The above results show the DFIG modeled system simulated that has extracted power from the wind turbine, and controlling the power as a function of wind speed varies. The main objective of a wind energy conversion system with DFIG control techniques is to extract as maximum power as possible from the wind and regulate it as needed. The system is monotonic because there is only one rotor or turbine speed that will produce the maximum power for each wind speed. However, a variable wind speed due to the application of an induction generator is connected by back to back converter and can control power flow to track the desired signal. It is seen that the generator can provide the maximum active power and nearly no reactive power, giving a unity power factor.

The simulations are done with the same wind speed source and reference power inputs to the system. The result shows an improved performance in terms of settling time, overshoot and rise time for active power. The response shows that the PI has a settling time of 1.0351 sec and an overshoot of 3.9 %. Whereas FLC has a settling time of 0.8021 sec and an overshoot of 2.8 %. The last STSMC has a settling time of 0.3314 sec and an overshoot of 2.2 %. According to this results, STSMC is better and more robust than the other two for both active and reactive power.

CHAPTER FIVE

5. CONCLUSIONS AND RECOMMENDATIONS

5.1. Conclusions

This thesis essentially sought to explain active and reactive power control schemes for DFIG-based wind turbine systems. The study thoroughly explains a wind turbine system's theoretical and mathematical model. The vector-control technique is used to independently control the flow of active and reactive power between the DFIG stator and the grid. Under random wind fluctuation, MATLAB Simulink is used to obtain the response characteristic. The simulation has demonstrated that the control strategy has a high ability to extract the most wind energy possible and adapt to a wind turbine at varying wind speeds. Three control strategies are used to manage the active and reactive power. Control techniques are compared using reference power tracking and stability analysis. Practically, PI controllers are used most often in wind power applications. It does, however, have a high initial overshoot issue based on the results above. When properly constructed, modern FLC can mitigate the limitations of PI controllers, however fuzzy controllers might produce errors if they are not properly designed. The STSMC controller is characterized by high precision, stability, simplicity, quick response, and robustness.

Based on the outcomes of the simulation with the wind speed altering its value, the response shows that the PI has a settling time of 1.0351 sec and an overshoot of 3.9 %. Whereas FLC has a settling time of 0.8021 sec and an overshoot of 2.8 %. The last STSMC has a settling time of 0.3314 sec and an overshoot of 2.2 %. So, it is suggested as a potential replacement controller to govern the active and reactive power of DFIG more than others in a balanced grid system.

5.2. Recommendations

The controller comparison to control active and reactive power was the main topic of the study. Based on the study STSMC has better performance in wind power systems, so it is very recommendable to use in practical applications.

Research Fund Acknowledgement

This research project is funded by Adama Science and Technology University under the grant number ASTU/SM-R/574/22, Adama, Ethiopia.

REFERENCES

Abad, G. (2016). Power Electronics and Electric Drives for Traction Applications. In *Power Electronics and Electric Drives for Traction Applications*. https://doi.org/10.1002/9781118954454

Abad, G., López, J., Rodríguez, M. A., Marroyo, L., & Iwanski, G. (2011). Doubly Fed Induction Machine. In *Doubly Fed Induction Machine*. https://doi.org/10.1002/9781118104965

Ackermann, T., & Söder, L. (2002). An overview of wind energy-status 2002. *Renewable and Sustainable Energy Reviews*, *6*(1–2), 67–127. https://doi.org/10.1016/S1364-0321(02)00008-4

Ahmed, W. K. (2013). Mechanical modelling of wind turbine: Comparative study. *International Journal of Renewable Energy Research*, *3*(1), 94–97.

Alta, H. (n.d.). *Ismail H. Altaş - Fuzzy Logic Control in Energy Systems with Design Applications in MatLab_Simulink-IET (2017).pdf*.

Becheri, H., Bousarhanne, I. K., Harrouz, A., Glaoui, H., & Belbekri, T. (2018). Maximum Power Point Tracking of Wind Turbine Conversion Chain Variable Speed Based on DFIG. *International Journal of Power Electronics and Drive Systems (IJPEDS)*, *9*(2), 527. https://doi.org/10.11591/ijpeds.v9.i2.pp527-535

Benbouhenni, H., Belaidi, A., Benbouhenni, H., Boudjema, Z., & Belaidi, A. (2018). Using Three-Level Fuzzy Space Vector Modulation Method to Improve Indirect Vector Control Strategy of a DFIG Based Wind Energy Conversion Systems. *International Journal of Smart Grid*. https://doi.org/10.20508/ijsmartgrid.v2i3.15.g16

Berhanu, M., Mekonnen, Y., Leidhold, R., Mamo, M., Muluneh, Z., & Sarwat, A. (2018). Analysis of a Doubly Fed Induction Generator Through Modeling and Simulation. *2018 IEEE PES/IAS PowerAfrica, PowerAfrica 2018*, 652–657. https://doi.org/10.1109/PowerAfrica.2018.8521094

Boubzizi, S., Abid, H., El hajjaji, A., & Chaabane, M. (2018). Comparative study of three types of controllers for DFIG in wind energy conversion system. *Protection and Control of*

Modern Power Systems, *3*(1), 1–12. https://doi.org/10.1186/s41601-018-0096-y

Burton, T., Jenkins, N., Sharpe, D., & Bossanyi, E. (2011). Conceptual Design of Horizontal Axis Wind Turbines. In *Wind Energy Handbook*. https://doi.org/10.1002/9781119992714.ch6

Chandrasekaran, S. (2014). *Grid Connected Doubly Fed Induction Generator Based Wind Turbine under LVRT*. *March*, 191.

Cherifi, D., & Miloud, Y. (2020). Hybrid control using adaptive fuzzy sliding mode control of doubly fed induction generator for wind energy conversion system. *Periodica Polytechnica Electrical Engineering and Computer Science*, *64*(4), 374–381. https://doi.org/10.3311/PPee.15508

Christensen, V. (2009). Ecopath with Ecosim: linking fi sheries and ecology 1 Why ecosystem modeling in fi sheries? *WIT Transactions on State of the Art in Science and Engineering*, *34*, 1755–8336. https://doi.org/10.2495/978-1-84564

Djeriri, Y., & Massoum, A. (n.d.). *A Comparative Study Between Field Oriented Control and Sliding Mode Control for Dfig Integrated in Wind Energy S ... A COMPARATIVE STUDY BETWEEN FIELD ORIENTED CONTROL*.

European Wind Energy Association. (2012). Wind Energy - The Facts. In *Wind Energy - The Facts*. https://doi.org/10.4324/9781849773782

Faculty, T. A., Qiao, W., & Fulfillment, I. P. (2008). Integrated Control of Wind Farms , Facts Devices and the Power Network Using Neural Networks and Adaptive Critic Designs Integrated Control of Wind Farms , Facts Devices and the Power Network Using Neural Networks and. *Computer Engineering*, *August*.

Fletcher, J., & Yang, J. (n.d.). *Introduction to Doubly-Fed Induction Generator for Wind Power Applications*.

Ganthia, B. P., & Barik, S. K. (2020). Steady-State and Dynamic Comparative Analysis of PI and Fuzzy Logic Controller in Stator Voltage Oriented Controlled DFIG Fed Wind Energy Conversion System. *Journal of The Institution of Engineers (India): Series B*, *101*(3), 273–286. https://doi.org/10.1007/s40031-020-00455-8

Haile, E. A., Worku, G. B., Beyene, A. M., & Tuka, M. B. (2021). Modeling of doubly fed induction generator based wind energy conversion system and speed controller. *Journal of Energy Systems*, *5*(1), 46–59. https://doi.org/10.30521/jes.854669

Hamane, B., & Member, M. L. D. (n.d.). *Direct Active and Reactive Power Control of DFIG based WECS using PI and Sliding Mode Controllers*. *5*.

Hussein, A. T., Manara, B., & Recherche, C. De. (2004). *flow control.* 580–584.

Ibrahim, R. K., & Watson, S. (n.d.). *Wind turbine simulation model for the study of combined mechanical and electrical faults*.

J.~Marques, H.~Pinheiro, H.~A.~Gründling, J.~R.~Pinheiro, & H.~L.~Hey. (2003). A Survey of Variable-Speed Wind Turbine System. *Proceedings of the 7th {B}razilian Power Electronics Conference (COBEP 2003)*, 732–738.

Jaballaafou, A., Madi, A. A., Addaim, A., & Intidam, A. (2020). Wind Power Production based on DFIG: Modeling and Control by ADRC. *20th IEEE Mediterranean Electrotechnical Conference, MELECON 2020 - Proceedings*, 517–522. https://doi.org/10.1109/MELECON48756.2020.9140611

Junyent-ferré, A., Gomis-bellmunt, O., Sumper, A., & Sala, M. (2010). *Simulation Modelling Practice and Theory Modeling and control of the doubly fed induction generator wind turbine*. *18*, 1365–1381. https://doi.org/10.1016/j.simpat.2010.05.018

Khalfallah, T., Cheikh, B., Tayeb, A., & Champenois, G. (2015). Power control of wind turbine based on fuzzy sliding-mode control. *International Journal of Power Electronics and Drive Systems*, *5*(4), 502–511. https://doi.org/10.11591/ijpeds.v5.i4.pp502-511

Mabrouk, H., & Boumediene, A. (2018). *The controlling of the DFIG Based Wind Energy Conversion System modeling and simulation*. *7*(May), 34–39.

Mazouz, F., Belkacem, S., Colak, I., & Drid, S. (2018). *Direct Power Control of DFIG by Sliding Mode Control and Space Vector Modulation*. 462–467.

Mitra, S. C. • M., & Sengupta, S. (2006). Electric Power Quality. In *ISBN 978-94-007-0634-* (Vol. 1999, Issue December).

O'Dwyer, A. (2006). Handbook of PI and PID controller tuning rules, 2nd Edition. In *Handbook of PI and PID Controller Tuning Rules, 2nd Edition*. https://doi.org/10.1142/P424

Qiao, W. (2009). Dynamic modeling and control of doubly fed induction generators driven by wind turbines. *2009 IEEE/PES Power Systems Conference and Exposition, PSCE 2009*. https://doi.org/10.1109/PSCE.2009.4840245

Rajendran, S., & Jena, D. (2014). Control of Variable Speed Variable Pitch Wind Turbine at Above and Below Rated Wind Speed. *Journal of Wind Energy, 2014*, 1–14. https://doi.org/10.1155/2014/709128

Rao, D. S. (2012). *Grid Connected DFIG With Efficient Rotor Power Flow Control Under Sub & Super Synchronous Modes of Operation*. *1*(6), 1–6.

Rekioua, D. (2014). *Wind Power Electric Systems*.

Sellami, M. H. (n.d.). *W IND E NERGY D EVELOPMENTS , P OTENTIAL*.

Senani, F., & Rah, A. (n.d.). *Active and Reac ctive Power Control of f DFIG using PI I and DPC controllers*.

Senapati, S. K. (2014). Modelling and Simulation of a Grid Connected Doubly Fed Induction Generator for Wind Energy Conversion System. *2014*.

Singh, M., & Santoso, S. (2012). Dynamic models for wind turbines and wind power plants. *Wind Power: Systems Engineering Applications and Design Models, October*, 93–204.

Sumathi, S., Ashok Kumar, L., & Surekha, P. (2015). Solar PV and Wind Energy Conversion Systems: Introduction to Theory, Modeling with MATLAB/SIMULINK, and the Role of Soft Computing Techniques. In *Green Energy and Technology*.

Tamaarat, A. (2019a). Active and Reactive Power Control for DFIG Using PI, Fuzzy Logic and Self-Tuning PI Fuzzy Controllers. *Advances in Modelling and Analysis C*, *74*(2–4), 95–102. https://doi.org/10.18280/ama_c.742-408

Tamaarat, A. (2019b). *Active and Reactive Power Control for DFIG Using PI , Fuzzy Logic and Self-Tuning PI Fuzzy Controllers d φ*. *74*(2), 95–102.

Tapia, A., Tapia, G., & Ostolaza, J. X. (2003). *Modeling and Control of a Wind Turbine Driven*

Doubly Fed Induction Generator. *18*(2), 194–204.

Thomas, T. (2020). *Event analysis and real-time validation of doubly fed induction generator-based wind energy system with grid reactive power exchange under sub-synchronous and super-synchronous modes*. *August*, 1–21. https://doi.org/10.1002/eng2.12282

Tiwari, R., & Babu, N. R. (2016). Recent developments of control strategies for wind energy conversion system. *Renewable and Sustainable Energy Reviews*, *66*, 268–285. https://doi.org/10.1016/j.rser.2016.08.005

Wu, M., & Xie, L. (2018). Calculating steady-state operating conditions for DFIG-based wind turbines. *IEEE Transactions on Sustainable Energy*, *9*(1), 293–301. https://doi.org/10.1109/TSTE.2017.2731661

Zouggar, E. O., Chaouch, S., Abdeslam, D. O., & Abdelhamid, A. L. (2019). Sliding control with fuzzy type-2 controller of wind energy system based on doubly fed induction generator. *Instrumentation Mesure Metrologie*, *18*(2), 137–146. https://doi.org/10.18280/i2m.180207

APPENDICES

APPENDICE A

Inertia of Generator, gearbox & wind turbine model

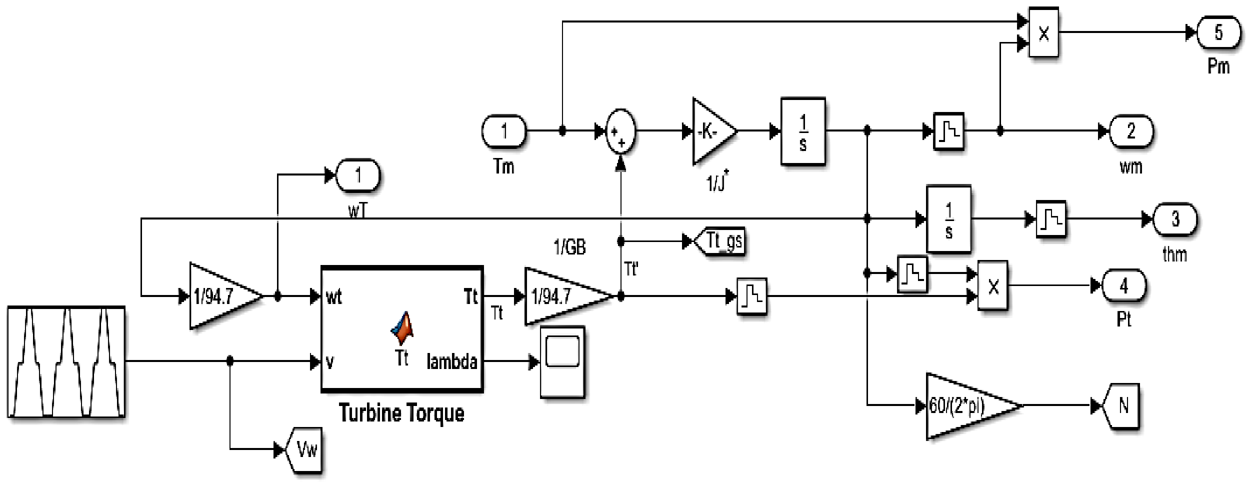

Figure A-1: Wind Turbine Model

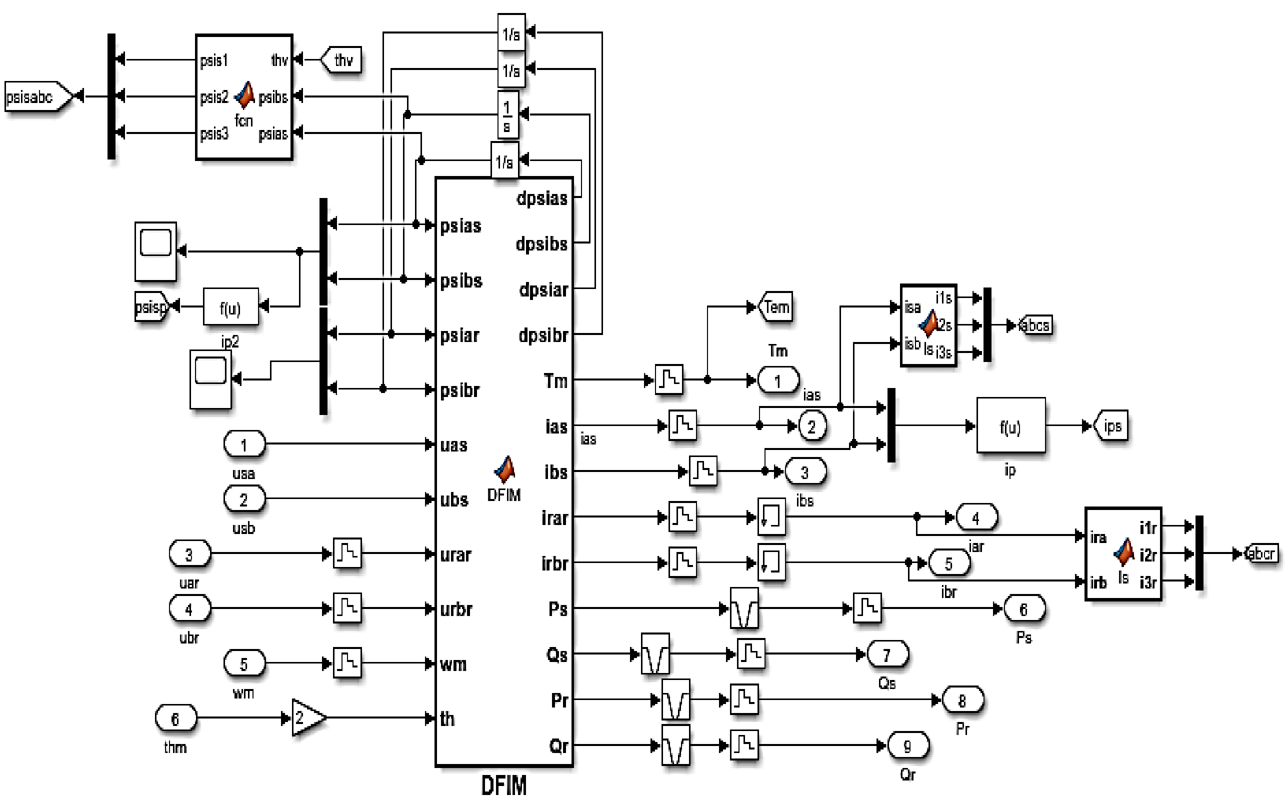

Figure A-2: DFIM Model

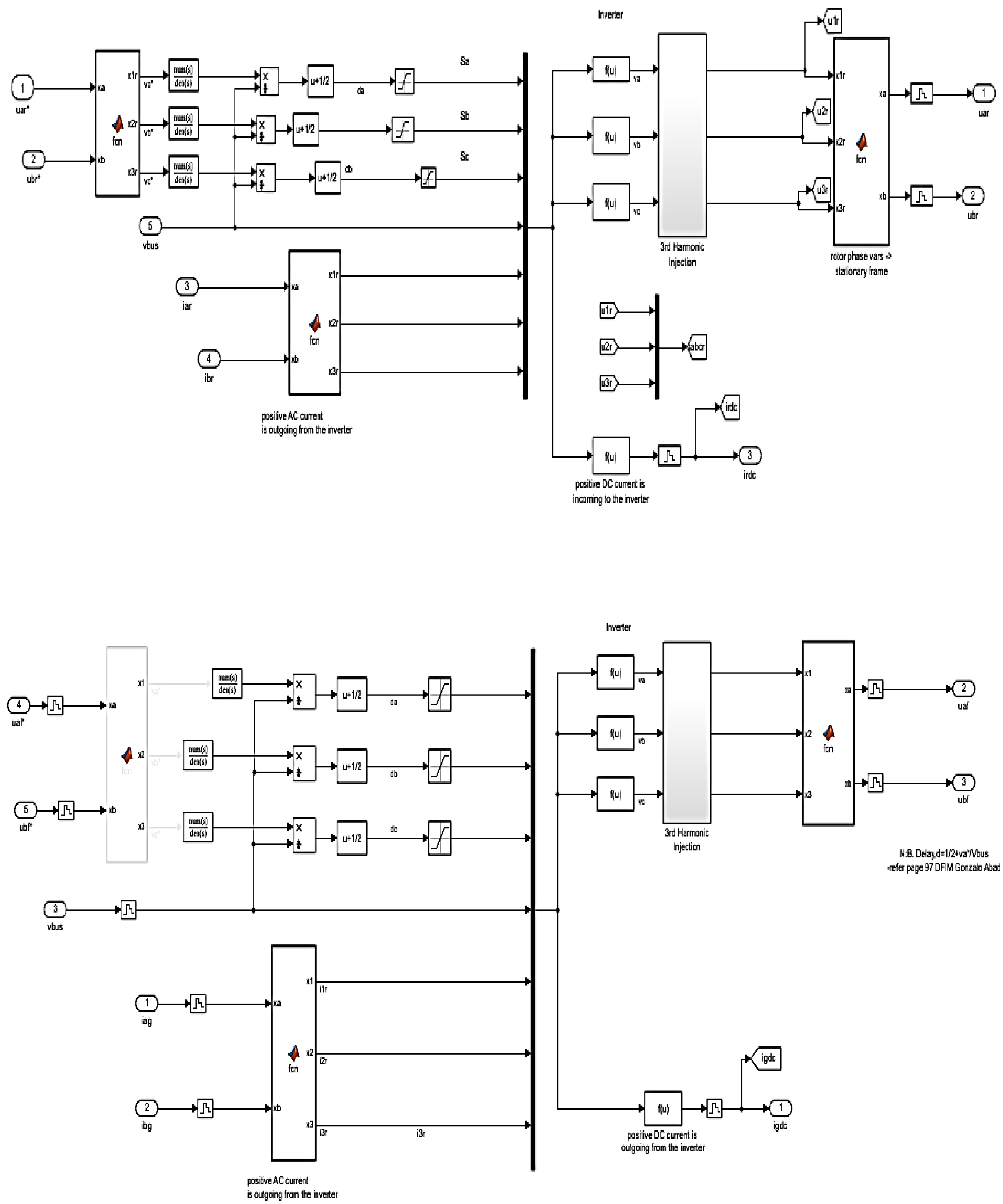

Figure A-3: RSC and GSC Model

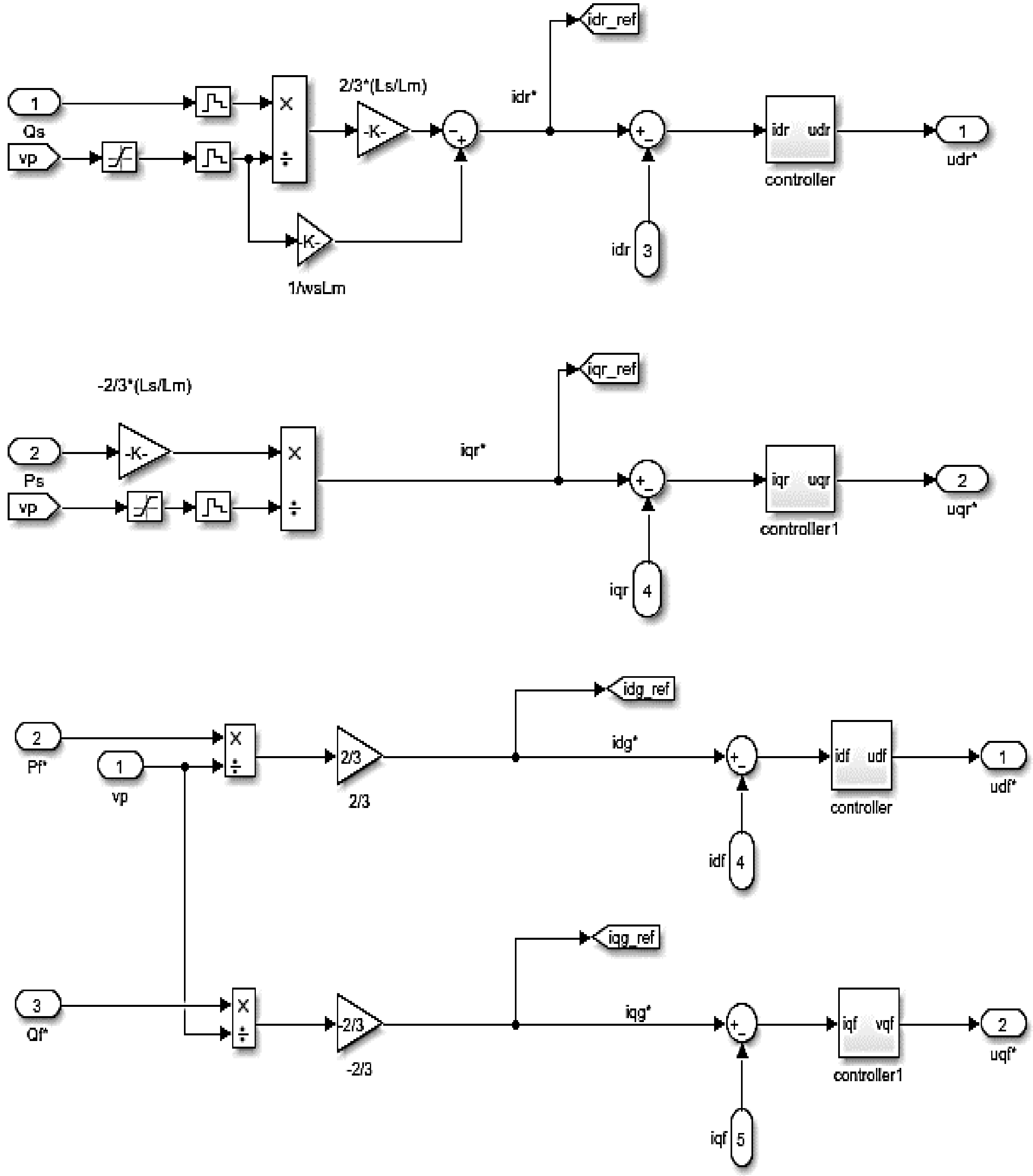

Figure A-4: RSC and GSC Control Loop

APPENDICE B

MATLAB Code

```
%%DFIG Parameters->rotor parameter referred to the stater to stator side
f = 50;                       % stator frequency(Hz)
Ps = 2e6;                     % rated stator power(W)
n = 1500;                     % rated rotational speed(rev/min)
Vs = 690;                     % rated stator voltage(V)
Is = 1760;                    % rated stator current(A)
Tem = 12732;                  % rated torque(N.M)

p = 2;                        % pole pair
u = 1/3;                      % stator/rotor turns ratio
Vr = 2070;                    % rated rotor voltage (non-reached)(V)
smax = 1/3;                   % maximum slip
Vr_stator = (Vr*smax)*u;      % rated rotor voltage referred to stator(v)
Rs = 2.6e-3;                  % stator resistance(ohm)
Lsi = 0.087e-3;               % leakage inductance(stator & rotor)(H)
Lm = 2.5e-3;                  % magnetizing inductance(H)
Rr = 2.9e-3;                  % rotor resistance referred to stator(ohm)
Ls = Lm + Lsi;                % stator inductance(H)
Lr = Lm + Lsi;                % rotor inductance(H)
Vbus = Vr_stator*sqrt(2);     % DC de bus voltage referred to stator(v)
sigma = 1 - Lm^2/(Ls*Lr);
Fs = Vs*sqrt(2/3)/(2*pi*f);   % stator flux(aprox.)(Wb)

J = 127;                      % inertia
D = 1e-3;                     % damping

fsw = 4e3;                    % switching frequency(Hz)
Ts = 1/fsw/50;                % sample time (sec)

%PI Regulator
tau_i = (sigma*Lr)/Rr;
tau_n = 0.05/4;
wni = 100*(1/tau_i);
wnn = 1/tau_n;

kp_id = (2*wni*sigma*Lr)-Rr;
kp_iq = kp_id;
ki_id = (wni^2)*Lr*sigma;
ki_iq = ki_id;
kp_n = (2*wnn*J)/p;
ki_n = ((wnn^2)*J)/p;

% Three blade wind turbine model

N = 100;                       % gearbox ratio
Radio = 42;                    % radio
ro = 1.225;                    % air density

% Cp and Ct curves
```

```
beta = 0;                     % picth angle
ind2 = 1;

for lambda=0.1:0.01:11.8

    lambdai(ind2)=(1./((1./(lambda-0.02.*beta)+(0.003./(beta^3+1)))));
    Cp(ind2)= 0.73.*(151./lambdai(ind2)-0.58.*beta-0.02.*beta^2.14-
13.2).*(exp(-18.4./lambdai(ind2)));
    Ct(ind2)= Cp(ind2)/lambda;
    ind2=ind2+1;
end
tab_lambda=(0.1:0.01:11.8);

% Kopt for MPPT
Cp_max = 0.44;
lambda_opt = 7.2;
Kopt = ((0.5*ro*pi*(Radio^5)*Cp_max)/(lambda_opt^3));

% Power curve in function of wind speed
P = 1.0e+06*[0,0,0,0,0,0,0,0.0472,0.1097,0.1815,0.2568,0.3418...
    0.4437,0.5642,0.7046,0.8667,1.0518,1.2616,1.4976,1.7613,2.0534,...
    2.3513,2.4024,2.4024,2.4024,2.4024,2.4024,2.4024];
V = [0.0000,0.5556,1.1111,1.6667,2.2222,2.7778,3.3333,3.8889,4.4444,...
    5.0000,5.5556,6.1111,6.6667,7.2222,7.7778,8.3333,8.8889,9.4444,...
    10.0000,10.5556,11.1111,11.6667,12.2222,12.7778,13.3333,13.8889,...
    14.4444,15.0000];

figure
subplot(1,2,1)
plot(tab_lambda,Ct,'linewidth',1.5)
xlabel('lambda')
ylabel('Ct')
subplot(1,2,2)
plot(V,P,'linewidth',1.5)
grid
xlabel('wind speed (m/s)')
ylabel('power(w)')

% Grid side converter
Cbus = 80e-3;                             % DC bus capacitance
Rg = 20e-6;                               % grid side filter's resistance
Lg = 400e-6;                              % grid side filter's inductance
Kpg = 1/(1.5*Vs*sqrt(2/3));
Kqg = -Kpg;
% PI regulators
tau_ig = Lg/Rg;
wnig = 60*2*pi;
kp_idg = (2*wnig*Lg)-Rg;
kp_iqg = kp_idg;
ki_idg = (wnig^2)*Lg;
ki_iqg = ki_idg;
kp_v = -1000;
ki_v = -300000;
```